Supplementary Cementitious Materials: Assessment of Test Methods for New and Blended Materials

Saif Al-Shmaisani
Ryan Kalina
Katelyn O'Quinn
Jae Kyeong Jang
Michael Rung
Raissa Ferron
Maria Juenger

Technical Report Documentation Page

1. Report No. FHWA/TX-21/0-6966-1	2. Government Accession No.	3. Recipient's Catalog No.
4. Title and Subtitle Supplementary Cementitious Materials: Assessment of Test Methods for New and Blended Materials		5. Report Date Submitted: December 2020; Published March 2021
		6. Performing Organization Code
7. Author(s) Saif Al-Shmaisani, Ryan Kalina, Katelyn O'Quinn, Jae Kyeong Jang, Michael Rung, Raissa Ferron, and Maria Juenger		8. Performing Organization Report No. 0-6966-1
9. Performing Organization Name and Address Center for Transportation Research The University of Texas at Austin 3925 W. Braker Lane, 4th Floor Austin, TX 78759		10. Work Unit No. (TRAIS)
		11. Contract or Grant No. 0-6966
12. Sponsoring Agency Name and Address Texas Department of Transportation Research and Technology Implementation Division P.O. Box 5080 Austin, TX 78763-5080		13. Type of Report and Period Covered Technical Report September 2017 – January 2021
		14. Sponsoring Agency Code
15. Supplementary Notes Project performed in cooperation with the Texas Department of Transportation.		

16. Abstract

In Texas, and most of the U.S., Class F fly ash is the most used supplementary cementitious material (SCM) due to the many benefits it provides to concrete. In recent years, the availability of Class F fly ash has decreased as many coal-fired power plants have shut down. Plants that have not shut down are required to install various emission control systems that can significantly alter the type of fly ash produced. As the face of fly ash production continues to change, the usability of non-traditional fly ashes and fly ash alternatives in concrete must be evaluated. As the number of new SCM sources rises to meet demand, rapid tests are necessary to screen out poor-performing materials and long-term performance testing is needed to qualify promising materials for use in concrete mixtures. In this study, both rapid SCM screening tests and long-term performance of non-traditional, blended fly ashes were examined. For rapid screening, both R^3 testing (ASTM C1897) and a lime reactivity test were successful at screening out inert materials. By pairing the R^3 test with an extra step in bound water testing, it is also possible to distinguish between pozzolanic and hydraulic reactivity of SCMs. With respect to non-traditional, blended fly ashes, it was determined that fly ashes that do not meet the definition of a Class F fly ash but do meet the chemical and physical property requirements performed comparably to a traditional Class F fly ash in most cases. Most of the performance differences were negligible and can be remedied through the addition of limestone, gypsum, or chemical admixtures, except for sulfate resistance. The poor sulfate resistance of some non-traditional fly ashes can be directly linked to the presence of certain crystalline phases, making the ash perform more like a Class C fly ash than a Class F fly ash.

17. Key Words Concrete, Fly Ash, Supplementary Cementitious Material, Pozzolan, Reactivity, Testing		18. Distribution Statement No restrictions. This document is available to the public through the National Technical Information Service, Springfield, Virginia 22161; www.ntis.gov.	
19. Security Classif. (of report) Unclassified	20. Security Classif. (of this page) Unclassified	21. No. of pages TBD	22. Price

Form DOT F 1700.7 (8-72) Reproduction of completed page authorized

THE UNIVERSITY OF TEXAS AT AUSTIN
CENTER FOR TRANSPORTATION RESEARCH

Supplementary Cementitious Materials: Assessment of Test Methods for New and Blended Materials

Saif Al-Shmaisani
Ryan Kalina
Katelyn O'Quinn
Jae Kyeong Jang
Michael Rung
Raissa Ferron
Maria Juenger

Disclaimers

Author's Disclaimer: The contents of this report reflect the views of the authors, who are responsible for the facts and the accuracy of the data presented herein. The contents do not necessarily reflect the official view or policies of the Federal Highway Administration or the Texas Department of Transportation (TxDOT). This report does not constitute a standard, specification, or regulation.

Patent Disclaimer: There was no invention or discovery conceived or first actually reduced to practice in the course of or under this contract, including any art, method, process, machine manufacture, design or composition of matter, or any new useful improvement thereof, or any variety of plant, which is or may be patentable under the patent laws of the United States of America or any foreign country.

Engineering Disclaimer

NOT INTENDED FOR CONSTRUCTION, BIDDING, OR PERMIT PURPOSES.

Research Supervisor: Maria C. Garci Juenger

Acknowledgments

Table of Contents

List of Tables

List of Figures

Chapter 1. Introduction

1.1. Motivation

Currently in Texas, fly ash, a coal combustion product, is the most commonly used SCM and is typically used to replace 15–35% of portland cement by mass. ASTM C618 [1] categorizes fly ash in two different classes: Class C fly ash, containing greater than 18% calcium oxide, and Class F fly ash, consisting of a maximum of 18% of calcium oxide. The use of fly ash in concrete affects both the fresh state and hardened state properties in positive ways by increasing the workability, reducing bleeding, improving pumpability, reducing the heat of hydration, increasing strength gain at later ages, and refining the pore structure to reduce permeability [2]. Class F fly ash is used predominantly in Texas and in most of the U.S. due to its ability to provide resistance to alkali-silica reaction (ASR) as well as sulfate attack [3].

In 2019, the U.S. generated approximately 71.3 million metric tons of coal combustion products, 37% (approximately 26.6 million metric tons) of which was fly ash. Of the 26.6 million metric tons of fly ash, 16.1 million metric tons (61%) were utilized in other industries [4]. Based on American Coal Ash Association (ACAA) data [4,5], the percentage of fly ash utilized has increased by 5% between 2018 and 2019, while the amount produced has dropped 19%. This can be largely attributed to competing fuel sources for electricity generation, such as natural gas, as well as emission standards issued by the EPA in 2011 requiring coal-fired power plants to install emission control systems, which, in turn, alters the composition of the fly ash. Natural gas and renewable energy have become more price competitive, so because of this, no new coal-fired power plants have been constructed in the U.S. since 2013, with plant retirements forecasted through 2040 [6]. In the last five years, there have been 324 coal-fired power generator closures in the U.S., and the U.K. is set to have its remaining coal-fired power plants retired by 2025 [7]. This presents a problem for the U.S. infrastructure, following a study conducted by the American Road and Transportation Builders Association (ARTBA) [8], which estimates that concrete production will increase more than 50% through 2033 [9].

In order to prepare for the upcoming shortage in fly ash supply, it is of interest to explore potential alternatives for Class F fly ash. Many power plants have started to burn blends of different coals, which results in fly ash with a different composition than a traditional Class F fly ash. Suppliers have also started to blend Class C and Class F fly ash to compensate for the lack of supply of Class F fly ash. Since the final products of these two processes have different compositions than a

traditional Class F fly ash, they must be tested to qualify their use in concrete. With the high demand for concrete and the low availability of Class F fly ash, rapid screening methods must be developed to identify promising materials and reject poor performers. This document presents an overview of research on fly ashes from blended coal sources, blended fly ashes, and reactivity tests for supplementary cementitious materials (SCMs).

Additionally, for these SCMs to be used in Texas Department of Transportation (TxDOT) projects, they must meet TxDOT requirements. Permissible SCMs for hydraulic cement concrete mixture designs are designated in Section 4.2.6 of Item 421 in the 2014 edition of the TxDOT Standard Specifications for Construction and Maintenance of Highways, Streets, and Bridges [10]. Section 4.2.6 specifies the use of Class C and F fly ashes, ground-granulated blast furnace slag (GGBFS), silica fume, and metakaolin. Use of SCMs other than those outlined in Section 4.2.6 depends on the ability of the concrete mixture design utilizing that SCM to limit expansion from alkali-silica reaction (ASR) to 0.08%, per testing procedures in ASTM C1567 [11] when dealing with fine, intermediate, or coarse aggregate with ASTM C1260 [12] values greater than 0.10%.

Besides durability improvements, TxDOT also recognizes other properties of concrete mixtures that are changed with the use of SCMs, such as heat of hydration, setting times, and water demand. Therefore, these properties will be discussed for the materials of interest.

1.2. Literature Review

1.2.1. Supplementary Cementitious Materials

1.2.1.1. Blended Coal Fly Ashes

In 2011, the EPA issued emission standards requiring coal-fired power plants to install emission control systems, which, in turn, reduces the quality of the fly ash. Other methods to help meet these standards include changing the burning process or changing the coal type that is burned. These methods alter the chemical properties of the fly ash produced by the coal plants and change their effects on cementitious mixtures. In Texas, power plants are increasingly burning Powder River Basin (PRB) coal to comply with air quality regulations, either exclusively or in blends with Texas Lignite Coal (TLC). PRB coal has a higher lime content than TLC, so the fly ash produced has a higher calcium content and is classified as Class C [13,14]. When the two coal sources are blended, the fly ash can be either a Class F or a Class C, depending on the proportions used.

Class F fly ashes resulting from blended PRB and TL coals may have different chemical properties than fly ashes made from burning 100% TLC. However, the fly ashes can still meet the ASTM C618 criteria for Class F classification. Given that Class C and Class F perform very differently with respect to control of heat of hydration, sulfate attack, and alkali-silica reaction, it's not clear if these blends will perform like a Class F fly ash. To our knowledge, there is no published literature comparing the performance of blended coal fly ashes to traditional Class F fly ashes.

1.2.1.2. Blended Fly Ashes

ASTM C1697 [15] allows the blending of Class C and Class F fly ash. The standard currently requires that the fly ashes to be blended meet ASTM C618 [1] specifications. Similar to fly ashes resulting from blended coals, fly ashes resulting from blended ashes may have similar composition to Class F fly ash, but it is not clear that they will behave as a Class F fly ash in concrete.

In 1998, Naik et al. [16] made a case for blending fly ashes. The researchers hypothesized that a blend of Class C and Class F fly ashes would produce a quicker rate of hydration reaction in a cementitious mixture compared to Class F fly ash, while maintaining a more favorable microstructure than a straight portland cement mixture. Three fly ash blends were created: 75% Class C and 25% Class F fly ash, 50% Class C and 50% Class F fly ash, and 25% Class C and 75% Class F fly ash. These blends were mixed at a 40% replacement of cement in concrete mixtures and compared to two controls, a straight portland cement concrete and a concrete with 35% Class C fly ash. The concretes were tested for compressive strength, tensile strength, flexural strength, drying shrinkage, abrasion resistance, salt scaling resistance, and chloride permeability. Results showed that the blending of Class C and Class F fly ash had a significant effect on the properties tested, demonstrating that up to 50% of Class C fly ash can be replaced by Class F fly ash.

Antiohos et al. [17,18] also tested blends of Class C and Class F fly ashes from Greece. Prior to blending, the fly ashes were ground using a ball mill to obtain ashes of similar particle size. Similar to Naik et al. [16], the researchers created three fly ash blends at the same proportions. Mortar compression tests were conducted on these blended ashes at 20% and 30% cement replacement and compared to three controls, a straight portland cement mortar as well as mortars containing both original fly ashes at 20% and 30% cement replacement. Compression test results showed that the 20% fly ash blend mortars outperformed the controls at later ages with the highest strength mortar containing the blend with equal proportions of both fly ashes. At 30% replacement, compressive strength had a direct correlation to active silica content with the blend possessing the highest active silica content

having the highest compressive strength. Active silica content can be tested in accordance to European Standard (EN) 197-1 [19] and correlates with the amount of the total silica content that is soluble. Synergistic action was also claimed for the fly ash blend mortars to account for the increment observed in compressive strength testing. The authors believed that the instant hydration of free lime present in high-lime ash temporarily increased the alkalinity of the mixture creating an "internal activation" process. This increase in alkalinity assists in the dissociation of firm glassy chains of the low-lime ash, releasing additional active centers, resulting in this synergistic effect. In 2007, Antiohos et al. [20] tested an additional Class C fly ash with lower active silica and higher CaO content than the original Class C fly ash tested. This Class C fly ash was ground and blended with the same Class F fly ash used in the previous study at 50% Class C-50% Class F fly ash and 25% Class C-75% Class F fly ash. Mortar compression tests were conducted on the new blended ashes and the previous blended ashes, blended at the same proportions, at 20% and 30% cement replacement and compared to four controls, a straight portland cement mortar as well as mortars containing all three original fly ashes at 20% and 30% cement replacement. Results agreed with the previous study, showing that blends with equal contributions from each fly ash were the most effective at 20% replacement, while performance at 30% replacement was highly dependent on the active silica content. In addition to compressive strength testing, pozzolanicity and hydration product development tests were performed.

In a study by Tanikella [21], twenty different fly ashes were characterized for their physical and chemical properties (thirteen Class C and seven Class F fly ashes) and studied in both binary and ternary paste systems. Mixtures with a 20% cement replacement by each individual fly ash were created and tested for the following properties: the initial set time, the rate of strength gain (strength-activity index), the heat of hydration, and the non-evaporable water and calcium hydroxide contents at various ages. These mixtures were also compared to a control portland cement mixture. Once testing was completed, a linear regression analysis was performed for each individual test with the independent variables consisting of the physical and chemical properties of the fly ash. For each test, a model was created used the combination of independent variables that had the most significant effects. Once models were created for both the Class C and Class F fly ashes, ternary pastes were mixed using an orthogonal array that defined specific compositions for each mixture and were analyzed and modeled in the same way as the binary systems. At the end of testing, it was observed that the properties of the ternary binder systems were not a weighted linear combination of the properties of binary pastes prepared from individual fly ashes. Nonetheless, the most influencing variables of the ternary blends were identified for each test.

Few studies have tested the performance of fly ash blends in sulfate attack and alkali-silica reaction. Recently, Franklin and Rhodes [22] made a case for blending fly ashes along the guidelines in ASTM C1697. They claimed that blended fly ashes can be used where Class F fly ash is specified, as long as the sum of the oxides, alkalis, and LOI are kept with the limits. They showed data demonstrating that the blended ashes behave in between the Class F and Class C ashes with respect to sulfate attack (C1012 [23]) and ASR (C1567 [11]).

In 1986, Mehta [24] conducted a study on the effect of fly ash composition on sulfate resistance of cement. Sixteen fly ash samples were tested with varying calcium contents and were blended with Type I portland cement at 25 and 40% replacement of cement. Mehta concluded that the resistance to sulfate attack depended solely on the type of aluminate phase present in the hydrated system at the time of exposure. In cases when hydrated cement pastes contained monosulfate hydrate or calcium aluminate hydrates prior to sulfate immersion, expansion would take place due to ettringite formation. When hydrated cement pastes contained ettringite prior to sulfate immersion, they would perform satisfactorily.

In 2011, Dhole et al. [25] evaluated the sulfate resistance of mortars containing high-calcium and low-calcium fly ash, along with ternary blends containing both high and low-calcium fly ash. The results showed that binary mixtures containing Class F fly ash showed significantly improved sulfate resistance compared to the control portland cement mixture. As the level of Class F fly ash increased, the expansion values decreased. Binary mixtures containing Class C fly ash revealed the opposite behavior. These mortars contained significant quantities of reactive calcium aluminate and monosulfate, which produced abundant ettringite when immersed in sulfate solution, leading to expansion in the bars. Formation of monosulfate and calcium aluminate hydrates at early ages can be linked to increased contents of phases such as C_3A, $C_4A_3\check{S}$, alkali sulfates, and reactive calcium aluminate glass in fly ashes. Analysis of the fly ashes used in the study found that fly ashes containing a calcium content of up to 15% CaO had insignificant amounts of C_3A. However, the C_3A content increased significantly as the calcium content increased past 15%. In ternary mixtures made with Class C fly and Class F fly ashes, with lower amounts of reactive alumina phases, sulfate resistance was improved compared to the control mixture. Ternary mixtures containing high percentages of Class C fly ash and low percentages Class F fly ash were able to control expansion better than the control cement mortar, but not enough to provide adequate protection. Mixtures containing high percentages of Class F fly ash and low percentages of Class C fly ash had good performance and were crack-free even after a year. Additionally, it was found that a combination of

50:50 Class C and Class F fly ash in a mixture with 25 to 30% cement replacement would perform satisfactorily in sulfate exposure.

In a study by Shehata and Thomas [26], eighteen different fly ashes were tested for their ability to prevent expansion due to ASR. Data showed that, at a 25% replacement level, low calcium, low alkali fly ashes (<20% CaO and <4% Na_2O_{eq}) controlled ASR expansion very well. The researchers concluded that a fly ash's ability to mitigate expansion is directly correlated with calcium, alkali, and silica content, where the minimum level of replacement required to control expansion generally increases as calcium or alkali content of the fly ash increases, or as the silica content decreases. Accordingly, blending coal or blending fly ashes should result in predictable performance in concrete since oxide composition plays a major role. In another study by Shehata and Thomas [27], the alkali release characteristics were studied for blended cements. Results concluded that the total alkalis contributed from a fly ash with a CaO content greater than 20% were greater than those contributed from fly ashes with a CaO content less than 20%. Additionally, the total available alkalis for samples containing high-alkali fly ash were much higher than those contributed by lower alkali fly ash. This should be considered when blending fly ashes of high alkalinity with lower alkalinity fly ashes.

The potential problem with blending stems from the expectation that blends of coal or blends of ashes will perform according to the weighted average of their oxides. Fly ashes are generally characterized using x-ray fluorescence to obtain an oxide analysis. However, these oxides are bound in different phases in the fly ash depending on the coal burned and the burning conditions. While the majority of the oxides are bound in glassy phases, there are several types of glassy phases present and the composition of these phases impacts reactivity [28–32]. The crystalline phases present in Class C fly ashes are quite different than in Class F fly ashes. Durdzinski et al. [32] characterized four Class C fly ashes and found three to contain both C_3A and C_4AF in quantities from 1-9%. Aughenbaugh [29] likewise found C_3A in a Class C fly ash, but none of the eight Class F fly ashes tested contained cementitious phases. McCarthy et al. [33] claim that nearly all western U.S. (PRB) fly ashes contain C_3A or similar phases. The presence of crystalline aluminate phases can affect the gypsum balance of the cementitious system, which can affect setting [34] as well as affect the response of the system to sulfate attack, as was shown by Mehta [24] and Dhole et al. [25]. Additionally, interactions with chemical admixtures, particularly ones that adsorb on aluminate phases, are also likely to be impacted due to these phases present in blended ash systems. Blending these ashes with a Class F fly ash or other SCM only reduces the amount of the phases but does not eliminate them. Therefore, it is possible that some blends will

not behave as their weighted averages of oxide components but will be dominated by the phases present. This issue merits further investigation.

1.2.2. SCM Testing

ASTM C618 provides the specifications for fly ash and natural pozzolans for use in concrete. Some parts of the specification are prescriptive, and others are performance-based. The standard is problematic for natural pozzolans because it fails to screen out inert materials like finely ground quartz [35]. In order to qualify new sources of SCMs for use in Texas to accommodate the shortage in Class F fly ash, including blended fly ashes, the materials need appropriate screening, beyond the tests included in ASTM C618.

TxDOT Project 0-6717 [36] demonstrated that it is necessary to test SCMs more extensively than ASTM C618 demands. Testing in that project included material characterization such as x-ray diffraction and laser particle size analysis, pozzolanicity testing through measurement of calcium hydroxide consumption, and performance testing for ASR using ASTM C1293 (among many other tests performed). The tests provided assurance that the SCMs that performed well were appropriate for use in concrete. However, while such extensive testing is necessary for new SCMs (and is even recommended by ASTM C1709 [37] for new, alternative SCMs), it is impractical for testing every fly ash variant or blend that occurs in Texas when power plants change operations. Therefore, there is a need for simple, rapid screening tests.

1.2.2.1. Reactivity Tests

The prescriptive compositional (sum of SiO_2 + Al_2O_3 + Fe_2O_3) requirements in ASTM C618 are intended to ensure that the fly ash or natural pozzolan will react with calcium hydroxide in a pozzolanic reaction [38]. However, given that at least some part of these oxides may be bound in unreactive, crystalline phases (e.g. quartz or mullite), it is not a particularly effective requirement. Measuring the crystalline phases can be done using x-ray diffraction, but the glassy phases of fly ash and most SCMs are the reactive ones, so any prescriptive compositional specification would have to assess the composition of the glassy phases. The easiest way to evaluate glassy phase composition is by subtracting crystalline phases from the oxide composition to determine a bulk oxide composition of a glass [39]. This value can then be used to calculate characteristics of a glass, such as the glassy SiO_2/Al_2O_3 ratio or non-bridging oxygen/tetrahedral (NBO/T) that give indications of glass reactivity in alkaline solutions, such as in hydrating portland cement [39].

The best way to ensure pozzolanicity, however, is to test it. Since pozzolanicity reflects the ability of the SCM to consume calcium hydroxide (CH) to form calcium silicate hydrate (C-S-H), typically pozzolanicity tests involve measuring CH consumption, either directly or indirectly. Traditional accelerated methods include the modified Chapelle test [40], Frattini test [41], and lime reactivity test [42,43]. This section aims to provide background information on current reactivity tests and examine their reliability.

1.2.2.1.1. Active Silica

The amount of reactive silica in an SCM is commonly associated with the reactivity of the material. European Standard (EN) 197-1 defines the reactive silica content as "the fraction of the silicon dioxide which is soluble after treatment with hydrochloric acid (HCl) and with boiling potassium hydroxide (KOH) solution" [19]. The quantity of reactive silica is determined as the difference between the total silica content and the dry insoluble residues. In a study by Snellings and Scrivener [44], it was determined that the test for active silica cannot be simply extrapolated to simulate portland cement conditions and that this test is not suitable as an estimator for SCM reactivity.

1.2.2.1.2. Modified Chapelle Test

The modified Chapelle test aims to measure the amount of CH consumed by a pozzolan. As per instructions given in NFP 18-513 [40], 1 g of pozzolan and 2 g of CaO are combined in a volumetric flask with 250 mL of deionized water and then stirred at 85 ± 5 °C for 16 hours along with another flask that contains no pozzolan. The flasks are then cooled to ambient temperature using running water and a solution of 250 mL of deionized water and 60 g of sucrose are added to each flask. Both flasks are then stirred for 15 minutes. Following stirring, 200 mL of each solution is filtered, and 25 mL of the filtered solutions are removed to be titrated with 0.1 N hydrochloric acid. The volume to titrate both solutions is used to calculate the CH consumed by the pozzolan. In a study by Seraj and Juenger [45], it was observed that when compared to compressive strength results, the Chapelle test was efficient at identifying pozzolans with high early reactivity (7 and 28-day strengths) but was poor at identifying pozzolans with later reactivity (90-day strength). The Chapelle test also had high sensitivity to the particle size distribution of the SCMs, as well as the cooling rate and filter paper used. These inconsistencies make it more difficult to standardize the test. Additionally, quartz was tested as an inert filler and resulted in a non-zero value for CH consumption and must be tested more in order to determine if this is an issue with the test or the material.

1.2.2.1.3. Differential Scanning Calorimetry/Thermal Gravimetric Analysis (DSC/TGA) for Pozzolanicity

The objective of DSC/TGA testing is to determine the mass loss of water during the degradation of CH, which typically occurs between approximately 400 and 500 ºC [46]. TxDOT Projects 0-6717 [36] and 5-6717 [47] both implemented this technique to quantify the CH content in control pastes and pastes containing SCMs. The procedure in the study consisted of preparing sample mixtures with a predetermined cement replacement percentage and curing them until their target age was reached. Upon reaching the target age, the edges of the sample were removed and discarded in order to remove calcium hydroxide crystals that orient along the edges of the sample and walls of the container. Next, the sample was crushed to pass the No. 100 sieve (150 μm) and then placed in a vacuum desiccator for a minimum of two weeks to cease hydration. The samples were then ground to pass the No. 325 sieve (45 μm) and placed back under vacuum prior to DSC/TGA testing to prevent carbonation of the materials [47]. The DSC/TGA testing was performed utilizing a Mettler Thermogravimetric Analyzer, Model TGA/DSC 1. The heat flow and mass loss were recorded as the materials were heated from 40–1000 ºC at a rate of 20 ºC/min within a chamber with N_2 gas to prevent carbonation of the material while the test was underway. The DSC curve was used to pinpoint the exact start and end temperatures when the mass loss occurred [48]. The mass loss within this region is then used to calculate the amount of CH present in the tested sample, which was converted to the amount of CH per gram of cement by normalizing by ignited weight and accounting for the mass percent of SCM.

A significant issue with this test is the abundant opportunities for the sample to carbonate before being measured in the thermogravimetric analyzer. Other issues occur with the interpretation of the TGA curve, which typically significantly overestimates the actual content of CH in the samples [46,48]. Another drawback comes from the reaction between the SCMs and the calcium from existing C-S-H in the system [49]. This means that the consumption of CH would be much higher if no calcium was contributed from the existing C-S-H.

1.2.2.1.4. Frattini Test

The Frattini test aims to assess the pozzolanicity of a material by comparing the concentration of calcium present in a solution in contact with hydrated cement with the quantity of calcium capable of saturating a solution of the same alkalinity [41]. The procedure consists of mixing a blend of portland cement with a 30% replacement of the cement by an SCM at a water to solid ratio of five and is kept at 40°C for seven days. The suspension is then filtered and titrated to determine the saturation of the filtrate with respect to portlandite. Snellings and Scrivener [44],

performed the Frattini test on multiple different SCMs and concluded that it is unclear how the results can be translated to a quantitative indication of compressive strength since only the solution saturation with respect to portlandite is assessed.

1.2.2.1.5. Lime Reactivity Test

The Canadian standard for alternative SCMs [43] uses a lime reactivity test, and an Indian standard uses a similar one [42]. The test involves mixing the SCM with calcium hydroxide, sand, and an alkali source, then testing for compressive strength after a specified period. The assumption is that strength gain is due to formation of C-S-H, so this is an indirect method of evaluating pozzolanicity. The method is easy to perform and repeatable. Kasaniya et al. [50] have modified the lime reactivity test in what they call the University of New Brunswick Pozzolanic Reactivity Test (UNBPRT). The UNBPRT was optimized for calcium hydroxide to pozzolan ratio, water to binder ratio, curing time, solution composition, and temperature.

1.2.2.1.6. Rapid, Relevant, and Reliable (R^3) Test

A new reactivity test called the rapid, relevant, and reliable (R^3) test method was recently standardized in ASMT C1897 [51]. The goal of the R^3 test is to create an environment that isolates the reactivity of the SCMs separate from the reaction of portland cement clinker. The procedure consists of mixing portlandite, deionized water, potassium hydroxide (KOH), potassium sulfate (K_2SO_4), and calcite along with the SCM. These pastes are then cured at 40°C and tested in two methods: cumulative heat using isothermal calorimetry or bound water content using loss-on-ignition. The R^3 method has shown to be effective at distinguishing between inert and reactive materials [52]. Measuring calcium hydroxide consumption in theses pastes has also been able to separate hydraulic and pozzolanic reactivity [53,54]. Bound water tests are preferred in lieu of isothermal calorimetry to provide a cost-effective method to determine reactivity since the only equipment necessary is an oven that can reach 400°C.

1.2.2.1.7. Compressive Strength Development

Another means of evaluating pozzolanicity can be through compressive strength development of cement-SCM pastes or mortars. ASTM C618 tries to get at this through the strength activity index (SAI), but this test is ineffective at assessing pozzolanicity since it confounds reactivity with water demand by not having a constant water content and is too generous in its strength criteria (75% strength with a 20% replacement of cement with SCM)[35,38,55]. The SAI is so generous, in fact, that an inert quartz filler passes [35]. The SAI test is in the spirit that the SCM

should "do no harm" to compressive strength or workability. The test requires that mortars have a constant flow, not water-to-cementitious materials ratio. So, SCMs that cause poor workability will require high water contents, which reduces strength so much that the SCM does not pass the SAI. Because the test links workability and strength, it is not a good measure of the impact of the SCM on strength. Because of this, Bentz et al. [55] proposed a constant volume method for strength testing. The ASTM task group working on developing a new specification for natural pozzolans is considering a constant water-to-cementitious materials ratio by mass with a water reducer specified, similar to the ASTM C1240 standard for silica fume. Workability is still evaluated by mortar flow, but poor workability is reported and then compensated through the use of a water reducer. Workability in ASTM C618 is assessed through a mortar flow test.

There are other, more rigorous, means of using strength to evaluate pozzolanicity, including a method used by some Europeans called the k-value efficiency factor [56]. The k-value is defined as the portion of SCM in a cementitious mixture, which can be considered as equivalent to portland cement, having the same properties as a cementitious mixture without SCM. In this case, a portland cement mixture would have a k-value of 1. Papadakis and Tsimas [56] estimated these k-values using an empirical equation for compressive strength related to the water content, cement content, SCM content, cement type, and time and curing. This shows that the SCMs can easily substitute, equivalently, for portland cement up to a certain level. Also, it may be possible to insist that strength of an SCM-containing mixture increase at a faster rate than a cement-only mixture, a condition that is being considered in a new ASTM specification under development for ground glass pozzolans.

1.2.2.1.8. Issues with Reactivity Tests

One thing to consider when evaluating reactivity is that it can be difficult to differentiate in common test methods between the pozzolanic reaction and cementitious reactions (e.g. from Class C fly ash or slag) and filler effects (e.g. from ground limestone or quartz) [57]. Methods such selective dissolution and image analysis can be used to determine the degree of reaction of an SCM, but the former is prone to error and the latter is expensive and time consuming [58]. De-convoluting these reactions is an area of research that needs attention.

1.2.2.2. Other Tests

Interactions between SCMs and air entraining agents are addressed by standards for SCMs in different ways. ASTM C1709 [37] suggests using a foam index test, the procedures of which are outlined in the specification. ASTM C1240 [59] for silica fume includes a procedure for making a mortar with the SCM and an air

entraining agent and measuring the air content. These tests are important for fly ash characterization because the loss-on-ignition value does not correlate directly with air entrainer absorption. This is because activated carbon injection results in the presence of activated carbon, which can have low loss on ignition, yet a large impact on air entrainment [9]. Therefore, it is important to test air entrainment in addition to loss on ignition.

None of the tests specified in ASTM C618 evaluate interactions with water reducing admixtures. This is problematic because it is typical for concrete mixtures to contain at least one chemical admixture and it is well known that admixture incompatibility issues (oftentimes manifested in rheology, setting, strength gain, or cracking problems) can occur in the presence of SCMs.

Finally, a comment should be made about the performance of SCMs with cements that contain limestone fillers. There is evidence that limestone-SCM blends improve compressive strength in a synergistic way because of the formation of carboaluminate phases, particularly with high-alumina content SCMs [60]. Limestone can also improve setting time delays in high volume fly ash mixtures [61]. However, limestone can disrupt the gypsum balance of an SCM-containing mixture [60], so the interaction of SCMs and limestone-containing cements merits attention.

1.3. Materials Selected for Testing

To find a potential substitute for traditional Class F fly ash, several ashes were procured that meet ASTM C618 [1] Class F physical and compositional requirements. The materials were classified into the following categories:

- Production Class F fly ash produced from 100% Texas lignite coal

- Class F fly ashes produced from blends of Powder River Basin (PRB) and Texas lignite coal

- Fly ash blends of ASTM C618-conforming Class C and Class F fly ash, blended to meet the compositional requirements of an ASTM C618 Class F fly ash

- Fly ashes that do not meet ASTM C618 specifications and have been remediated to meet the compositional and physical requirements

- A Class F fly ash procured from an international source

The material designations, classifications, and sources are presented in Table 1.1 for these materials.

Table 1.1: Procured Class F Fly Ashes

Designation	Material Classification	Source
F-G	Production Class F Fly Ash	Texas
F-Z		Ohio
BA-P		Alabama
BA-S	Blended Class C and F Fly Ash	Arizona
BA-V		Texas
BC-B	Blended Coal Fly Ash	Texas
BC-M		Texas
RM-S3	Remediated Class F Fly Ash	Arizona
RM-S9		Arizona
I-S	International Class F Fly Ash	Spain

In addition to these Class F fly ashes procured directly from suppliers, a Class C fly ash and a milled bottom ash, produced at the same parent plant as F-G, were procured to be blended in-house at the University of Texas at Austin. Table 1.2 shows these materials, and Table 1.3 shows the blends made using them.

Table 1.2: Procured Class C Fly Ash and Milled Bottom Ash

Designation	Material Classification	Source
C-H	Class C Fly Ash	Oklahoma
MBA	Milled Bottom Ash	Texas

Table 1.3: In-House Blended Materials

Designation	Material Classification	Blend Proportions
BA-B	Blended Milled Bottom Ash and Class F Fly Ash	40% MBA/60% F-G
BA-H	Blended Class C and F Fly Ash	54% C-H/46% F-G

To determine the effectiveness of reactivity testing, a variety of materials were procured, including materials that possess pozzolanic or hydraulic reactivity, or a combination of the two, or are inert. Table 1.4 shows the material designations, classifications, and sources.

Table 1.4: Materials Procured for Reactivity Testing

Designation	Material Classification	Source
Q	Inert Quartz Powder	West Virginia
C-H	Class C Fly Ash	Oklahoma
F-G	Production Class F Fly Ash	Texas
MBA	Milled Bottom Ash	Texas
M-D	Metakaolin	Missouri
P-O	Overburden Pumicite	New Mexico
P-P	Pure Pumicite	New Mexico
RM-S9	Remediated Class F Fly Ash	Arizona
S	Slag Grade 100	Illinois
T-P	Pumiceous Tuff	Arizona

To perform paste, mortar, and concrete testing, cements and aggregates were procured. Two cements, one with a low limestone content (<5%) and one with a higher limestone content (>5%), were procured. Both cements were sourced in Texas and are designated OPC and PLC, respectively. The low limestone cement was used for the majority of the testing, while the higher limestone cement was used on select samples. Additionally, a fine aggregate from Texas that was previously confirmed to be reactive using ASTM C1260 [12] was procured for alkali-silica reactivity testing. For ASTM C1293 [62] testing, a limestone coarse aggregate from Texas was procured. For all other concrete testing, a Colorado River sand and gravel from Texas were used as the fine and coarse aggregate, respectively.

Chapter 2. Material Characterization

Prior to conducting performance and reactivity testing, compositional and physical analysis was performed on the supplementary cementitious materials (SCMs). Characterization was completed to compare material properties with performance. Additionally, testing in accordance with ASTM C311 [63] was performed to ensure fly ash alternatives met the chemical and physical requirements specified in ASTM C618 [1] for Class F fly ash. Table 2.1 outlines the characterization tests performed. Testing was performed at the University of Texas at Austin, unless otherwise noted. Material characterization was not performed on materials blended in-house. For these materials, compositional and physical properties were determined as the weighted sum of their individual components.

Table 2.1: Material Characterization Tests

Test Method	Property Measured
X-ray Fluorescence	Oxide Composition
Oven Drying	Moisture Content
Oven Drying	Loss on Ignition
Pycnometer	Density
No. 325 Wet Sieve	Fineness
Autoclave	Soundness
Mortar Compression Testing	Strength Activity Index
Mortar Flow	Water Requirement
Flame Photometer	Available Alkali
X-ray Diffraction	Crystalline and Bulk Amorphous Composition
Laser Diffraction	Particle Size Distribution
Scanning Electron Microscopy	Particle Shape

2.1. Characterization Procedures and Results

2.1.1. Oxide Composition

X-ray fluorescence (XRF) testing, performed at the Texas Department of Transportation (TxDOT), was used to determine the oxide compositions of the materials. Non-traditional Class F fly ashes must meet the oxide composition requirements set by ASTM C618 [1]. This includes a 50% minimum sum of the silicon dioxide (SiO_2), aluminum oxide (Al_2O_3), and ferric oxide (Fe_2O_3) and a maximum calcium oxide (CaO) content of 18%. A maximum sulfur trioxide (SO_3)

content of 5% is also included in the standard. Table 2.2 shows the results from XRF testing.

Table 2.2: Oxide Compositions of Materials

Material	SiO_2 (%)	Al_2O_3 (%)	Fe_2O_3 (%)	CaO (%)	MgO (%)	SO_3 (%)	Na_2O (%)	K_2O (%)	SiO_2+ Al_2O_3+ Fe_2O_3 (%)
F-G	54.81	21.19	4.72	11.24	2.52	0.45	0.15	0.99	80.71
F-Z	43.89	19.20	18.05	7.53	0.80	2.69	0.56	2.09	81.14
BA-B	54.65	21.34	5.01	11.17	2.47	0.40	0.13	0.95	80.99
BA-H	46.64	20.33	5.05	16.97	4.23	0.94	0.89	0.76	72.02
BA-P	45.30	20.26	9.93	12.69	2.88	1.06	1.19	1.58	75.50
BA-S	50.86	22.80	5.15	10.82	2.42	0.88	1.83	0.93	78.81
BA-V	45.40	17.76	7.33	18.58	4.44	1.18	1.28	0.87	70.49
BC-B	55.22	18.24	6.12	11.64	2.82	0.50	0.46	1.25	79.58
BC-M	51.10	19.26	5.05	14.10	3.76	0.72	0.68	1.42	75.41
RM-S3	52.36	22.91	5.71	8.25	0.90	3.92	1.29	0.93	80.97
RM-S9	62.60	18.83	4.10	2.87	0.64	0.23	2.39	2.46	85.52
I-S	57.41	20.08	9.32	2.87	1.65	0.57	2.24	1.82	86.81
Q	99.20	0.21	0.13	0.18	0.03	0.09	0.02	0.03	99.54
C-H	39.69	19.61	5.32	21.85	5.68	1.36	1.52	0.56	64.62
MBA	54.40	21.58	5.43	11.06	2.39	0.33	0.10	0.89	81.41
M-D	54.57	36.02	2.90	0.41	0.35	0.05	0.00	1.37	93.49
P-O	64.89	11.75	2.55	1.09	0.31	0.03	3.78	3.97	79.18
P-P	73.99	13.08	2.08	0.33	0.00	0.04	4.40	4.27	89.14
S	35.24	10.61	1.50	39.01	10.74	2.63	0.30	0.54	47.35
T-P	72.47	14.14	1.80	1.96	1.18	0.05	2.82	5.05	88.41

Most of the fly ash alternatives meet the requirements for a Class F fly ash as set by ASTM C618, except for BA-V due to its CaO content greater than the 18% maximum. The 18% limit set on CaO content for Class F fly ash was recently added, after performance testing had started on the procured materials. Prior to this addition, BA-V met the previous requirements for a Class F fly ash. Therefore, BA-

V is presented throughout the report as an alternative to traditional Class F fly ash, although it no longer meets the criteria for a Class F fly ash in ASTM C618.

2.1.2. Moisture Content and Loss on Ignition

Moisture content (MC) and loss on ignition (LOI) of the materials were measured in accordance with ASTM C311 [63] to ensure the fly ash alternatives met the requirements set by ASTM C618 [1] for Class F fly ash. ASTM C618 limits MC and LOI of Class F fly ash to 3% and 6%, respectively. Results from MC and LOI testing on the fly ash alternatives are shown in Table 2.3.

Table 2.3: MC and LOI of Materials

Material	MC (%)			LOI (%)		
F-G	0.46	±	0.09	0.17	±	0.01
F-Z	0.74	±	0.04	2.15	±	0.01
BA-B	0.57	±	0.13	0.22	±	0.01
BA-H	0.49	±	0.05	0.34	±	0.10
BA-P	0.65	±	0.02	1.06	±	0.02
BA-S	3.30	±	0.09	1.40	±	0.10
BA-V	0.70	±	--	0.70	±	--
BC-B	0.62	±	0.01	0.25	±	0.05
BC-M	0.62	±	0.09	0.16	±	0.05
RM-S3	0.93	±	0.03	1.45	±	0.01
RM-S9	0.54	±	0.06	0.38	±	0.04
I-S	0.66	±	0.08	1.00	±	0.15

Red text indicates material that does not meet ASTM C618 requirements for a Class F fly ash

As-received, BA-S did not meet the moisture content requirements set by ASTM C618. This can be remedied by the supplier by drying the fly ash prior to distribution or adjusting blend proportions.

2.1.3. Density

Density measurements are performed on fly ashes to ensure uniformity compliance between separate batches of materials. Since the materials procured for this study came from a single batch, density was only measured for concrete mixture

proportioning. Measurements were completed at TxDOT using a gas-comparison pycnometer and results are presented in Table 2.4.

Table 2.4: Physical Properties of Materials

Material	Density (g/cm³)	Fineness (%)	Soundness (%)
F-G	2.34	24.43	-0.02
F-Z	2.57	12.34	-0.04
BA-B	2.47	22.01	-0.01
BA-H	2.50	19.33	0.02
BA-P	2.51	14.21	0.02
BA-S	2.33	11.19	0.02
BA-V	2.71	6.30	-0.06
BC-B	2.49	15.34	0.02
BC-M	2.50	16.54	-0.03
RM-S3	2.23	21.44	-0.04
RM-S9	2.25	17.21	-0.04
I-S	2.43	15.04	-0.02
Q	2.64	--	--
C-H	2.63	14.98	0.06
MBA	2.66	18.39	0.01
M-D	2.72	--	--
P-O	2.57	--	--
P-P	2.40	--	--
S	2.93	--	--
T-P	2.47	--	--

2.1.4. Fineness

Fineness of the materials was measured in accordance with ASTM C311 [63] to ensure the fly ash alternatives met the requirements set by ASTM C618 [1] for Class F fly ash. Testing is conducted by wet sieving a material through a 45µm (No. 325) sieve and. The amount of material retained on the sieve is then calculated and cannot exceed 34% to meet Class F fly ash criteria. Results from fineness testing

are shown only for the fly ash alternatives in Table 2.4. All the fly ash alternatives met the fineness criteria for a Class F fly ash.

2.1.5. Soundness

Soundness of the materials was measured in accordance with ASTM C311 [63] to ensure the fly ash alternatives met the requirements set by ASTM C618 [1] for Class F fly ash. Testing is conducted by measuring the amount of autoclave expansion of paste bars. The expansion of the paste bars must remain below 0.8% to meet Class F fly ash criteria. Results from soundness testing were provided by the material suppliers and are shown only for the fly ash alternatives in Table 2.4.

2.1.6. Strength-Activity Index and Water Requirement

The strength-activity index (SAI) and water requirement for the materials were measured in accordance with ASTM C311 [63] to ensure the fly ash alternatives met the requirements set by ASTM C618 [1] for Class F fly ash. Mortar mixtures were made with a varying water to cementitious materials ratio (w/cm) to achieve a flow within ± 5 of the control portland cement mixture. Once the flow requirements were met, mortar was cast into 2 in. cubes and tested in compression at 7 and 28 days in accordance with ASTM C109 [64]. Compressive strength of the mortar cubes must be at a minimum of 75% of the portland cement control at 7 or 28 days to meet Class F fly ash criteria. Results from SAI and water requirement testing were provided by the material suppliers and are shown only for the fly ash alternatives in Table 2.5. Testing was not performed on in-house blends but results for their individual components are presented.

Table 2.5: SAI and Water Requirement for Mortars

Material	SAI (%) 7 Days	SAI (%) 28 Days	Water Requirement (%)
F-G	82	92	95
F-Z	76	80	101
BA-P	93	92	95
BA-S	79	88	97
BA-V	93	112	91
BC-B	86	91	94
BC-M	89	103	94
RM-S3	81	85	99
RM-S9	79	90	101
I-S	89	89	97
C-H	104	102	96
MBA	87	88	98

2.1.7. Available Alkali

ASTM C311 [63] procedures were followed to determine available alkali of the fly ashes presented as the equivalent sodium oxide content (Na_2O_e). The samples were prepared by dry mixing 5 g of SCM with 2 g of hydrated lime, adding 10 mL of water, and mixing until the sample was uniform. The mixtures were then sealed in a plastic vial and stored at 38°C for 28 days.

When the samples were ready for testing, the contents of the vial were removed, broken up, and ground with water to create a uniform slurry containing no lumps. The slurry was transferred into a beaker where water was added to bring the total volume of the sample to 200 mL. The sample was left for 1 hour on a magnetic stirrer, after which the sample was then filtered through a medium-textured filter paper into a 500 mL volumetric flask and washed with hot water 8 to 10 times. The filtrate was neutralized with dilute HCl (1+3) using 1 to 2 drops of phenolphthalein solution as the indicator. The solution was cooled to room temperature and then deionized water was added to fill the remaining portion of the volumetric flask. Flame photometry was utilized to determine the amount of sodium and potassium oxides in the solution, measured in ppm. The values obtained were then converted to percent oxides for sodium and potassium and then converted to the equivalent

sodium oxide ($Na_2O_e = Na_2O + 0.658\ K_2O$). The soluble alkali contents of the fly ashes are presented in Table 2.6.

Table 2.6: Available and Total Alkalis (Percent by Mass of SCM)

Material	Available			Total
	Na_2O (%)	K_2O (%)	Na_2O_e (%)	Na_2O_e (%)
F-G	0.19	0.46	0.49	0.79
F-Z	0.36	1.00	1.02	1.93
BA-B	0.16	0.42	0.43	0.75
BA-H	0.81	0.47	1.12	1.39
BA-P	0.90	0.93	1.51	2.23
BA-S	1.15	0.37	1.39	4.01
BA-V	0.70	0.36	0.94	1.85
BC-B	0.46	0.55	0.82	1.02
BC-M	0.47	0.77	0.98	1.61
RM-S3	0.73	0.41	1.00	1.90
RM-S9	1.01	0.47	1.32	2.44
I-S	1.09	0.86	1.66	3.45

2.1.8. Crystalline and Bulk Amorphous Composition

Quantitative X-ray diffraction (XRD) was performed to determine the crystalline composition and bulk composition of the amorphous phases in the materials. Samples were prepared by first grinding 2.5 g of SCM using a ceramic mortar and pestle until all the material passed through a No. 325 sieve to ensure adequate packing in the XRD sample holder. The material was then mixed with a reference material, zincite (ZnO), at 10% by mass in an agate mortar and pestle. A small amount of isopropanol was added to the powder mixture to ensure a homogenous dispersion of the powders. Samples were then dried in an oven at 60°C for a short period of time (less than 10 minutes) and placed in a vacuum desiccator until testing.

Once the samples were ready for testing, the powders were packed into discs for analysis in a Rigaku MiniFlex II. To minimize preferential orientation of the crystals, a razor blade was used to form perpendicular cuts along the surface of the powder before a glass slide was used to press down the powder without twisting.

Samples were then run using a continuous scan at a measurement range of 5° to 75° 2θ, a step size of 0.02° 2θ at a rate of 0.5° 2θ per second, a tube voltage of 40 kV, and a tube current of 15 mA. The XRD pattern provides a plot (diffractogram) of x-ray intensities throughout the measurement range, which can be found for all samples in Appendix A. Crystalline phases were first identified using Jade before completing the quantitative analysis using PDXL2. The composition of the amorphous content was then determined as the difference of the oxides present in the crystalline phases from the XRF data. Crystalline compositions of the samples are presented in Table 2.7-Table 2.9. The bulk amorphous compositions for all the materials are shown in Table 2.10.

Table 2.7: Amorphous Contents and Main Crystalline Phases Present in Coal Combustion Products (CCPs)

Phase Name	C-H (%)	F-G (%)	F-Z (%)	I-S (%)	BC-B (%)	BC-M (%)	MBA (%)
Amorphous	75.39	82.84	77.07	80.46	82.24	75.10	65.85
Albite	--	--	--	--	--	--	--
Anhydrite	0.93	--	2.39	--	--	--	0.50
Anorthite	--	--	--	--	--	--	18.47
Augite	--	--	--	--	--	--	2.63
Clinoptilolite-Na	--	--	--	--	--	--	--
Cristobalite	--	--	--	--	--	--	--
Gehlenite	3.43	--	--	--	--	--	--
Hematite	--	0.47	2.49	0.77	0.32	--	--
Kalsilite	--	--	--	--	--	--	--
Lime	0.47	0.40	0.75	--	--	--	--
Magnetite	--	--	4.43	6.83	0.42	--	--
Mullite	2.25	6.73	6.78	3.46	3.06	4.14	5.12
Periclase	2.32	--	--	--	--	1.98	0.37
Portlandite	--	--	--	--	--	--	--
Tricalcium Aluminate	7.53	--	--	--	--	3.89	--
Quartz	7.68	9.56	6.10	8.48	13.96	14.90	7.56

Table 2.8: Amorphous Contents and Main Crystalline Phases Present in Blended or Remediated CCPs

Phase Name	BA-B (%)	BA-H (%)	BA-P (%)	BA-S (%)	BA-V (%)	RM-S3 (%)	RM-S9 (%)
Amorphous	76.04	78.82	84.89	66.34	80.22	71.83	83.04
Albite	--	--	--	4.16	--	--	--
Anhydrite	--	0.50	0.55	--	0.62	--	--
Anorthite	7.39	--	--	--	--	--	--
Augite	1.05	--	--	--	--	--	--
Clinoptilolite-Na	--	--	--	13.52	--	--	--
Cristobalite	--	--	--	3.58	--	--	--
Gehlenite	--	1.85	--	--	--	--	--
Hematite	0.28	0.22	1.39	--	--	--	--
Kalsilite	--	--	--	--	--	2.36	--
Lime	0.24	0.44	0.20	--	0.34	--	0.41
Mullite	6.09	4.31	3.20	5.51	3.52	15.37	9.58
Periclase	0.15	1.25	1.34	--	1.67	--	0.84
Portlandite	--	--	--	--	--	2.46	--
Tricalcium Aluminate	--	4.07	2.02	--	3.80	--	0.12
Quartz	8.76	8.54	6.42	6.89	9.85	7.98	6.01

Table 2.9: Amorphous Contents and Main Crystalline Phases Present in Natural Pozzolans and Slag

Phase Name	M-D (%)	P-O (%)	P-P (%)	S (%)	T-P (%)
Amorphous	77.01	84.89	90.47	95.46	66.84
Albite	--	4.27	--	--	7.84
Anatase	1.19	--	--	--	--
Anorthoclase	--	15.51	--	--	14.70
Hematite	0.39	--	--	--	--
Lime	0.20	--	--	--	--
Merwinite	--	--	--	4.54	--
Mullite	1.94	--	--	--	--
Muscovite	7.29	--	--	--	--
Sanidine	--	4.14	8.38	--	--
Quartz	12.17	7.23	1.15	--	10.62

Table 2.10: Bulk Amorphous Composition and NBO/T of Materials

Material	SiO$_2$ (%)	Al$_2$O$_3$ (%)	Fe$_2$O$_3$ (%)	CaO (%)	MgO (%)	SO$_3$ (%)	Na$_2$O (%)	K$_2$O (%)	SiO$_2$/ Al$_2$O$_3$	NBO/T
F-G	43.36	16.35	4.25	10.83	2.52	0.45	0.15	0.99	4.39	0.12
F-Z	35.88	14.33	11.13	5.80	0.80	1.29	0.56	2.09	3.88	-0.01
BA-B	40.41	14.27	4.65	9.17	2.17	0.40	0.13	0.95	4.35	0.11
BA-H	36.48	15.02	4.83	13.03	2.97	0.65	0.89	0.76	3.87	0.50
BA-P	37.98	17.20	8.55	11.01	1.54	0.73	1.19	1.58	3.79	0.27
BA-S	27.20	16.35	5.09	10.64	2.42	0.88	0.75	0.63	3.79	0.12
BA-V	34.56	13.80	7.33	15.63	2.77	0.82	1.28	0.87	4.34	0.61
BC-B	40.40	16.05	5.37	11.64	2.82	0.50	0.46	1.25	5.14	0.21
BC-M	35.03	14.83	5.05	11.68	1.78	0.72	0.68	1.42	4.50	0.34
RM-S3	39.15	11.12	5.71	6.39	0.90	3.92	1.29	0.23	3.88	-0.04
RM-S9	53.88	11.91	4.10	2.39	0.00	0.23	2.39	2.46	5.64	-0.08
I-S	47.95	17.60	1.73	2.87	1.65	0.57	2.24	1.82	4.85	-0.08
C-H	30.63	13.88	5.32	14.90	3.36	0.81	1.52	0.56	3.43	0.83
MBA	36.00	11.13	5.24	6.67	1.64	0.33	0.10	0.89	4.28	0.10
M-D	37.90	32.30	2.51	0.41	0.35	0.05	0.00	0.69	2.57	-0.50
P-O	41.49	7.18	2.55	1.09	0.31	0.03	1.80	2.75	9.37	0.02
P-P	67.34	11.52	2.08	0.33	0.00	0.04	4.16	3.19	9.60	-0.01
S	33.58	10.61	1.50	36.69	10.19	2.63	0.30	0.54	5.64	2.48
T-P	46.51	9.80	1.80	1.96	1.18	0.05	0.61	4.40	8.70	0.04

Once the amorphous composition has been calculated, the network modifier content can be used to express the level of reactivity of the SCMs [39,65]. In a pure silicate glass, silicate tetrahedra are linked at each corner to exactly one other silicate tetrahedron (T). This structure can be affected by the introduction of alkali and alkaline earth metals (M$_2$O and M'O), which are considered network modifiers [65,66]. The M+ cations, such as potassium and sodium, destabilize the glass network by bonding to oxygen atoms for charge balance, preventing them to act as a bridge between silicon atoms, thus creating non-bridging oxygens (NBO) [65,66]. The glass present in fly ash and pozzolans typically consists of alkali and alkaline earth aluminosilicate glass. Aluminum is known to act as a network former due to its ability to be tetrahedrally coordinated in place of silicon, resulting in a net charge of -1 on the tetrahedron, which must be balanced by a cation in the interstices [66]. By using the NBO/T parameter, the reactivity of the fly ash and pozzolans can be assessed. NBO/T (shown in Table 2.10) was calculated using the amorphous oxide atomic percentages, which were converted from the mass percentages, using Equation 1.1 from Diaz-Loya et al. [65].

$$\frac{NBO}{T} = \frac{2(Na_2O + K_2O + CaO + MgO - Al_2O_3)}{(SiO_2 + Al_2O_3 + Fe_2O_3)}$$

$\qquad$ (1.1)

NBO/T values typically range from 0 to 4, where a value of 0 represents a fully polymerized network of silicon tetrahedra with little reactivity, and a value of 4 implies that there are no oxygen-bridged tetrahedral, so the glass has a high reactivity [39,65]. Negative NBO/T values are due to insufficient amounts of network modifiers to charge balance all the Al^{3+}, resulting in no network modifiers available to prevent oxygen atoms from bridging neighboring tetrahedra [39]. This causes the aluminum to take on 6-coordination, which has a lower reactivity than the 4-coordination aluminum that occurs when its charge is sufficiently balanced [39,67].

The vitreous SiO_2/Al_2O_3 ratio can also be used to evaluate the reactivity of fly ash and pozzolans in high alkaline environments, such as in portland cement mixtures and geopolymers. Optimum ratios have been identified for geopolymers, with metakaolin having an optimum range of 2.0-4.3, Class C fly ash performing best when the ratio is below 4.3, and Class F fly ash showing improved reactivity at low SiO_2/Al_2O_3 ratios [39]. The amorphous oxide atomic percentages were used to calculate the SiO_2/Al_2O_3 ratios, which are shown in Table 2.10.

2.1.9. Particle Size Distribution

Particle size distribution of the materials was determined through laser diffraction. Samples were dispersed in isopropanol and particle size was measured using a Malvern Mastersizer 2000 Laser Diffraction Particle Size Distribution Analyzer. The results are presented as the particle diameters at 10%, 50%, and 90% of the cumulative particle size distribution in Table 2.11.

Table 2.11: Particle Size Distribution of Materials

Material	d_{10} (µm)	d_{50} (µm)	d_{90} (µm)
F-G	2.1	16.7	96.3
F-Z	2.2	17.6	80.0
BA-B	3.2	23.2	88.3
BA-H	2.1	14.4	80.9
BA-P	1.5	11.8	73.2
BA-S	2.1	12.4	56.8
BA-V	1.5	11.9	50.5
BC-B	1.5	11.4	67.2
BC-M	1.4	11.6	66.1

Material	d_{10} (μm)	d_{50} (μm)	d_{90} (μm)
RM-S3	2.3	20.2	94.3
RM-S9	1.9	18.1	84.5
I-S	1.5	11.5	72.3
Q	4.4	16.2	40.3
C-H	2.0	12.4	67.8
MBA	4.8	32.8	76.4
M-D	2.4	19.5	55.8
P-O	1.4	5.9	28.6
P-P	1.6	5.2	14.0
S	1.5	8.6	25.2
T-P	1.6	7.3	25.2

2.1.10. Scanning Electron Microscopy

Scanning electron microscopy (SEM) was performed on the fly ashes to determine the particle shape of the materials. It has been shown that particle shape and size of fly ash can affect the performance of cement-based materials, which can be altered during the blending or remediation process [68]. SEM samples were mounted using carbon conductive tape on a SEM stub. To reduce charging, a sputter coater (Electron Microcopy Sciences) coated specimens for a 30-second gold/palladium (60:40) at a current of 40 mA. Samples were loaded in a FEI Quanta 650 SEM and images were taken under high vacuum and an accelerating voltage of 20 kV. SEM images can be found in Appendix B.

Chapter 3. Reactivity Testing

With the decrease in availability of Class F fly ash in Texas, new sources and materials are being tested as potential alternatives. Due to the high demand for these materials, rapid screening methods are necessary to expedite their use in concrete. Table 3.1 shows the tests selected to assess the filler effects, cementitious reactions, and pozzolanic reactions of the supplementary cementitious materials (SCMs) selected for this testing (Table 1.4).

Table 3.1: Reactivity Tests

Test Method	Sample Type	Reactions Measured
Isothermal Calorimetry	Cement-SCM Pastes	Filler
	R^3 Mixtures	Pozzolanic
	SCM-Water/Alkaline	Pozzolanic
X-Ray Diffraction	Hydrated Pastes	Cementitious
Loss on Ignition	R^3 Mixtures	Pozzolanic
Thermogravimetric Analysis	R^3 Mixtures	Pozzolanic
	Cement-SCM Pastes	Pozzolanic
Compressive Strength	Cement-SCM Mortars	Strength Development
	Lime-SCM Mortars	Pozzolanic

3.1. Reactivity Tests

3.1.1. Isothermal Calorimetry

3.1.1.1. Cement-SCM Pastes

Isothermal calorimetry was performed on cement-SCM pastes to examine the effects the procured SCMs have on the hydration kinetics of cement, including filler effects. Filler effects can be attributed to two main mechanisms: increased space and enhanced nucleation [69]. Since fillers do not produce any hydrates, more space is available for cement hydrates to form. Enhanced nucleation occurs when the filler is finer than the cement, which provides additional nucleation sites on the surfaces of the inert material for cement phases to form. It should be noted that isothermal calorimetry results for SCM-cement pastes cannot identify whether or not an SCM is pozzolanic. These tests only determine if the SCM alters the hydration kinetics of cement through filler effects or through the SCM's own hydraulic reactivity.

Pastes consisted of 25 g cementitious material and a w/cm of 0.45. For pastes containing SCMs, 25% of the cement was replaced by mass. Pastes were mixed for 2 min using an overhead laboratory mixer at 1600 rpm and then placed into a glass ampoule, sealed, and inserted into a TAM Air (Thermometric or TA Instruments) isothermal calorimeter at 23°C. Heat release of the pastes was then measured for 72 h. Figure 3.1 and Figure 3.2 show the rates of heat evolution of the pastes.
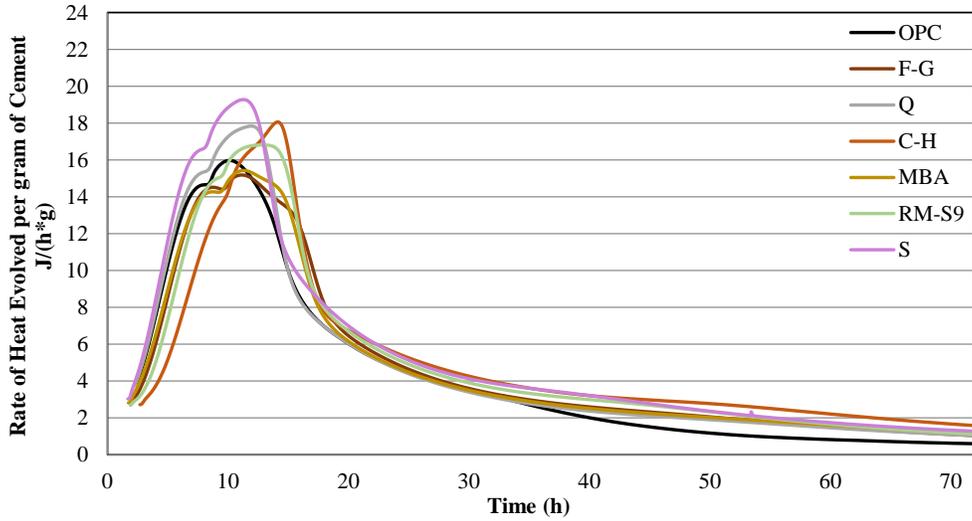
Figure 3.1: Rate of heat evolution of cement pastes containing control materials and SCMs
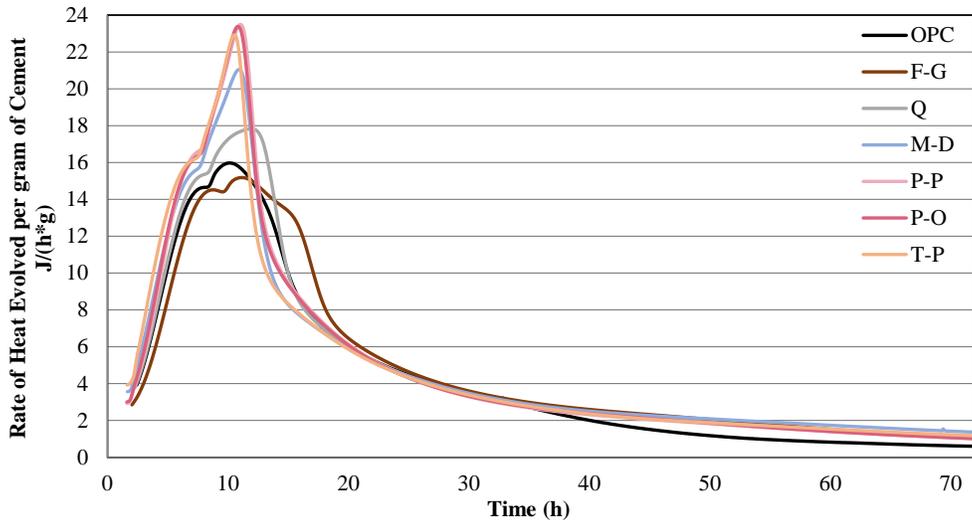
Figure 3.2: Rate of heat evolution of cement pastes containing control materials and natural pozzolans

28

In Figure 3.1, Q increases the rate of heat evolution in paste per gram of cement, despite being an inert material due to filler effects. At early ages, slow reacting and low reactivity materials act as a filler, including low-calcium fly ashes and milled bottom ash [69]. Therefore, it is expected that F-G and MBA pastes would behave similarly to Q paste due to filler effects. Differences in Figure 3.1 between F-G, MBA, and Q are due to the particle sizes of these materials, as shown in Table 2.11. Since F-G and MBA have larger particle sizes than Q, they do not provide increased nucleation sites, although they still provide increased space for cement hydrates to form.

C-H is a high calcium fly ash that contains tricalcium aluminate and free lime, which are reactive crystalline phases that can accelerate and alter cement hydration reactions [69]. This results in a heat evolution curve for C-H paste that has an amplified second peak that starts to overlap the main hydration peak in Figure 3.1. The increase in rate of heat evolution per gram of cement of S paste compared to OPC paste can be attributed to the hydraulic properties of slag.

In Figure 3.2, the main hydration peak of natural pozzolan pastes occurred sooner than the control OPC paste due to the smaller particle sizes of the materials as shown in Table 2.11. Additionally, an amplification of the second peak is observed for the natural pozzolan pastes. This is likely due to a combination of filler effects and reactive alumina in the natural pozzolans while attributing no additional sulfates. The increase in aluminates in the system results in a quicker depletion of the sulfates in the system, which can result in an amplification of the second peak [69].

The observed filler and hydraulic behaviors of the SCMs in Figure 3.1 and Figure 3.2 provide information on how the materials will affect early-age concrete performance, but do not serve as screening tools for SCM reactivity. In order to measure SCM reactivity, both pozzolanic and hydraulic, other types of tests are needed.

3.1.1.2. Rapid, Relevant, and Reliable (R^3) Mixtures

An isothermal calorimetry test protocol for SCMs called the rapid, relevant, and reliable (R^3) test method recently standardized in ASTM C1897 [51] is being used to evaluate the reactivity of SCMs. The goal of the R^3 test is to create an environment that isolates the reaction of the SCMs without the use of portland cement. Mixtures are composed of five different solid components: (1) one of the SCMs or quartz, (2) portlandite (Ca(OH)$_2$), or CH in cement chemistry notation), (3) calcite, (4) potassium hydroxide (KOH), and (5) potassium sulfate (K$_2$SO$_4$). CH is added at a 3:1 mass ratio to the SCM to provide an excess amount of CH for

consumption by the SCM. Calcite is added as an excess counter anion for the AFm phase. KOH and K_2SO_4 are added to deionized water to produce an activating solution, while the solution-to-binder ratio of the system was 1.2. The cumulative heat is measured using an isothermal calorimeter at 40ºC for 7 days, and higher values suggest greater SCM reactivity. Similar to cement-SCM paste calorimetry, R^3 mixtures are mixed for 2 minutes using an overhead laboratory mixer at 1600 rpm. The cumulative heats for the R^3 mixtures at 7 days are shown in Figure 3.3.
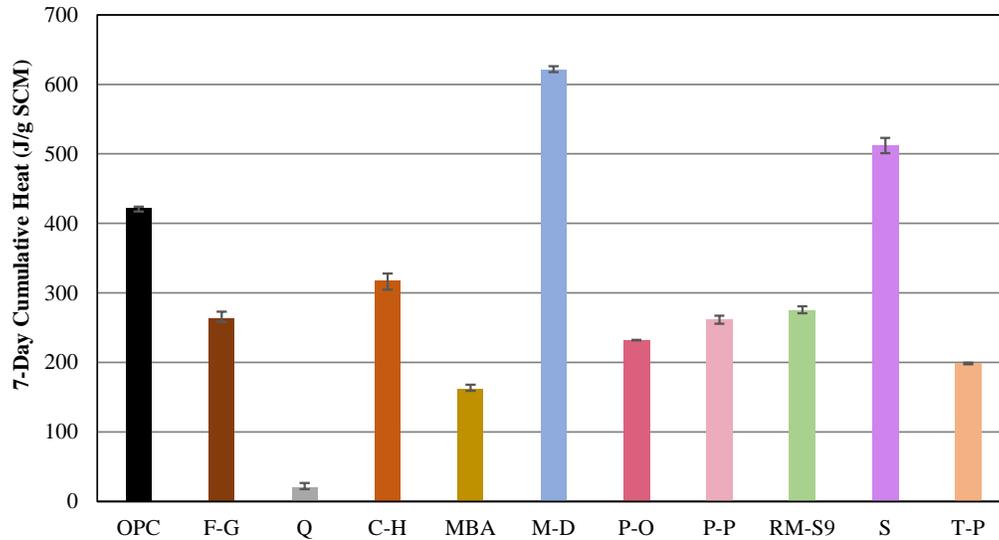
Figure 3.3: 7-day cumulative heat release of R^3 mixtures at 40°C

In Figure 3.3, the inert quart mixture, Q, had a substantially lower cumulative heat value at 7 days than the rest of the mixtures, indicating that the test is effective at distinguishing between inert and reactive materials. OPC and S mixtures had higher cumulative heat values at 7 days than most of the mixtures, except for M-D, due to their hydraulic properties. The hydraulic properties of the Class C fly ash mixture, C-H, also attributed to the higher cumulative heat value than the other ashes and pumices. M-D mixture had the highest cumulative heat value at 7 days, which is due to metakaolin being a silica and alumina-rich material. CH, in the R^3 mixture, reacts with the silica and alumina present in M-D to form both calcium aluminate and calcium silicate hydrates. The formation of calcium aluminate hydrates generates more heat than calcium silicate hydrates, leading to higher heat release values for M-D since it has a higher alumina content than the other materials, as shown in Table 2.2 [70,71]. It is clear from the results in Figure 3.3 that the R^3 isothermal calorimetry test can correctly identify inert and reactive SCMs, but does not distinguish between hydraulic and pozzolanic reactivity.

3.1.1.3. SCM-Water/Alkaline Solution Pastes

Isothermal calorimetry was also performed on pastes containing only the SCM mixed with water to identify the self-cementitious reactions of the SCMs. The idea was to create an environment that only measures heat from hydraulic reactions in order to separate hydraulic from pozzolanic SCMs. The same mixture proportions and procedure were used as for cement-SCM pastes, but with a 100% cement replacement of the cement with the SCM by mass. The cumulative heats for the SCM-water pastes are shown in Figure 3.4 and Figure 3.5.
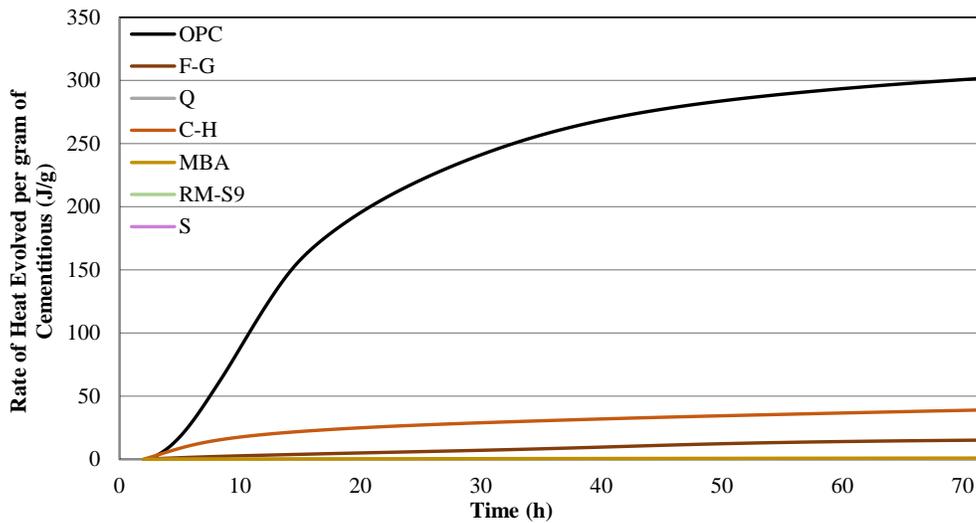
Figure 3.4: Cumulative heat evolved of control and SCM-water pastes
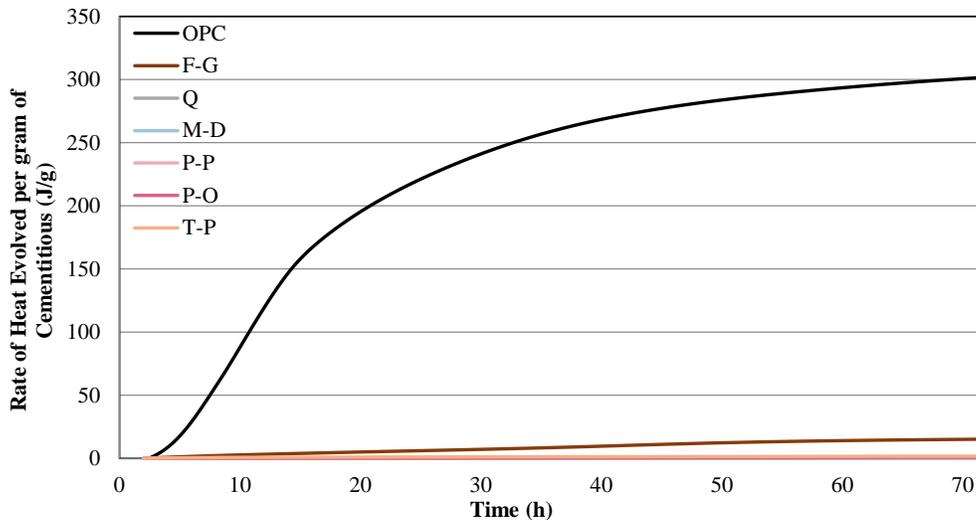
Figure 3.5: Cumulative heat evolved of control and natural pozzolan-water pastes

31

It is apparent from both Figure 3.4 and Figure 3.5 that only OPC, C-H, and F-G pastes released any measurable heat by the end of 3 days. Slag paste was expected to have a higher cumulative heat value than both C-H and F-G due to its latent hydraulic properties, but it did not generate any heat at the end of 3 days. It was determined that in order for the latent hydraulic properties of slag to be apparent, an alkaline solution would be necessary. Therefore, it was concluded that isothermal calorimetry of SCM-water paste mixtures is ineffective at distinguishing between hydraulic and pozzolanic SCMs.

In the next test, a 0.3 M potassium hydroxide solution was used for SCM-alkaline solution pastes, to match the potassium concentration of R^3 mixtures, at a 0.9 solution-to-SCM ratio. The samples were prepared using the same procedure as for cement-SCM pastes, and heat release was measured for 3 days at 40°C. The temperature was increased from 23 to 40°C to help facilitate the reaction of the SCMs. The cumulative heat values at 3 days of the SCM-alkaline solution pastes are presented in Figure 3.6.
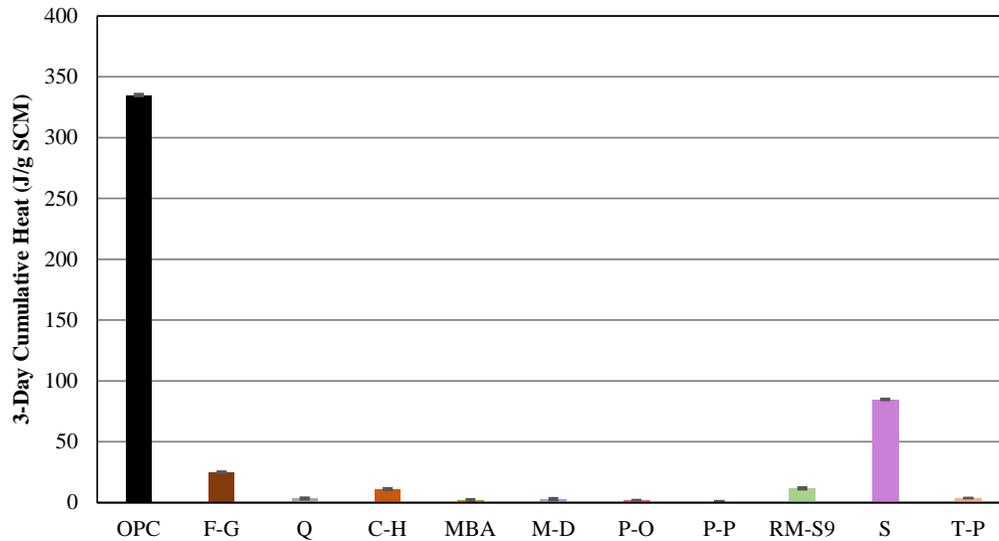
Figure 3.6: 3-day cumulative heat release of SCM-alkaline solution pastes at 40°C

Both the OPC and S pastes in Figure 3.6 have the highest cumulative heat values at 3 days showing that the test clearly identifies hydraulic materials. However, pastes containing F-G and RM-S9, both low-calcium fly ashes (Table 2.2), show a measurable heat release due to some form of geopolymerization. This can lead to false positives when identifying hydraulic materials. Additionally, the Class C fly ash paste, C-H, had a lower cumulative heat value than F-G despite having a higher calcium content. C-H paste began to stiffen prior to being inserted in the calorimeter. The rapid reaction of C-H prevented a complete measurement of the heat release. This can lead to false negatives in the test as well, with quick reacting

materials appearing non-hydraulic. Therefore, it was concluded that calorimetry testing on SCM-alkaline solutions is ineffective at distinguishing between hydraulic and pozzolanic SCMs.

3.1.2. X-ray Diffraction

3.1.2.1. Hydrated Pastes

X-ray diffraction (XRD) analysis was on conducted on select pastes from SCM-alkaline solution calorimetry testing to determine through the presence of cementitious reaction products if hydraulic reactions were indeed occurring under these testing conditions. After 3 days, samples were removed from the calorimeter and paste was extracted from the glass ampoule. Hydrated pastes were then placed under vacuum at 30 mm-Hg for a minimum of 2 weeks to stop hydration [48]. Samples were then ground using a ceramic mortar and pestle until all the material passed through a No. 325 sieve to ensure adequate packing in the XRD sample holder. The powders were packed into sample holders for analysis in a Bruker D8. To minimize preferential orientation of the crystals, a razor blade was used to form perpendicular cuts along the surface of the powder before a glass slide was used to press down the powder without twisting. Samples were then run using a continuous scan at a measurement range of 5° to 75° 2θ, a step size of 0.02° 2θ at a rate of 2° 2θ per second, a tube voltage of 40 kV, and a tube current of 30 mA. The main crystalline phases present in the hydrated pastes are presented in Table 3.2.

Table 3.2: Main Crystalline Phases in Hydrated SCM-Alkaline Solution Pastes

Designation	Main Crystalline Phases
OPC	Portlandite, C_3S, C_2S, C-S-H, Calcite, Ettringite, Gypsum
C-H	Quartz, Mullite, Periclase, Calcite
F-G	Quartz, Mullite, Hematite
S	C-S-H, Merwinite

Only OPC and S alkaline solution pastes contained cementitious reaction products when analyzed in XRD. This agrees with the results from calorimetry testing, where OPC and S pastes had the highest measurable heat values. Although F-G and C-H pastes produced heat in calorimetry testing, they contained no hydration products. Since the sodium aluminosilicate hydrate (N-A-S-H) gel formed during geopolymerization is amorphous and, therefore, not easily measured by XRD, it is possible that the heat released from F-G and C-H is from geopolymerization. This confirms that calorimetry on SCM pastes with alkaline solutions is not appropriate for separating pozzolanic from hydraulic reactions.

3.1.3. Loss on Ignition

3.1.3.1. R^3 Mixtures

ASTM C1897 [51] includes an alternative method to isothermal calorimetry to assess SCM reactivity using the same R^3 mixtures and curing time. The procedure involves measuring the loss on ignition in a furnace between 40°C and 350°C. This mass loss is related to the water chemically bound to hydration products, such as calcium silicate hydrates, calcium aluminate hydrates, and other minor hydrates [46,72]. A higher mass loss indicates a higher amount of chemically bound water, meaning that the SCM has greater reactivity.

Excess R^3 mixtures from isothermal calorimetry testing were cast into sealed plastic vials and cured in an oven at 40°C for 7 days. After the curing period, the samples were removed from the vials and crushed, resulting in a paste. Following crushing, 10 g of the paste was spread evenly on a petri dish and placed back in the 40°C oven to dry for 24 ± 1 hours. The samples were weighed then calcined at 350°C for 2 hours to determine the mass loss between the two temperatures. The results from this bound water testing are shown in Figure 3.7.
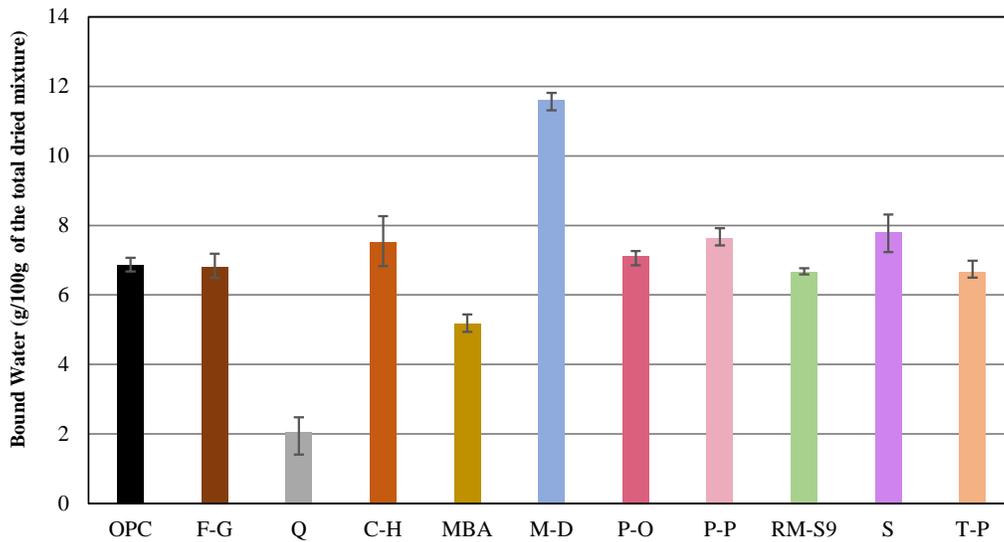
Figure 3.7: 7-day bound water content of R^3 mixtures at 40°C

Similar to results from R^3 isothermal calorimetry testing, the inert quartz mixture, Q, had the lowest bound water value of all the materials, showing that the test is effective at separating inert and reactive materials. The bound water values of OPC, S, and M-D mixtures were lower relative to other materials than their cumulative heat values, while the pumices were higher. This is likely due to some hydration reactions generating more heat, while binding similar amounts of water to hydration

products with a lower heat release. M-D mixture had the highest bound water value at 7 days, agreeing with its high cumulative heat value in Figure 3.3. The formation of calcium aluminate hydrates bind more water than calcium silicate hydrates, leading to higher bound water values [70,71]. Therefore, the bound water method in ASTM C1897 [51] is equally effective as the calorimetry method at screening inert materials, though there are some differences in the methods if one wants to make an interpretation regarding the "degree" of reactivity.

While the R^3 tests in ASTM C1897 [51], both through calorimetry and bound water measurement, successfully screen inert SCMs from reactive ones, neither can distinguish between pozzolanic and hydraulic reactivity. Therefore, an additional step was added to the standardized bound water test to measure the water bound to the remaining CH in the mixture [73]. After weighing the samples at the end of the bound water test, the samples were returned to the oven and heated to 500°C for an additional 2 hours. The mass loss between 350 and 500°C can be used as an estimate for unreacted CH in the mixture. The results from this test, herein denoted as the R^3P test, are presented in Figure 3.8.
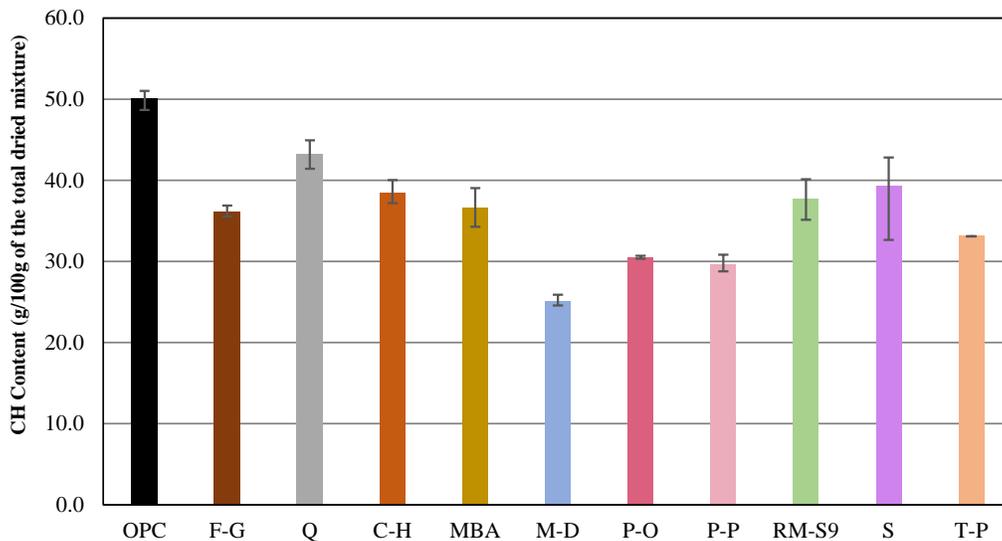
Figure 3.8: R^3P calcium hydroxide content of R^3 mixtures at 7 days

It is apparent in Figure 3.8 that OPC mixture has a higher CH content than the inert material. That is because OPC is producing additional CH as it reacts and does not react with any of the CH present in the mixture, so there is more CH in the final mixture. The remaining mixtures all had CH content lower than Q, showing that they are reacting pozzolanically, consuming CH through the pozzolanic reaction. The mixtures with slag (S) and Class C fly ash (C-H) consume the least CH of the SCMs, as expected since their reactivity is more from hydraulic reactions than pozzolanic ones. It can be concluded that running the R^3P test can help distinguish

between pozzolanic and hydraulic materials, but the analysis of results needs careful attention.

The results from R^3 isothermal calorimetry and R^3P testing can be paired to distinguish between inert and reactive materials, and hydraulic and pozzolanic reactivity. Thresholds, adapted from Suraneni et al. [53] and Kalina et al. [35], were used to separate reactivity types into categories, shown in Figure 3.9. A material is classified as inert if it had a CH content in R^3P testing greater than 40 g/100 g of the total dried mixture and a 7-day cumulative heat in R^3 testing below 100 J/g SCM. A material is classified as pozzolanic, less reactive if it had a CH content between 25 and 45 g/100 g of the total dried mixture and a 7-day cumulative heat between 100 and 350 J/g SCM. A material is classified as pozzolanic, more reactive if it had a CH content below 35 g/100 g of the total dried mixture and a 7-day cumulative heat greater than 350 J/g SCM. A material is classified as hydraulic, less reactive if it had a CH content greater than 45 g/100 g of total dried mixture and a 7-day cumulative heat between 100 and 350 J/g SCM, and hydraulic, more reactive if it had a CH content greater than 35 g/100 g of total dried mixture and a 7-day cumulative heat greater than 350 J/g SCM. While more work is needed to define and refine the thresholds in Figure 3.9, it is apparent that this is a promising method to rapidly categorize SCM reactivity. Furthermore, the same type of plot in Figure 3.9 can be developed for R^3 bound water and R^3P test results, with similar effectiveness.
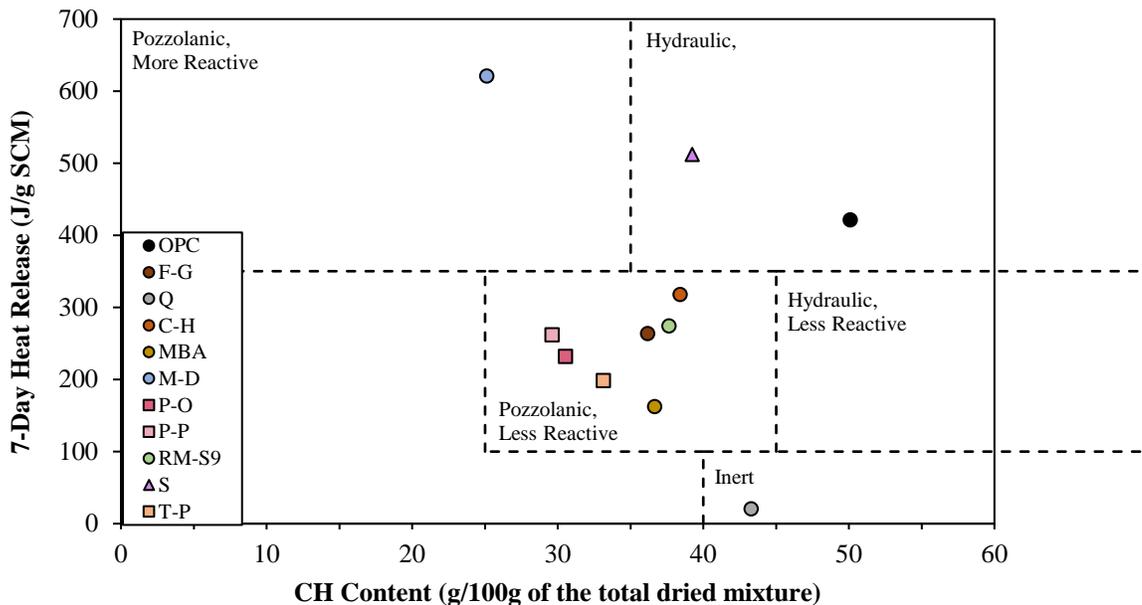
Figure 3.9: Classifications of SCMs based on reactivity using the 7-day heat release of R^3 mixtures at 40°C and CH content of R^3 mixtures using the R^3P method. Thresholds adapted from Suraneni et al. [53] and Kalina et al. [35]

3.1.4. Thermogravimetric Analysis

3.1.4.1. R^3 Mixtures

The R^{3}P test assumes that the water lost between 350°C and 500°C is due to the decomposition of CH. Thermogrametric analysis (TGA) testing was done on the same samples to verify this assumption.

After crushing samples down for R^3 bound water testing, excess sample was placed under vacuum at 30 mm-Hg for a minimum of 2 weeks to stop hydration [48]. Samples were then ground using a ceramic mortar and pestle until all the material passed through a No. 325 prior to running differential scanning calorimetry (DSC) and thermogravimetric analysis (TGA). 10 mg of sample was measured for mass loss between 40 and 550°C using a Mettler Thermogravimetric Analyzer, Model TGA/DSC 1 at a rate of 20°C/min within a N$_2$ gas filled chamber flowing at a rate of 50 mL/s to prevent carbonation. The DSC curve was used to determine the start and end of CH decomposition along the TGA curve, typically between 400 and 500°C [46]. This mass loss was used to determine the CH content of R^3 mixtures and was then compared to the results in R^{3}P testing (referred to as single point measurement) in Figure 3.10.
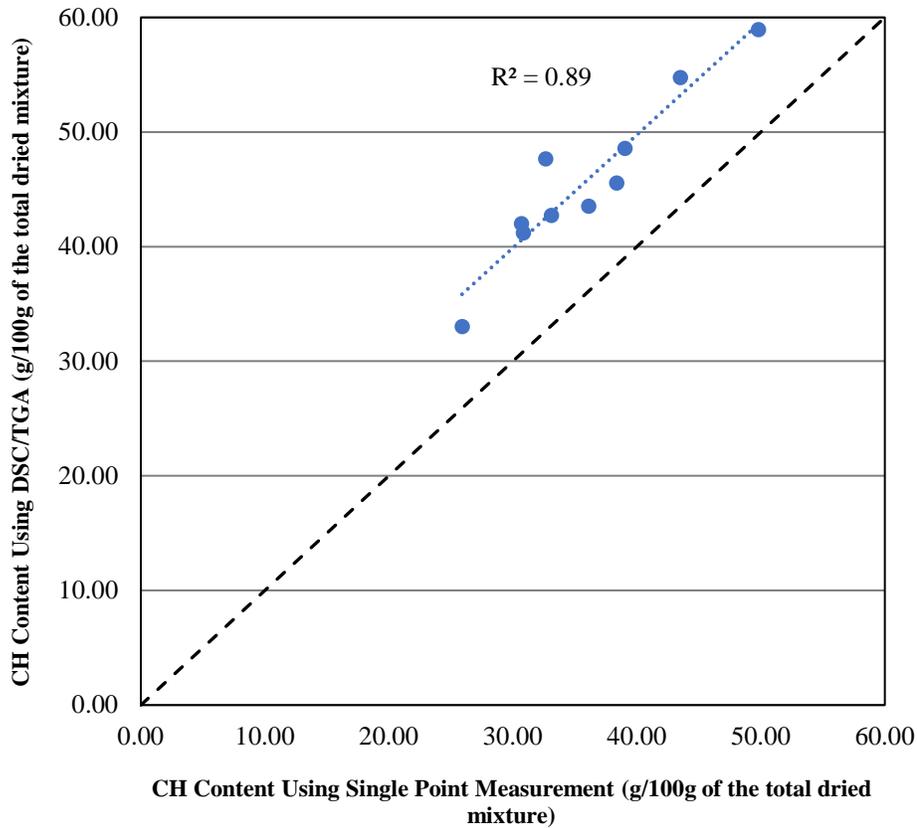
Figure 3.10: CH content of R^3 mixtures at 7 days using DSC/TGA vs R^3P

The results in Figure 3.10 show that the CH contents of R^3 mixtures were higher when measured using the DSC/TGA method than through loss on ignition in a furnace (single point measurement); this is apparent by the data points being skewed higher than the black dotted line of equality in Figure 3.10. This difference in measured CH contents could be due to carbonation during the 24-hour drying period prior to calcining in the R^3P method. To determine if the R^3P method is a suitable replacement for using DSC/TGA, a least squares regression line was fit to the data. A strong correlation was found between the results, suggesting that while the values measured are different, the trends are the same, validating the use of the R^3P method as a quicker, cheaper, and more user-friendly method to DSC/TGA.

3.1.4.2. Cement-SCM Pastes

A traditional way to assess pozzolanic reactivity is by measuring the CH content of cement-SCM pastes over time through DSC/TGA, as was performed in TxDOT Projects 0-6717 [36] and 5-6717 [47]. When pastes have lower CH contents than a control cement-only paste or a paste containing cement and quartz, this suggests that the pozzolanic reaction has occurred, reducing CH in the mixture.

Pastes consisted of a 25% replacement of the cement with SCM by mass and a w/cm of 0.45 and were mixed using the same procedure as was used for isothermal calorimetry for cement-SCM pastes. After mixing, pastes were poured into four separate plastic containers and placed in a curing room at 23°C and 100% relative humidity to be removed at 1, 7, 28, or 90 days. Upon reaching a testing age, one of the containers was removed from the curing room and the outer edges of the sample were cut and discarded to prevent bias in the results due to CH crystals that orient along the surface of the container [74]. The remaining sample was then crushed to pass a No. 100 sieve (150 µm) and placed under vacuum at 30 mm-Hg for a minimum of 2 weeks to stop hydration [48]. Samples were then prepared and measured in the same manner as TGA testing on R^3 mixtures, except the testing temperature range was increased from 40 to 1000°C. CH content of cement-SCM pastes normalized per gram of anhydrous cement are presented in Figure 3.11.
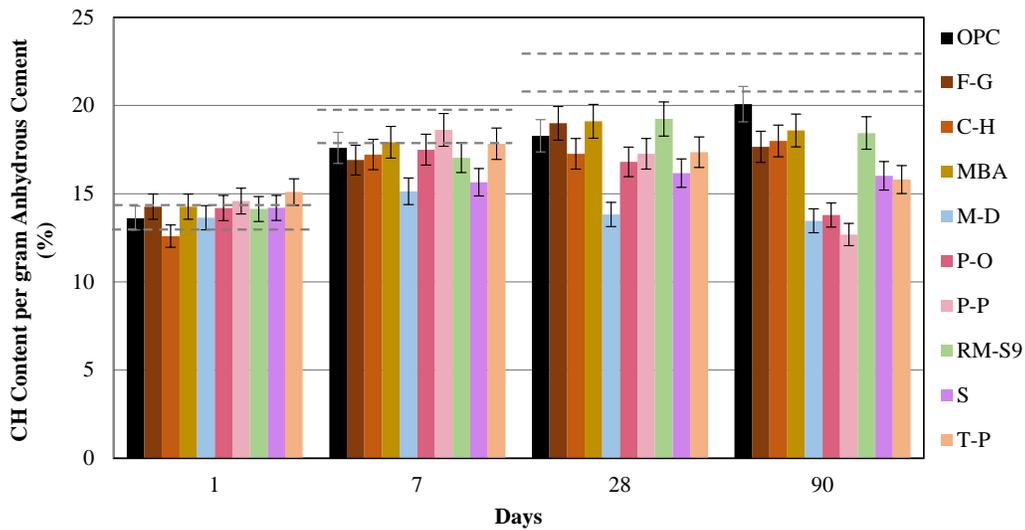
Figure 3.11: CH content of cement-SCM pastes at 25% replacement of the cement by mass with gray dashed lines indicating Q paste calcium hydroxide content with 5% error

Due to limited replicate testing, a representative error of 5% was applied to the results, adapted from Kim and Olek [48]. The CH content of Q paste is represented by the gray dashed lines at each age with an upper and lower line indicating ± 5% of the measured value. At 1 day, none of the SCMs are reacting to form or consume CH, resulting in all pastes having similar CH contents to each other and the OPC and Q pastes. By 7 days, both M-D and S pastes had lower CH contents than OPC and Q pastes, while the remaining pastes did not. Metakaolin is known to rapidly consume CH when used in cement-based systems due to its high pozzolanic reactivity [75]. Although S paste had a comparable CH content to M-D at 7 days, it has been shown that this is not due to pozzolanic reaction, but rather a decrease

39

in the initial formation of CH in slag-cement systems [75]. At later ages, the CH content of S paste does not change and remains below that of OPC and Q pastes. This can make it difficult to determine whether low CH content of a paste is related to decreased initial formation or consumption of CH.

By 90 days, all the cement-SCM pastes had lower CH contents than Q paste, indicating that they are all pozzolanic. Both P-O and P-P pastes had considerable decreases in CH content by 90 days, resulting in similar CH contents to M-D paste. M-D paste had similar CH contents between 28 and 90 days, which is likely due to limited reactants and space for hydrates to precipitate in [76]. Additionally, most of the pastes had lower CH contents than OPC paste at 90 days as well, except for MBA paste, indicating that it is the least pozzolanic material of the SCMs tested.

While measuring CH content of cement-SCM pastes at 90 days gives a very good indication of whether or not an SCM is pozzolanic, there are some problems with universally suggesting this method for pozzolanicity assessment: (1) the test is not standardized and would be difficult to standardize, (2) the test takes 90 days, (3) the test uses expensive DSC/TGA equipment, and (4) the test can be misleading for materials such as slag. Therefore, this test is recommended for researchers interested in understanding SCM behavior, but not for routine screening of materials.

3.1.5. Compressive Strength

3.1.5.1. Cement-SCM Mortars

ASTM C618 [1] uses compressive strength development to assess SCM reactivity through the strength activity index (SAI). This test is problematic, as discussed earlier, because of the variable w/cm used, making it difficult to isolate the role of the SCM on strength from the role of the water content. Therefore, for this study, w/cm was fixed when evaluating the ability of compressive strength to assess SCM reactivity. It should be noted that the impact of SCMs on strength development is related not just to SCM reactivity, but also to their ability to impact cement hydration kinetics among other factors.

Compressive strength testing of mortars was conducted in accordance with ASTM C109 [64]. Mortars consisted of a 25% replacement of the cement with SCM by mass and a fixed w/cm of 0.485. Standard graded sand, as specified by ASTM C109 [64], was used at a ratio of 2.75 to the cementitious material. Mortars were cast into 2 in. cubes to be tested at 1, 3, 7, 28, 56, and 90 days. Figure 3.12 shows the results from mortar compressive strength testing.
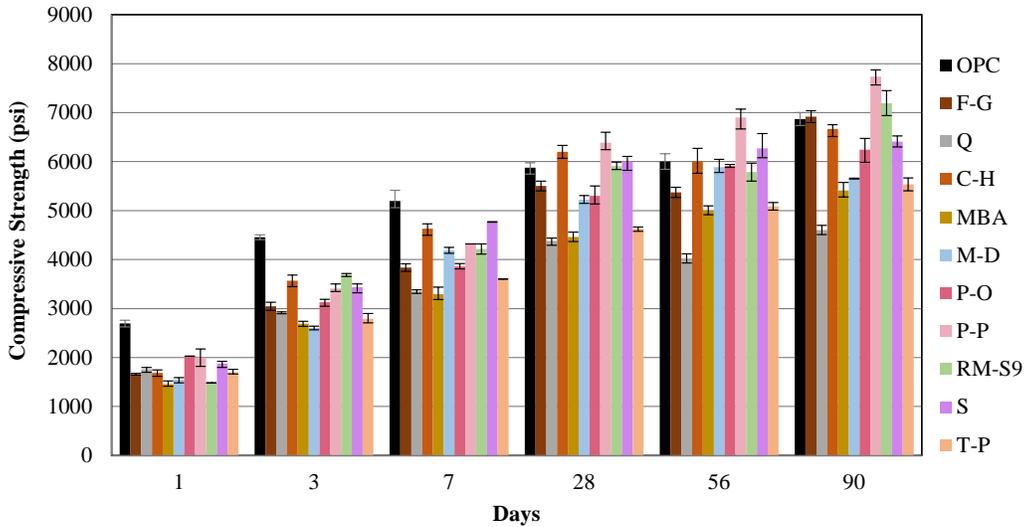
Figure 3.12: Mortar cube compressive strength results of cement-SCM mortars

Results from mortar cube compressive strength testing showed unreliable results with some mortars decreasing in compressive strength at later ages. To verify the results, mortar compressive strength testing was repeated using 2 in. by 4 in. cylinders since they have been found to have better precision [77]. Mortar cylinders were tested at 3, 7, 28, and 90 days and the results are presented in Figure 3.13.
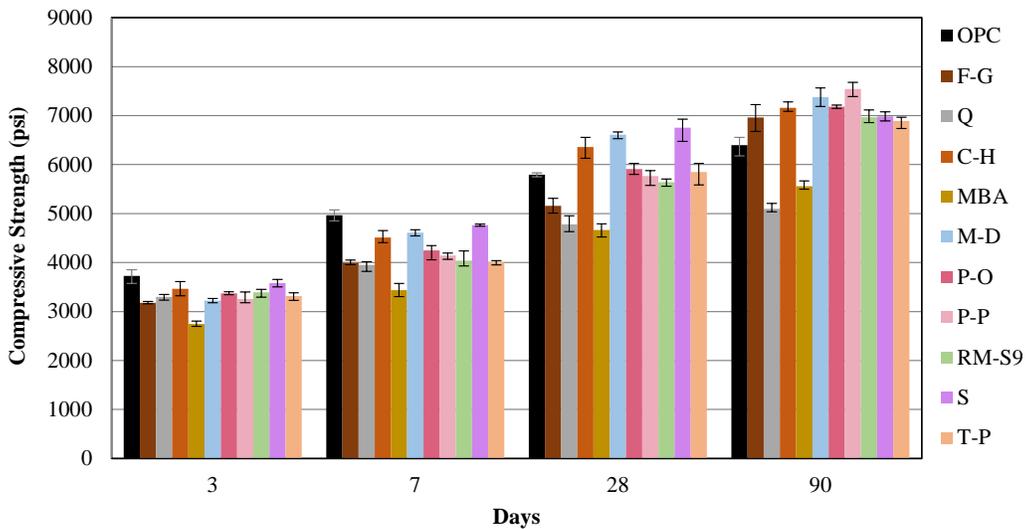
Figure 3.13: Mortar cylinder compressive strength results of cement-SCM mortars

At 3 days, all the SCM mortars had comparable or lower compressive strength to Q mortar (Figure 3.13). This is expected since most SCMs act as fillers at early ages. By 7 days, only C-H, M-D, and S mortars had higher compressive strengths than Q mortar. The early age strength gain for C-H and S mortar can be attributed

to the hydraulic properties of Class C fly ash and slag. Metakaolin is a fast-reacting pozzolan, which allows M-D mortar to increase strength at early ages. Since M-D mortar had similar compressive strength values at 7 days as C-H and S, it can be difficult to determine if early strength gain is related to hydraulic reactivity or fast pozzolanic reactivity. At 28 days, most of the mortars had higher compressive strengths than Q mortar, except for MBA mortar. However, MBA mortar saw a larger strength gain between 7 and 28 days. The lower early age compressive strength of MBA mortar compared to Q mortar can be related to the larger particle size of MBA than Q, as shown in Table 2.11. At 90 days, all the mortars had higher compressive strengths than Q mortar, with most also having higher compressive strength than OPC mortar, except for MBA mortar. This indicates that MBA is the least reactive material tested, as was seen in other reactivity tests. Additionally, by 90 days many other mortars had comparable strengths to M-D mortar showing that slower reacting materials can reach the same degree of reaction as fast-reacting materials at later ages.

It can be concluded from mortar compressive strength tests that the 90 day strength of mortars is a good indicator of SCM reactivity. Using earlier ages to assess SCM reactivity can be misleading since the pozzolanic reaction is slow for many SCMs.

3.1.5.2. Lime-SCM Mortars

Recently, a modified lime reactivity test method was developed, known as the University of New Brunswick Pozzolanic Reactivity Test (UNBPRT) [50]. Reactivity of materials is determined through compressive strength of lime mortars. Similar to R^3 testing, UNBPRT binder contains SCM, CH, and calcium carbonate. CH is added to the binder at a 1:2 ratio to the SCM and calcium carbonate is added at a 1:15 ratio to the binder. The same potassium sulfate solution used in R^3 testing is used for UNBPRT mortar at a water-to-binder mass ratio of 0.65 and standard graded sand is added at a mass ratio of 2.5 to the binder. Although the test was designed using 2 in. cubes, 2 x 4 in. cylinders were used instead for their improved precision [77], as was seen in cement-SCM mortar testing. After casting, cylinders were stored in a sealed container over water at 23°C for 24 hours. After the 24-hour period, the container was moved to an oven at 40°C for 2 days and then demolded. Once demolded, the cylinders were submerged in distilled water in sealed containers at 40°C for an additional 4 days. Some mortars were too soft to be removed from their molds at 3 days and were left in the mold over water at 40°C until they were stiff enough to be removed, or at the end of the 7-day curing process. At 7 days, the containers were removed from the oven and allowed to reach room temperature before being tested in compression. Figure 3.14 shows the results from UNBPRT. Thresholds were proposed by Kasaniya [78], where an inert material

would have a compressive strength below 2 MPa at 7 days, low reactivity would have a strength of 2-5 MPa, moderate reactivity 5-10 MPa, high reactivity 10-20 MPa, and very high reactivity would have a compressive strength greater than 20 MPa.
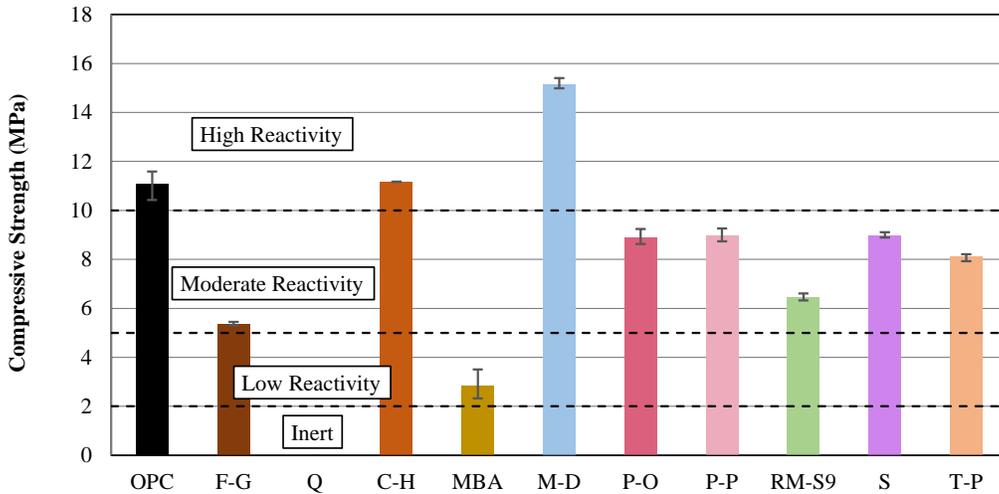
Figure 3.14: Compressive strength results of UNBPRT mortars at 7 days

At 3 days, F-G, Q, and MBA UNBPRT mortars were too soft to be removed from their molds at 3 days and were not demolded until the 6 days, for F-G and MBA mortars, and 7 days for Q mortar. At 7 days, Q UNBPRT mortar was not set enough to be tested in compression and was assigned a compressive strength value of zero. All other UNBPRT mortars were able to be tested in compression, indicating that the materials are reactive. As was seen in other reactivity tests, MBA was determined to have the lowest reactivity in the UNBPRT while M-D had the highest. The UNBPRT does not separate between pozzolanic and hydraulic reactivity, despite being called a pozzolanicity test. However, it uses the same equipment as the SAI test, in addition to a 40°C oven, and is more effective at screening out inert materials. Therefore, the UNBPRT is a promising method of screening inert from reactive materials in a 7-day period with limited need for new or advanced testing equipment.

Chapter 4. Admixture Interaction Testing

The objective of the testing presented in Chapter 4 was to investigate interactions between the SCMs and chemical admixtures since some SCMs are known to cause admixture incompatibilities as discussed in Section 1.2.2.2. The first phase was to assess the interaction effects of the fly ashes with an air-entraining agent (AEA) in accordance with the foam index test, air-entrainment of mortar test, and air void spacing analysis. The second phase was to evaluate interaction effects between the SCMs and high-range water reducers via shear rheology tests.

4.1. Interaction with Air-Entraining Agent

4.1.1. Foam Index Test

Initial testing of the interaction effects between the SCMs and an AEA was performed using the foam index test. The foam index test is a test that is used to rapidly determine the relative levels of AEA needed for materials that affect air-entrainment in concrete. As there are different variations of the test, the procedure used is summarized here:

1) Determine the initial solution concentration for the AEA to use for the test.

    a) A dilution ratio of 1:20 was selected. This results in a 5 vol.% AEA solution. For example, this can be achieved by adding 10 mL of AEA to 200 mL of water.

2) In a small, capped bottle, add 25 g of cementitious material and mix it well via shaking. (Note, when an SCM is used, add 16.75 g of cement and 8.25 g of SCM to the bottle).

3) In a different small, capped bottle (e.g., a 250 ml wide-mouth Nalgene®-type container with a tight-fitting cap) add 50 g water.

4) Add the cementitious material from Step 2 to the water in Step 3. Using the cap, close the bottle and shake the bottle for 10 seconds. This is the initial agitation phase.

5) Stop shaking the bottle. Open the lid and add 20 µL of 5% AEA solution.

6) Close the lid of the bottle and shake it for 20 seconds.

7) Open the lid and allow the sample to sit for 20 seconds. If a metastable foam is noticed after 20 seconds (see Figure 4.1), then the test is done. If not, proceed to Step 8.

8) Open the lid of the bottle and add an additional 20 µL of 5% AEA solution to the sample.

9) Repeat steps 7 and 8 until a stable foam is observed.

10) Record the total number of drops of air entraining admixture solution added to achieve a stable foam (n) and the solution concentration of the air entraining admixture solution used (C), and the drop volume (d).

Figure 4.1: Example of a stable foam

SCMs were evaluated using Sika® AIR. The manufacturer's recommended dosage is 16-195 mL per 100 kg of cementitious material (cm). Table 4.1 presents the results from the foam index test. The total volume of AEA per 100 kg of sample was calculated using Equation 4.1:

$$AEA = n \; x \; d \; x \; C \qquad (4.1)$$

where n = total number of drops to achieve a stable foam, d=20 µL, and $C = 0.05$.

Table 4.1: AEA Demand as Determined via the Foam Index Test

Designation	Total AEA (mL/100 kg cm)
OPC	0
PLC	4
Q	4
F-G	12
F-Z	32
BA-B	12
BA-H	12
BA-P	44
BA-S	8
BA-V	8
BC-B	8
BC-M	8
RM-S3	80
RM-S9	12
I-S	32

Note: One 20 µL drop of AEA diluted to 5% is equivalent to 4 mL of AEA per 100 kg of cm

Most of the samples had AEA demand of 12 mL or less, but there is a substantial difference between the samples that had the lowest and highest AEA demand. The RM-S3 paste had an AEA demand significantly larger than the other samples. This may be due to the sulfate treatment process used for this fly ash. Air void analysis was then conducted on concrete samples containing RM-S3 and BA-P due to their high foam index values.

4.1.2. Air Void Spacing Analysis

Air void analysis was completed on concrete specimens containing RM-S3 and BA-P due to their high foam index values, as well as F-G as a control. Concrete samples were dosed with 106 mL/100 kg cm of Sika® AIR. This dosage was selected because it is the median value of the product recommended dosage range. Concrete mixture design consisted of a 25% cement replacement with the SCM by mass and a 0.485 w/cm. The cementitious content was designed to contain 564 lb/yd³. Colorado River gravel was used as the coarse aggregate at a fixed content of 1800 lb/yd³. An assumed value of 2 vol.% was used for entrapped air. The Colorado River sand was used as the fine aggregate, and its content was adjusted to complete the remaining cubic yard volume in the concrete mixture. Table 4.2 shows an example of a concrete mixture design for air void analysis.

Table 4.2: F-G Concrete Mixture Design for Air Void Analysis

Component	Amount (lb/yd^3)
OPC	423
F-G	141
Water	296
Coarse Aggregate	1804
Fine Aggregate	1258
Air	2 vol.%
AEA	270 mL

After mixing, concrete was cast into a 4 x 8 in. cylinder and cured for 56 days prior to being sent to TxDOT for testing. The entrained air content determined through air void spacing analysis is shown in Table 4.3. Desirable spacing factors are less than 0.02 mm (0.008 in.), since values less than 0.02 mm indicate that the concrete should be adequately protected against freeze thaw damage.

Table 4.3: Results from Air Void Spacing Analysis

Designation	Entrained Air Content (%)	Spacing Factor (in.)
F-G	7.73%	0.00334
BA-P	6.04%	0.00437
RM-S3	5.32%	0.00709

The results shown in Table 4.3 reflect the foam index results in Table 4.1. Since BA-P and RM-S3 required more AEA to achieve a stable foam in the foam index test, less air was entrained in concrete containing these fly ashes when compared to F-G concrete at the same AEA dosage. As a result, it should be noted that more AEA is required to achieve a target entrained air content when using these fly ashes.

4.1.3. Air-Entrainment of Mortar

Admixture interactions were further explored with the air-entrainment of mortar test in accordance with ASTM C311 [63]. This was conducted using a commercial neutralized Vinsol resin solution prepared in accordance with ASTM C226 [79]. Mixtures consisted of 300 g of cement, 75 g of SCM, and 1125 g of 20-30 mesh size standard sand. First, the water content was adjusted for each mixture to give a flow of 80 to 95, and then the amount of neutralized Vinsol resin solution was varied to produce an air content of 18 ± 3%. In this test, two test mixtures were performed with target air contents of 15-18% and 18-21%. Then, the amount of neutralized Vinsol resin to produce 18% air content was determined by linear interpolation between the two test mixtures. The air content of the test mixtures was

calculated using Equations 4.2 and 4.3, where P is the percent of mixing water plus Vinsol resin solution based on mass of cement, D is the density of the SCM in mg/m^3 and W_a is the mass per unit volume (g/mL) of mortar determined by ASTM C185 [3].

$$Air\ content, volume\ \% = 100(1 - \frac{W_a}{W_c}) \quad (4.2)$$

$$W_c = \frac{300+1125+75+(300 \times P \times 0.01)}{\frac{300}{3.15}+\frac{1125}{2.65}+\frac{75}{D}+\frac{300 \times P \times 0.01}{1}} \quad (4.3)$$

The air-entrainment of mortar results are presented in Table 4.4. This test procedure estimates a linear trend for AEA needed for an air content of 18 ± 3%. When three points were determined within the range, it is questionable whether a linear approximation is valid, especially at air contents near 15%. Additionally, the water content is iterated to produce a given flow from 80 to 95, which can result in two test mixtures with different P values. The mass per volume of the mortar has a large effect on the air content calculation, causing concern as to whether one can interpolate between two mixtures with different P values accurately due to the difference in water content. In initial tests, Sika® AIR was used because it is more available; however, concerns about the test results occurred due to the high dosages of AEA required and additional water needed. Due to the availability of the materials and concerns about the accuracy of the test, only four samples were tested. When comparing the results from these tests with the foam index testing results, there was not good agreement. For example, in the foam index test, the F-Z paste required four times the amount of AEA to reach a stable foam than the BA-S paste. However, in the ASTM C311 air entrainment test, the F-Z mortar required 1.55 mL less of AEA than the BA-S mortar to achieve an air content of 18%. This discrepancy was another reason for discontinuing the test.

Table 4.4: Air-Entrainment of Mortar Results

Designation	AEA to Achieve 18% Air Content (mL)
OPC	1.48
F-Z	3.43
BA-S	4.98
RM-S9	4.89

4.2. Interaction with High-Range Water Reducers

Paste rheology was conducted on select materials that could have potential issues with high-range water reducers. Testing was conducted using an Anton Paar MCR

301 rheometer. For all paste rheology testing, mixtures consisted of 500 g of cementitious materials with a 25% replacement of cement by mass for each SCM and a water-to-cementitious materials (w/cm) ratio of 0.45. Mixing procedures followed ASTM C1738 [80] using a high-shear mixer. Water chilled to 5°C was used for mixing in order to maintain a paste temperature of 23 ± 3°C due to the heat generated from the high-shear mixer.

4.2.1. Saturation Dosage

Saturation dosages for a high-range water reducer (HRWR) were determined for each paste using Sika® ViscoCrete® 2110. The HRWR was added to the mixing water prior to the addition of the dry material. Paste mixtures were created starting at admixture dosages of 0.1 or 0.2% by weight of the cementitious materials (% wt. cm). After mixing, 19 mL of paste was transferred to the rheometer cup measuring system and subjected to a shear rate of 50 s^{-1} using a helical bob geometry at a controlled temperature of 23°C for 90 s. Once the 90 s were complete, a 3-minute rest period followed. After the rest period, the shear rate was increased from 1 s^{-1} to 50 s^{-1} (i.e., the up curve) and then decreased from 50 s^{-1} to rest (i.e., the down curve). Each shear rate was held for 45 s prior to changing to allow for the equilibrium stress to be achieved. The downward paste flow curves were then analyzed using the Bingham model (using the equilibrium stress values at each shear rate) to determine the paste's viscosity and yield stress values. The admixture dosage was increased in incremental dosages of 0.1%, and the rheology test was repeated (note: a new paste was prepared for each admixture dosage). The HRWR saturation dosage was determined as the minimum dosage to reach the stable minimum yield stress of the paste. The saturation dosage provides the maximum amount of HRWR to use in a mixture before it becomes unstable; however, dosages less than the saturation dosage are used in actual concrete mixtures to limit the risk of bleeding and segregation of the concrete mixture. Table 4.5 shows the saturation dosages for the ViscoCrete® 2110 for most of the SCMs selected for this testing.

Table 4.5: ViscoCrete® 2110 Saturation Dosages for Cement Pastes

Designation	Admixture Dosage (% wt. cm)
OPC	0.4
PLC	0.3
F-G	0.2
F-Z	0.3
BA-B	0.2
BA-V	0.2
RM-S3	0.2
RM-S9	0.4

The results shown in Table 4.5 indicate that the materials selected had no impact on the ViscoCrete® 2110 saturation dosage amounts. Most of the fly ashes had lower saturation dosages than the OPC, except for RM-S9, which required the same amount of HRWR.

4.2.2. Small Amplitude Oscillatory Shear Testing

Small amplitude oscillatory shear (SAOS) testing examines potential issues in the stiffening and setting behavior of the mixtures in the presence of an HRWR. An HRWR dosage of 0.1% was chosen for the pastes to ensure the dosage is not beyond the saturation point of the pastes. Three materials were selected for SAOS testing: F-G as a control, BA-V because of the fluidity of BA-V paste and its high calcium content, and RM-S3 for its high sulfate content. To ensure that the testing does not significantly disrupt the microstructure of the paste, the test is conducted in the linear viscoelastic region (LVER) so particles can recover elastically [81]. Testing was conducted once for each mixture at 16, 23, and 30°C to determine the impact of temperature on cement-HRWR interactions. Since BA-V paste was the most fluid of the three pastes, and therefore had the smallest LVER, a strain sweep was conducted to determine the critical strain where particles are no longer able to recover elastically. Once the critical strain was determined, a frequency sweep was performed to find the critical frequency. Table 4.6 shows the strain and frequency values chosen for SAOS testing at each temperature.

Table 4.6: Strain and Frequency Values for SAOS Testing

Temperature (°C)	Strain (%)	Frequency (Hz)
16	0.5	1
23	5×10^{-6}	1
30	0.0001	1

Once the strain and frequency values within the LVER were determined, SAOS tests were performed on the pastes for a test duration of 100 minutes and the storage modulus was measured. Figure 4.2 and Figure 4.3 show the evolution of the storage modulus over the duration of the testing period at each temperature for the tested pastes.
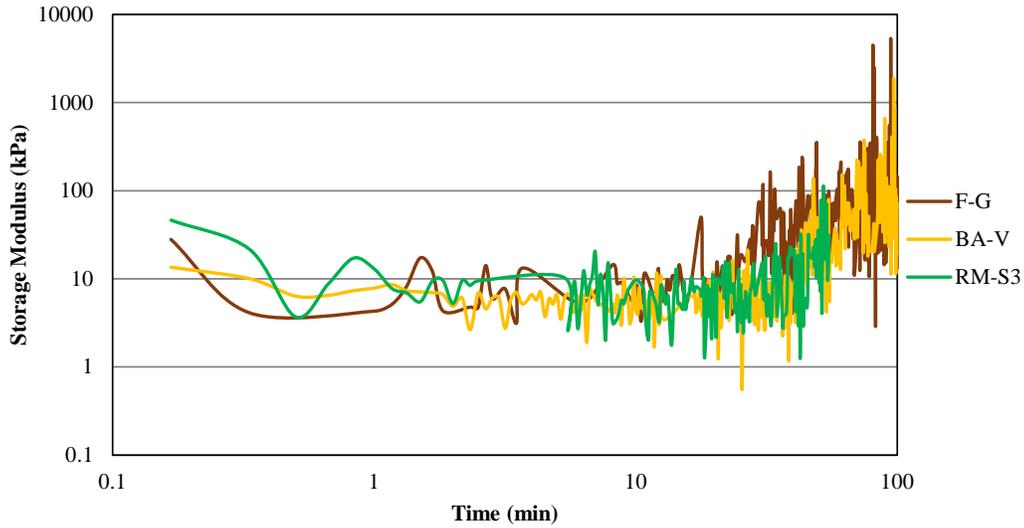
Figure 4.2: Storage modulus results for fly ash pastes at 23°C for 100 minutes
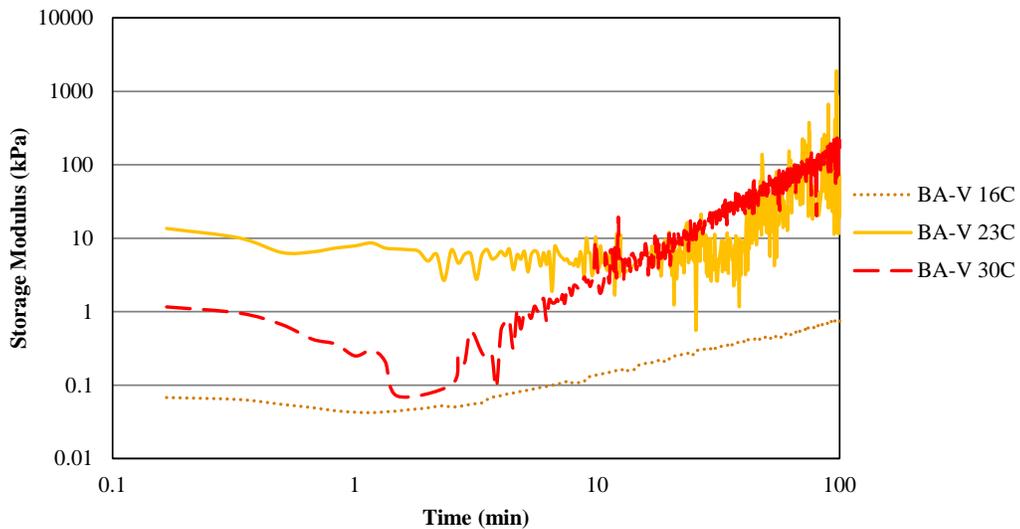
Figure 4.3: Storage modulus results for BA-V pastes at 16, 23, and 30°C for 100 minutes

SAOS testing at 23°C (Figure 4.2) showed that the fly ash pastes all behaved similarly, with the storage modulus increasing over time. The increase in storage modulus can be attributed to both soft colloidal interactions (i.e. electrostatic interactions) and formation early hydration products (e.g. calcium silicate hydrate).

51

Figure 4.3 shows the effects of temperature on storage modulus of BA-V cement paste. At lower temperatures, there is a slower gain in storage modulus in BA-V paste at 16°C than at higher temperatures. Thus, this indicates that the setting time of the mixture has increased. The structural rigidity of the system is higher than at lower temperatures, which is reflected by the rapid increase in storage modulus of BA-V paste at 30°C. While only the BA-V paste is shown here, all of the fly ashes, even the control, behaved similarly in SAOS testing. This indicates that no incompatibilities occurred.

Chapter 5. Concrete Property and Long-Term Durability Testing

Cement paste, mortar, and concrete testing was conducted on materials to examine property development and long-term durability. This testing is important for qualifying materials for use in concrete mixtures. Tests included isothermal calorimetry, rheology, and standardized ASTM tests as outlined in Table 5.1.

Table 5.1: Paste, Mortar, and Concrete Tests

Sample Type	Test Method	Property Measured
Pastes	Isothermal Calorimetry	Heat of Hydration
		Sulfate Optimization
	Rheology	Water Demand/Workability
Mortars	Drying Shrinkage (ASTM C311)	Drying Shrinkage
	ASTM C1567	ASR Control
	ASTM C1012	Sulfate Attack Control
Concrete	ASTM C143	Slump
	ASTM C231	Air Content
	ASTM C403	Setting Time
	ASTM C39	Compressive Strength
	ASTM C1202	Chloride Penetrability
	ASTM C1876	Bulk Electrical Resistivity
	ASTM C1293	ASR Control

5.1. Paste Testing

5.1.1. Isothermal Calorimetry

5.1.1.1. Heat of Hydration

Isothermal calorimetry was performed on cement-SCM pastes to determine the ability of the SCMs to reduce heat of hydration for use in thermal control plans. Mixture design and mixing procedure of calorimetry pastes are outlined in Section 3.1.1.1. Figure 5.1 and Figure 5.2 show the rate of heat evolution of cement pastes normalized per mass of paste, and Table 5.2 shows the cumulative heat after 3 days.
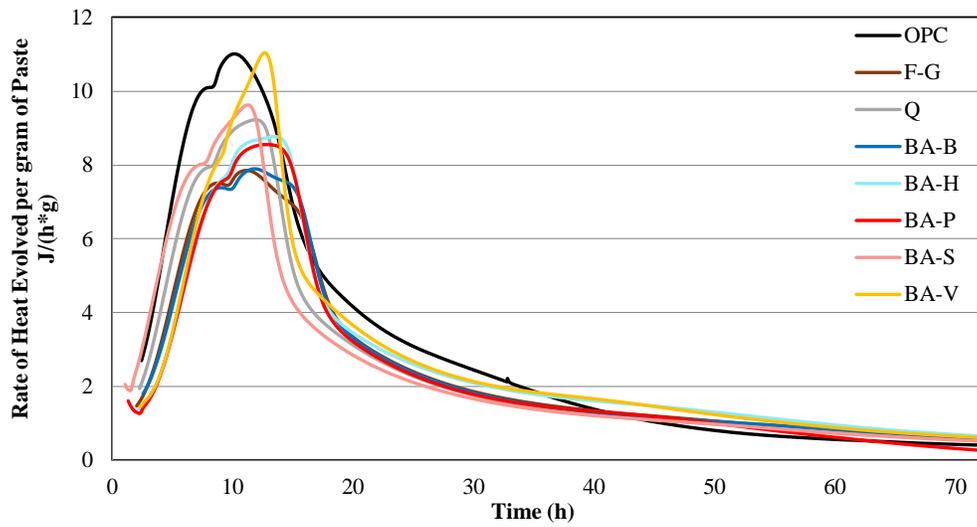
Figure 5.1: Rate of heat evolution of cement pastes containing control materials and blended fly ashes
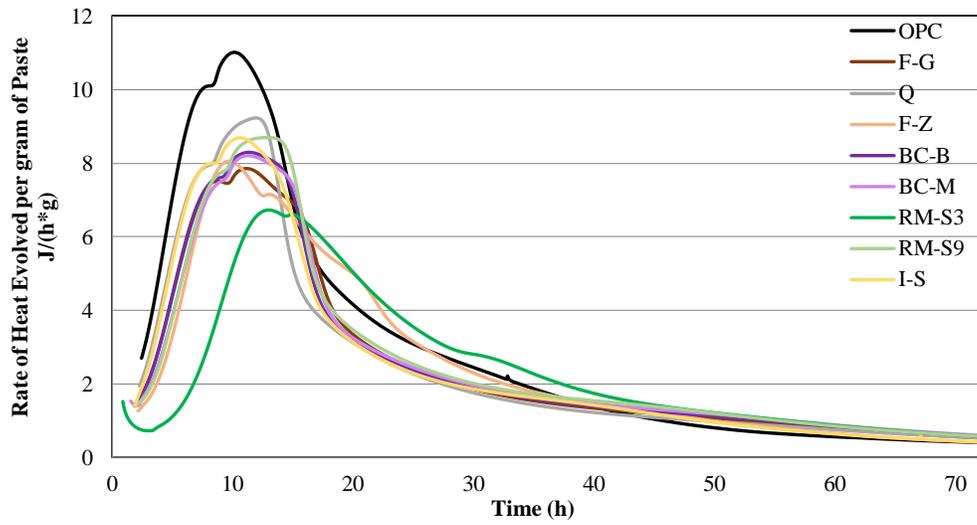
Figure 5.2: Rate of heat evolution of cement pastes containing control materials and fly ashes

54

Table 5.2: 3-Day Cumulative Heat Values of Cement Pastes

Designation	3-Day Cumulative Heat per gram of Paste (J/g)
OPC	208
Q	173
F-G	173
F-Z	181
BA-B	172
BA-H	184
BA-P	168
BA-S	173
BA-V	190
BC-B	176
BC-M	178
RM-S3	172
RM-S9	183
I-S	175

From Table 5.2, it is clear that all of the materials, including Q, reduce the cumulative heat released by the pastes in the first three days, suggesting that they are all appropriate for use in concrete thermal control plans.

In Figure 5.1, most of the materials reduced the maximum rate of heat released from the paste, except for BA-V. BA-V has the highest calcium content of the tested materials (Table 2.2) and has abundant tricalcium aluminate and free lime (Table 2.8), which are reactive crystalline phases that can accelerate and alter cement hydration reactions [69]. This results in a heat evolution curve for BA-V paste that has an amplified second peak that starts to overlap the main hydration peak. The hydration curve of BA-S paste also differs from the control Class F fly ash paste, F-G. The main hydration peak for BA-S paste occurs earlier than the other cement-SCM pastes. This is likely due to its smaller particle size in comparison to the other fly ashes as shown in Table 2.11. Additionally, BA-S paste has an amplified second peak, which can be attributed to the reactive alumina in the clinoptilolite phase (Table 2.8) [82]. The remaining pastes in Figure 5.1 had similar hydration curves to F-G paste.

In Figure 5.2, most of the cement-SCM pastes had similar hydration curves to F-G paste, except for RM-S3. RM-S3 is a sulfate-treated fly ash that comes from a coal-fired power plant that injects calcium hydroxide into the flux to react with SO_2 to reduce sulfur emissions. This reaction forms calcium sulfite ($CaSO_3$), which has a low solubility rate [83]. The presence of calcium sulfite in RM-S3 contributed to the delayed hydration peak and prolonged induction period of RM-S3 paste.

Amplification of the second peak and prolonged induction periods of cement paste are related to sulfate imbalances in the system. Sulfate imbalances can cause issues with setting time, sulfate resistance, and chemical admixture compatibility. This can be remedied through the addition of gypsum or limestone to increase or decrease the sulfates in the system, respectively [83–85].

5.1.1.2. Sulfate Optimization

To identify problems with sulfate optimization when SCMs are used with high limestone cements, isothermal calorimetry tests were repeated with a high limestone content cement. In this case, since the interest was on examining the impact of the SCMs on cement hydration, the rate of heat released was normalized against the mass of cement rather than the mass of paste. The rates of heat evolution are shown in Figure 5.3 and Figure 5.4.
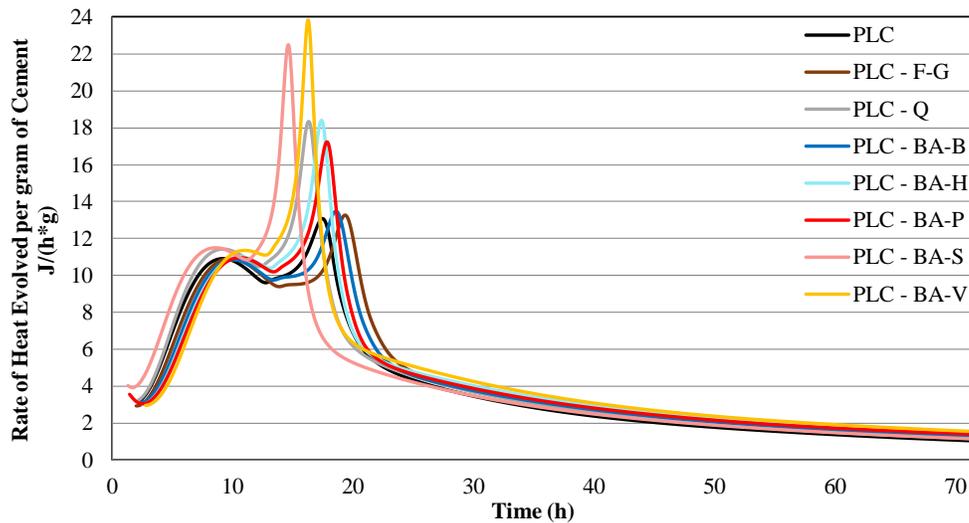
Figure 5.3: Rate of heat evolution of limestone cement pastes containing control materials and blended fly ashes
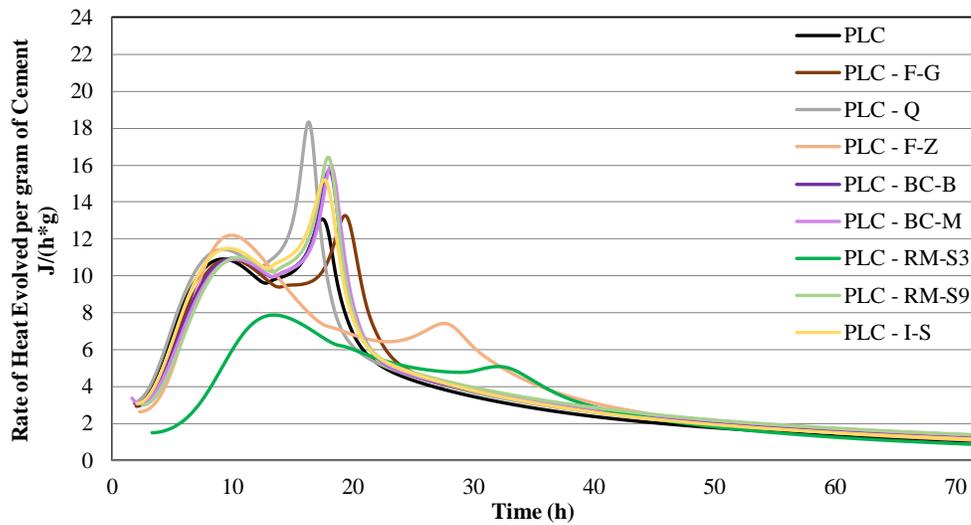
Figure 5.4: Rate of heat evolution of limestone cement pastes containing control materials and fly ashes

As mentioned previously, the addition of limestone to a cement system can cause a sulfate imbalance. This is evident by the amplified second peak in most mixtures in Figure 5.3 and Figure 5.4. To improve the sulfate balance of the system, gypsum was added to the control PLC paste and the paste with the highest second peak, BA-V. Lab grade gypsum was added as a percentage of the cement weight at 1% increments from 1-3%. Heat evolution curves are shown in Figure 5.5 and Figure 5.6 for gypsum additions for PLC and BA-V pastes, respectively.
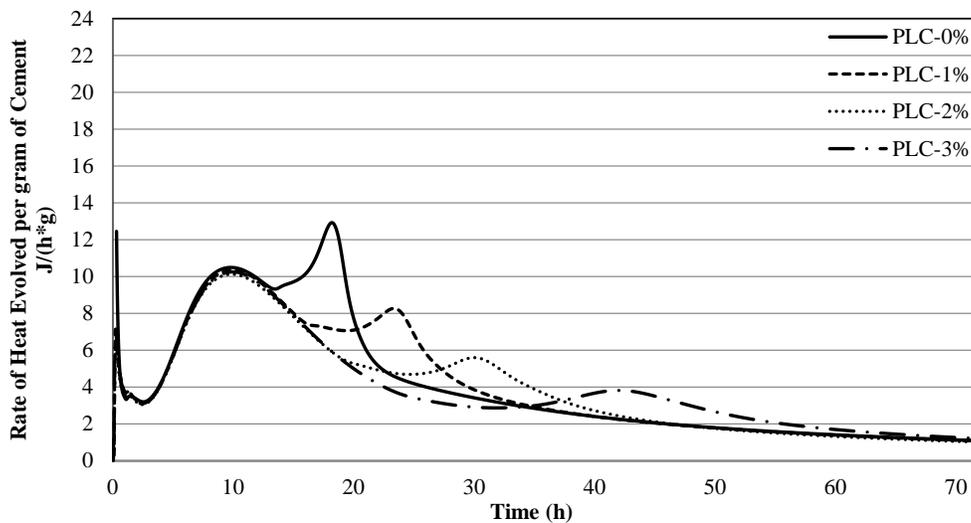
Figure 5.5: Rate of heat evolution of PLC paste with gypsum additions

57
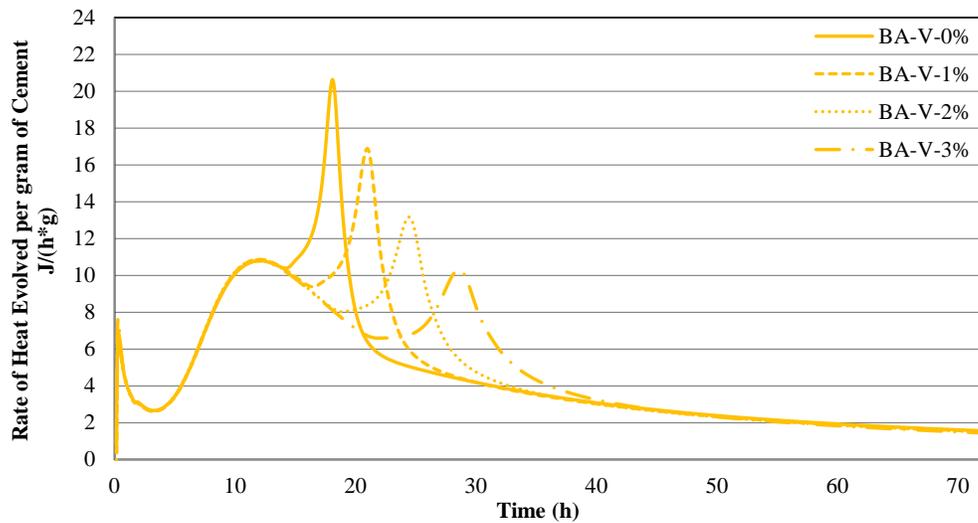
Figure 5.6: Rate of heat evolution of BA-V paste with gypsum additions

Results in Figure 5.5 and Figure 5.6 show that gypsum additions were effective at reducing the height of the secondary peak. However, this resulted in a delay in the secondary peak. It may not be possible to reduce the secondary peak without delaying its peak height. Eliminating the secondary peak with higher gypsum additions may be able to improve sulfate balance of the system [84].

5.1.2. Rheology

To characterize the water demand of the mixtures, rheological properties were measured. Paste mixture design and mixing procedure are outlined in Section 4.2. All mixtures containing SCMs were completed with a 25% replacement of the cement by mass. After mixing, paste samples were inserted into the rheometer and testing followed the procedure outlined in Section 4.2.1. Once testing was completed, the Bingham model was applied to the paste flow curves to determine the yield stress and viscosity of the pastes [86]. The paste flow curves are presented in Figure 5.7 and Figure 5.8. The yield stress was determined as the y-intercept of the trend line and the viscosity the slope. Table 5.3 shows the yield stress and viscosity for each paste.
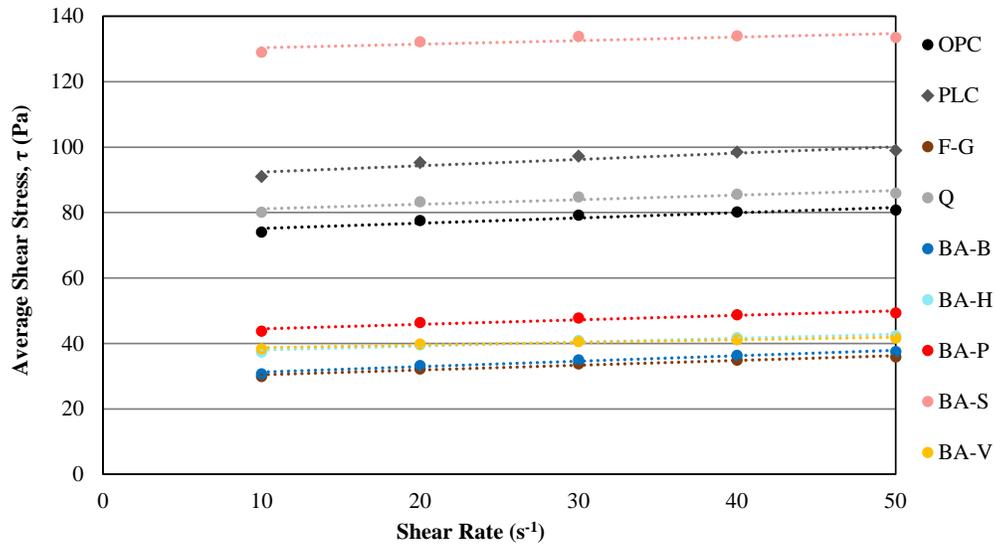
Figure 5.7: Flow curves of cement pastes containing control materials and blended fly ashes
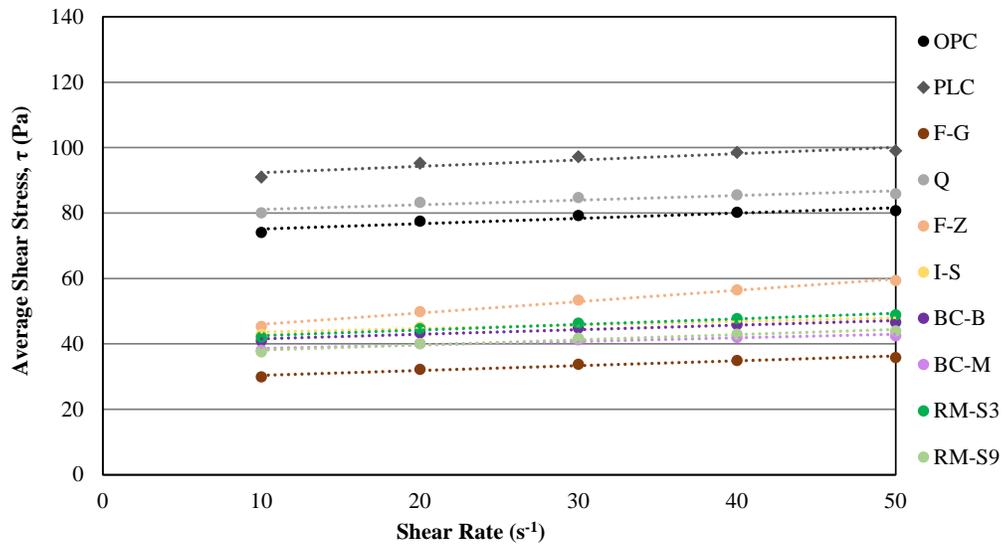
Figure 5.8: Flow curves of cement pastes containing control materials and fly ashes

59

Table 5.3: Bingham Parameters

Designation	Yield Stress (Pa)	Viscosity (Pa·s)
OPC	73.55	0.16
PLC	90.45	0.19
Q	79.76	0.14
F-G	28.95	0.15
F-Z	45.52	0.35
BA-B	29.58	0.17
BA-H	36.77	0.12
BA-P	43.14	0.14
BA-S	129.28	0.11
BA-V	37.98	0.08
BC-B	40.16	0.14
BC-M	37.54	0.11
RM-S3	40.88	0.17
RM-S9	36.56	0.16
I-S	42.52	0.11

All the SCM-containing pastes had similar or lower viscosities than the control fly ash, F-G, except for F-Z paste. This may cause issues with flowability and pumpability of concrete. Additionally, BA-S had the highest yield stress of all pastes, despite being a blend of Class C and F fly ash. This could be due to the smaller particle size of BA-S, as shown in Table 2.11. Additionally, BA-S contains angular particles, as shown in SEM images in Appendix B, which can increase the yield stress of the mixture due to interlocking of angular particles [68]. If a similar flow to a traditional Class F fly ash is desired when using BA-S, an HRWR can be used.

5.2. Mortar Testing

5.2.1. Drying Shrinkage

Drying shrinkage testing was performed in accordance with ASTM C311 [63] on mortar bars. The control cement mortar consisted of 500 g of cement at a constant w/cm of 0.485 and 1375 g of graded standard sand. Mortars containing SCMs had 125 g of the sand replaced with the SCM and w/cm was held constant at 0.485. Although the test proportions water based on flow, a constant w/cm was utilized to limit the number of variables in testing. Mortar bars were cured for 7-days in a lime water bath in accordance with ASTM C157 [87], and then the length and mass of the mortar bars were measured. After measuring, the bars were stored in air at 23°C for an additional 28 days. The relative increase in drying shrinkage and weight loss

compared to the control mixture were then calculated and are presented in Table 5.4.

Table 5.4: Drying Shrinkage and Weight Loss on Drying Relative to OPC Control

Designation	Relative Drying Shrinkage (%)	Relative Weight Loss (%)
Q	0.02	5.00
F-G	0.02	4.26
F-Z	0.00	5.29
BA-B	0.01	5.21
BA-H	0.03	3.91
BA-P	0.03	4.59
BA-S	0.03	4.90
BA-V	0.03	4.22
BC-B	0.01	3.34
BC-M	0.02	3.47
RM-S3	0.00	4.85
RM-S9	0.02	4.21
I-S	0.02	4.27

Since the w/cm was held constant at 0.485, replacing the sand with SCM resulted in a higher overall water content in the mortar compared to the control cement. This resulted in increased shrinkage and weight loss in most of the mortars. F-Z and RM-S3. F-Z and RM-S3 mortars did not have an increase in drying shrinkage compared to the control cement mortar. This is likely due to the high sulfate content of these fly ashes (Table 2.2), which leads to the formation of more ettringite, resulting in a greater volume of restraining, non-shrinking solid phases [88]. This helps reduce the amount of shrinkage occurring in these mortars. Although the shrinkage did not increase, the weight loss for both F-Z and RM-S3 mortars was comparable to the other fly ash mortars due to the increased water content compared to the control cement mortar. It can be concluded that the impact of any of these SCMs on drying shrinkage in concrete mixtures would be negligible.

5.2.2. Alkali-Silica Reaction

ASTM C1567 [11] was followed to evaluate the ability of the materials to control deleterious expansion due to alkali-silica reaction (ASR). Mixtures consisted of a graded fine aggregate, which was earlier found to be reactive through ASTM C1260 [12], at a ratio of 2.25 parts to the cementitious material by weight with a w/cm of 0.47. A cement replacement of 25% by mass was used for all SCMs. Expansion of the mortar bars was measured at 3, 7, 10, and 14 days. ASTM C1567 sets an

expansion threshold of 0.1% at 14 days. Mortar bars that expand beyond the threshold are deemed ineffective at mitigating ASR. Table 5.5 shows the results from ASTM C1567 testing. Red text indicates that the mortar bars have surpassed an expansion limit of 0.1%.

Table 5.5: ASR Mortar Bar Expansion Percentage at 14 Days

Designation	Percent Expansion		
OPC	0.41	±	0.01
Q	0.14	±	0.01
F-G	0.02	±	0.00
F-Z	0.10	±	0.00
BA-B	0.03	±	0.00
BA-H	0.08	±	0.01
BA-P	0.01	±	0.01
BA-S	0.04	±	0.01
BA-V	0.09	±	0.01
BC-B	0.03	±	0.00
BC-M	0.05	±	0.01
RM-S3	0.03	±	0.00
RM-S9	0.02	±	0.00
I-S	0.03	±	0.01

All the fly ashes were able to mitigate expansion due ASR in mortar. F-Z mortar expansion at 14 days was at the expansion limit, but it did not exceed the threshold.

5.2.3. Sulfate Resistance

Mortars were tested using ASTM C1012 [23] to assess the ability of the materials to reduce expansion due to sulfate attack. Mixtures consisted of standard graded sand at a ratio of 2.75 to the cementitious materials by mass and a w/cm of 0.485. A 25% replacement level by mass was used for all SCMs. Mortar bar expansion was evaluated for 18 months in accordance with ASTM C1012. Results from ASTM C1012 testing are presented in Table 5.6. Red text indicates that the mortar bars have surpassed an expansion limit of 0.1%. Yellow text for the F-G control fly ash means that the result is at the expansion limit of 0.1%.

Table 5.6: Sulfate Mortar Bar Expansion Percentages

ID	Weeks							Months				
	1	2	3	4	8	13	15	4	6	9	12	18
Q	0.01	0.01	0.01	0.02	0.23	1.36	--	--	--	--	--	--
F-G	0.01	0.01	0.01	0.01	0.02	0.02	0.03	0.03	0.04	0.06	0.10	0.16
F-Z	0.01	0.01	0.02	0.02	0.03	0.03	0.03	0.03	0.04	0.06	0.09	0.15
BA-B	0.01	0.01	0.02	0.01	0.02	0.03	0.05	0.08	0.22	0.51	0.74	1.50
BA-H	0.01	0.01	0.02	0.02	0.07	0.29	0.54	0.89	--	--	--	--
BA-S	0.01	0.01	0.01	0.01	0.02	0.02	0.02	0.02	0.02	0.04	0.03	0.03
BA-P	0.01	0.02	0.02	0.02	0.04	0.14	0.25	0.49	--	--	--	--
BA-V	0.01	0.02	0.02	0.02	0.06	0.24	0.46	--	--	--	--	--
BC-B	-0.01	0.00	0.01	0.01	0.02	0.02	0.03	0.04	0.08	0.19	0.32	0.45
BC-M	-0.02	-0.01	0.00	0.01	0.02	0.04	0.08	0.16	0.40	--	--	--
RM-S3	0.01	0.02	0.02	0.02	0.03	0.03	0.03	0.04	0.05	0.07	0.08	0.13
RM-S9	-0.02	-0.01	-0.01	-0.01	0.00	0.01	0.02	0.03	0.14	0.42	0.55	0.89
I-S	0.00	0.01	0.00	0.01	0.01	0.02	0.02	0.02	0.02	0.02	0.03	0.04

ACI 201 Guide to Durable Concrete [89] establishes expansion requirements for certain exposure classes, as shown in Table 5.7. Only the F-G, F-Z, BA-S, BC-B, RM-S3, and I-S fly ashes were able to meet the criteria for use in a sulfate environment. BC-B meets the requirements to be used in a Class 1 exposure condition; F-G, F-Z, and RM-S3 meet the requirements to be used in a Class 2 exposure condition; and BA-S and I-S were able to meet the requirements to be used in a Class 3 exposure condition.

Table 5.7: ACI 201 Sulfate Exposure Classifications

Exposure Class	Expansion Requirement
Class 1	Below 0.10% at 6 months
Class 2	Below 0.05% at 6 months or 0.10% at 12 months
Class 3	Below 0.10% at 18 months

Calcium aluminosilicate glass and reactive crystalline phases, such as tricalcium aluminate, gehlenite, and anhydrite have been shown to form sulfate attack-vulnerable hydration products. These reactive crystalline phases were found to be present in most of the fly ashes (Table 2.7 and Table 2.8) that failed to meet an exposure condition in sulfate resistance testing, except for BA-B. BA-B has a lower

amorphous content than most of the other fly ashes and consists of 40% MBA, which was found to have low reactivity in Chapter 3.

5.3. Concrete Testing

Concrete mixture design consisted of a 25% cement replacement with the SCM by mass and a 0.485 w/cm. The cementitious materials content was designed to be 564 lb/yd^3. Colorado River gravel was used as the coarse aggregate at a fixed content of 1800 lb/yd^3. An assumed value of 2 vol.% was used for entrapped air. The Colorado River sand was used as the fine aggregate, and its content was adjusted to complete the remaining cubic yard volume in the concrete mixture. Table 5.8 shows an example of a concrete mixture design for a straight cement mixture. This concrete mixture design was used for most concrete testing, apart from ASR testing.

Table 5.8: OPC Concrete Mixture Design

Component	Amount (lb/yd^3)
OPC	564
Water	297
Coarse Aggregate	1804
Fine Aggregate	1298
Air	2 vol.%

5.3.1. Fresh Concrete Properties

Slump and air content testing were performed in accordance with ASTM C143 [90] and C231 [91], respectively, on fresh concrete. Slump was measured once for each concrete mixture. Concrete used to measure slump was returned to the rotary drum mixer and mixed for an additional 30 seconds to reintegrate the sample prior to performing additional testing. When performing air content testing, unit weight of the concrete mixture was also measured. Similar to slump testing, air content testing was performed only once for each mixture. Table 5.9 shows the fresh concrete properties for each mixture.

Table 5.9: Fresh Concrete Properties

ID	Slump (in.)	Air Content (%)	Unit Weight (lb/ft^3)
OPC	7.4	3.9	145
Q	7.5	3.0	145
F-G	8.5	1.5	147
F-Z	8.5	1.8	148
BA-B	8.5	2.1	146
BA-H	8.5	1.7	146
BA-S	6.5	2.9	144
BA-P	9.5	1.6	147
BA-V	9.3	1.8	147
BC-B	9.5	1.2	148
BC-M	9.0	1.1	148
RM-S3	8.8	1.4	147
RM-S9	9.3	1.5	147
I-S	8.8	1.4	147

Most of the fly ash concretes performed similarly to the control Class F fly ash concrete, F-G, except for BA-S, which had the lowest slump of all the concrete mixtures. This confirms the results seen in paste rheology testing, which showed that BA-S paste had the highest yield stress (Table 5.3). This is likely due to the angular particles present in BA-S (Appendix B) and its relatively small particle size (Table 2.11). An HRWR can be used if a slump similar to F-G concrete is desired.

Time of set was also determined for all mixtures following ASTM C403 [92]. Mortar was separated from the coarse aggregate by sieving fresh concrete using a vibrating plate. The mortar was then stored in a cylindrical container and consolidated. ASTM C403 instructs to take the initial measurement 3 to 4 hours after concrete mixing and continue measurements at 30 min to 1-hour intervals until the concrete reaches final set. The results are shown in Figure 5.9 and Figure 5.10. Initial set occurs once the penetration resistance reaches 500 psi, whereas final set occurs once the penetration resistance reaches 4000 psi. Setting time was measured once for each of the concrete mixtures.
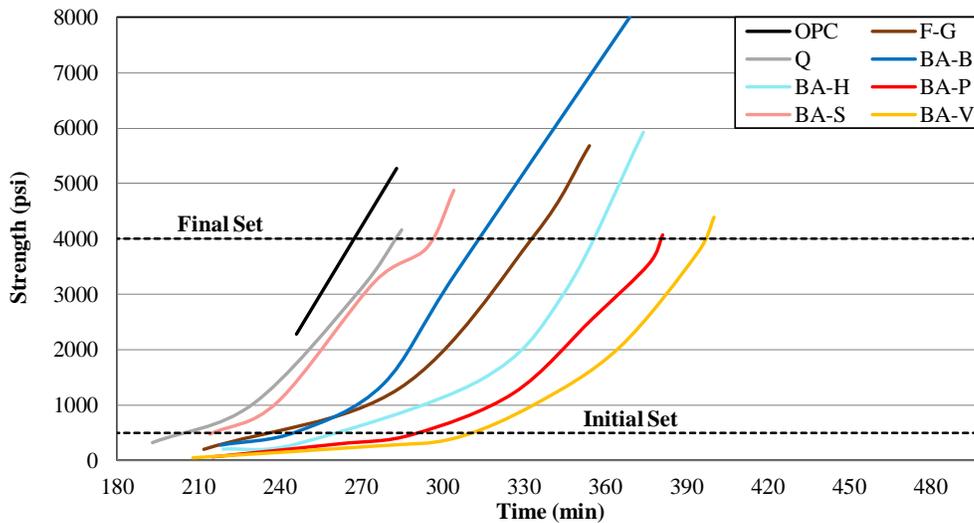
Figure 5.9: Time of set of concrete containing control materials and blended fly ashes
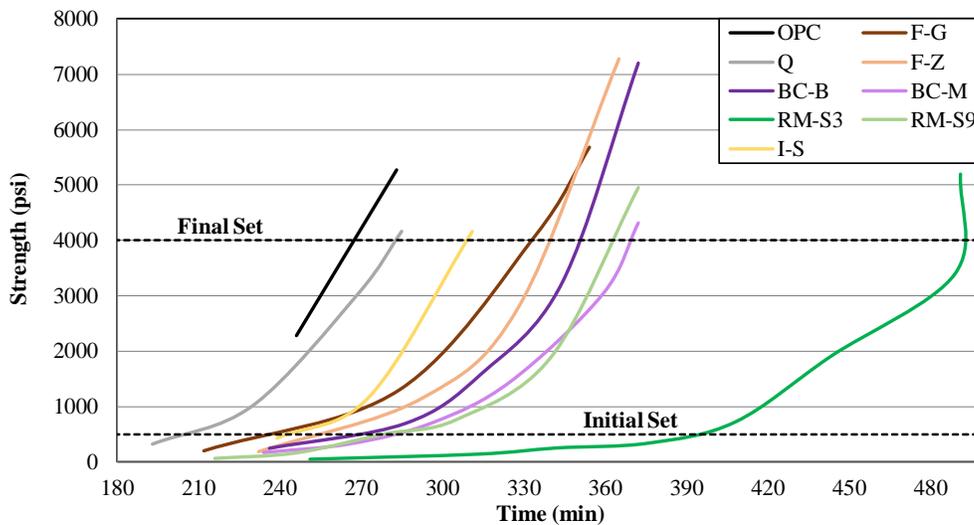
Figure 5.10: Time of set of concrete containing control materials and fly ashes

The initial measurement for OPC concrete occurred within the recommended time period of 3 to 4 hours after initial mixing but resulted in an initial penetration measurement above the initial set threshold. An initial set time of 224 minutes was estimated for OPC concrete by fitting a trend line to the curve. All SCMs delayed setting time compared to the control OPC mixture, with the RM-S3 fly ash causing significant delays. This agrees with results seen in heat of hydration testing in Figure 5.2, where the induction period of RM-S3 was prolonged. This is related to the high sulfate content of RM-S3 (Table 2.2). A delayed setting time can have negative effects on construction, causing plastic shrinkage and longer finishing

66

times [93]. It is possible that limestone or an accelerating admixture can reduce the final set time for RM-S3 concrete; however, further testing is warranted to verify that.

5.3.2. Compressive Strength

Once concrete mixing was completed, concrete was cast into 4 x 8 in. cylinder molds. Cylinders were stored at a 23°C for 24 hours before demolding and then moved to a curing room at 23°C and 100% relative humidity to be tested at 7, 28, 56, and 90 days. Compressive strength testing of concrete cylinders was performed in accordance with ASTM C39 [94]. Results are shown in Figure 5.11 and Figure 5.12.
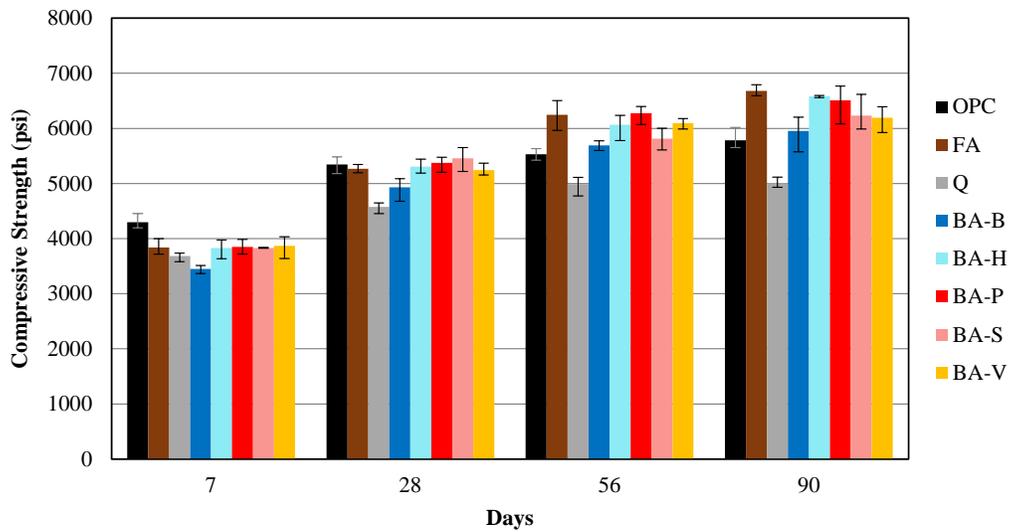
Figure 5.11: Compressive strength of concrete cylinders containing control materials and blended fly ashes
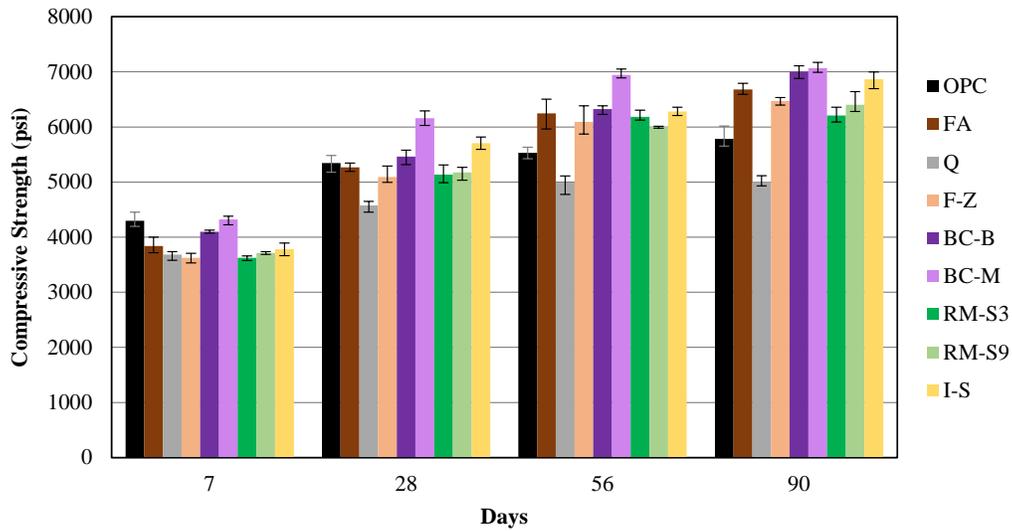
Figure 5.12: Compressive strength of concrete cylinders containing control materials and fly ashes

At 7 days, only BA-B concrete had a lower compressive strength than Q concrete. This is likely due to the larger particle size of BA-B compared to Q (Table 2.11) as well as the lower reactivity of MBA, which makes up 40% of BA-B. At 28 days and beyond, all concrete mixture, including BA-B, had higher compressive strengths than Q concrete. By 56 days, all the fly ash containing concretes had comparable or higher compressive strengths than OPC concrete. The results from concrete compressive strength testing indicate that all the fly ashes tested are pozzolanic and can increase long-term strength.

5.3.3. Rapid Chloride Penetrability

Rapid chloride penetrability testing (RCPT) was performed as outlined in ASTM C1202 [95]. RCPT was performed on 90 days concrete cylinders. The concrete cylinders were cut into 2-in. samples using an oil-lubricated concrete saw then were washed with soap and water to remove oil left from the saw and left to soak in soapy water overnight. Concrete samples were then rinsed and prepared for testing following ASTM C1202. The results are shown in Figure 5.13. Measurements were only completed once.
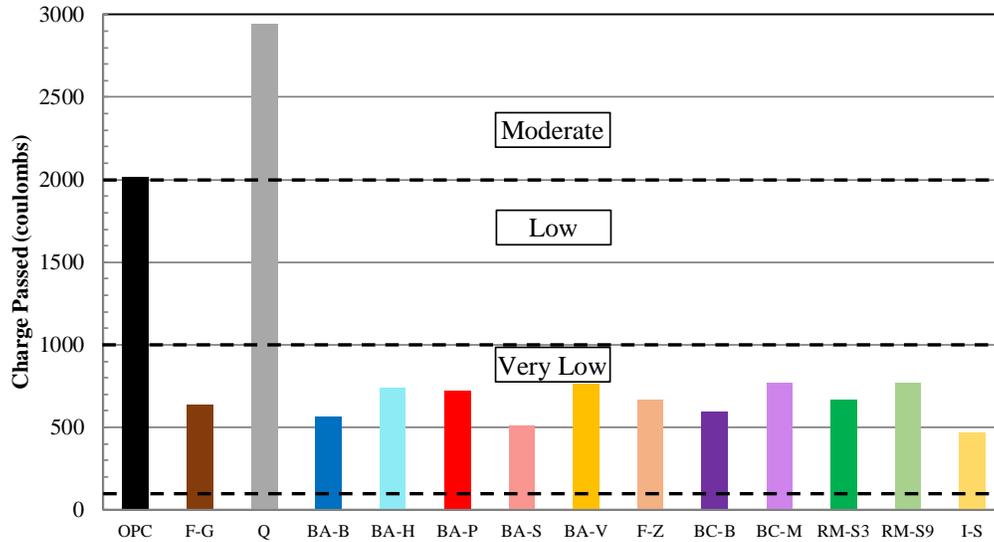
Figure 5.13: RCPT results of 90-day concrete cylinders containing control materials and SCMs with dashed lines indicating thresholds set by ASTM C1202

Despite the name of the test, RCPT measures the conductivity of a concrete sample rather than chloride penetrability. The conductivity can be correlated with permeability of the concrete, which gives an indication for how likely chloride ions will penetrate. Pozzolanic materials reduce the permeability of concrete by consuming CH and precipitating reaction products in available pore space, resulting in decreased pore connectivity [69,96]. Results from RCPT indicate that all the fly ashes are pozzolanic and were able to densify the pore structure of the concrete resulting in very low chloride ion penetrability based on thresholds set by ASTM C1202.

5.3.4. Bulk Electrical Resistivity

Bulk electrical resistivity was also measured for the concrete. Testing was conducted in accordance with ASTM C1876 [97]. For some of the cylinders, resistivity was measured directly on removal from the fog room as the cylinders reached 90 days (Table 5.10). For all mixtures, formation factor was also determined (Table 5.10). Once concrete cylinders reached 90 days of curing, they were submerged in a simulated pore solution with a resistivity of 0.127 ohm·m for 6 days. At the end of the 6-day period, samples were removed from the solution and blotted to remove excess liquid before being placed into the concrete electrical resistivity meter, and the resistivity was recorded. The formation factor was then calculated for the mixtures as a ratio of the bulk resistivity of the concrete to the resistivity of the simulated pore solution.

Table 5.10: Bulk Electrical Resistivity Results of Concrete Cylinders

ID	Resistivity (kΩ)	Formation Factor
OPC	--	540.4
Q	1.58	424.1
F-G	7.02	1325.8
F-Z	5.05	1297.5
BA-B	--	1178.1
BA-H	--	1046.2
BA-P	--	1109.0
BA-S	--	1460.8
BA-V	--	1008.5
BC-B	6.52	1266.1
BC-M	6.00	1303.8
RM-S3	6.08	1322.6
RM-S9	5.14	1228.4
I-S	8.60	1498.5

Resistivity of concrete is commonly associated with the permeability of the concrete, where a permeable concrete contains an interconnected pore structure that allows liquids and gases to pass through. The less permeable the concrete is, the less connectivity between pores, resulting in less liquid or gas passing through the matrix. This results in a more resistive and less permeable concrete. Measured resistivity values in concrete are also dependent on the resistivity of the pore solution. Therefore, measuring resistivity on concrete directly after curing combines information on both permeability and pore solution conductivity. Submerging samples in simulated pore solution results in all concrete samples having the same pore solution conductivity, thereby removing this variable. The formation factor, therefore, is only dependent on pore connectivity and is, thus, a good estimate of permeability. From Table 5.10, it is apparent that all of the SCM-containing mixtures had much higher formation factors than the control OPC and Q concretes, indicating that the SCMs reduce permeability.

5.3.5. Alkali-Silica Reaction

Alkali-silica reaction concrete mixtures varied slightly from other concrete mixture designs. A high alkali cement was used, and sodium hydroxide (NaOH) was added to the mixing water to increase the sodium equivalent (Na_2O_e) to 1.25% by mass of cement. The fine aggregate consisted of the same reactive sand used in ASR mortar

bar testing, while the coarse aggregate was non-reactive limestone that was graded in accordance with ASTM C1293 [62]. A w/cm of 0.45 was used for all mixtures, and a cement replacement of 25% by mass was used for all SCMs. Measurements were taken over the span of 2 years. Table 5.11 shows the expansion percentages of the mixtures. Red text indicates that the mortar bars surpassed the expansion limit of 0.04%.

Table 5.11: ASTM C1293 Expansion Percentages

ID	Day			Month					
	7	28	56	3	6	9	12	18	24
OPC	0.00	0.01	0.01	0.02	0.10	0.17	0.21	0.22	0.22
Q	0.00	0.00	0.00	0.00	0.00	0.00	0.01	0.01	0.01
F-G	0.00	0.01	0.01	0.01	0.01	0.01	0.01	0.01	0.01
F-Z	0.00	0.00	0.00	0.00	0.00	0.00	0.00	0.00	0.01
BA-B	0.00	0.00	0.00	0.00	0.00	0.00	0.00	0.00	0.00
BA-H	0.00	0.00	0.00	0.00	0.00	0.01	0.01	0.01	0.01
BA-S	-0.01	0.00	0.00	0.00	0.00	0.00	0.01	0.01	0.00
BA-P	0.00	0.00	0.00	0.00	0.00	0.01	0.01	0.01	0.01
BA-V	-0.01	-0.01	-0.01	-0.01	0.00	0.00	0.00	0.00	0.00
BC-B	-0.01	-0.01	0.00	0.00	0.00	0.00	0.00	0.00	0.00
BC-M	-0.01	-0.01	0.00	0.00	0.00	0.01	0.01	0.01	0.01
RM-S3	0.00	0.00	0.00	0.00	0.00	0.00	0.01	0.01	0.01
RM-S9	0.00	0.00	0.00	0.00	0.00	0.01	0.01	0.01	0.01
I-S	0.01	0.01	0.01	0.01	0.01	0.01	0.02	0.02	0.02

Only the control cement concrete, OPC, expanded beyond the 0.04% expansion limit set by ASTM C1293 after 2 years. Q, which failed ASR testing in mortar, was able to pass ASR testing in concrete. This may be due to leaching of alkalis during the testing duration in Q concrete, since Q concrete has a higher permeability than the other concrete mixtures, as was seen in RCPT (Figure 5.13) and bulk electrical resistivity testing (Table 5.10). The concrete prism test (ASTM C1293) has been considered to be more reliable than the mortar bar test (ASTM C1567) due to the harsh, unrealistic conditions that the mortar bars are subjected to in ASTM C1567 [98,99]. However, it has been shown that ASTM C1293 also has its shortcomings, such as leaching of alkalis and lower alkali loading for SCM-containing concrete mixtures [100]. Recent research [100] has shown that the newly standardized miniature concrete prism test (AASHTO T380) [101] may be a better test method to determine a materials ability to suppress deleterious expansion due to ASR.

Chapter 6. Analysis and Recommendations

6.1. Reactivity Tests

This study evaluated several available SCM reactivity tests to determine their ability to screen out inert materials and differentiate between pozzolanic and latent hydraulic materials. Successful, rapid reactivity testing will be helpful for rapidly screening poor performing materials and pre-qualifying materials for use. It was found that R^3 testing, newly standardized in ASTM C1897 [51], and the University of New Brunswick Pozzolanic Reactivity Test [50] were the most effective at screening out inert materials. Additionally, by measuring CH content of R^3 pastes using thermogravimetric analysis or single-point mass loss between 350 and 500°C, as done in the R^3P test, the values can be paired with heat release in R^3 isothermal calorimetry or R^3 bound water testing to distinguish between hydraulic and pozzolanic reactivity.

The following recommendations are made for screening out inert materials. The method used is dependent on the equipment available in a testing laboratory.

- If an isothermal calorimeter is available, the R^3 calorimetry method would be recommended for its reduced labor time and good reproducibility. Combining the results with the R^3P test would be recommended to further separate between hydraulic and pozzolanic reactivity.

- If there is not access to a calorimeter, either the UNBPRT or the R^3 bound water test are recommended. The UNBPRT requires the same equipment as the SAI test, with the addition of an oven at 40°C. This may be favorable to the R^3 bound water test, which additionally requires an oven that can hold stable temperatures at 350°C and a desiccant-filled chamber. It may be possible to combine the UNBPRT test with the R^3P test to separate between pozzolanic and hydraulic reactivity of materials; however, the UNBPRT is unable to differentiate between pozzolanic and hydraulic reactivity on its own.

The R^3 matrix and UNBPRT lime reactivity tests were the most effective at screening out inert materials in a short period of time. Since both tests are conducted in simulated environments to accelerate the material, additional testing should be conducted to confirm material performance in cement-based materials. This allows for a better understanding of the limitations of material reactivity in concrete than is provided in the R^3 and UNBPR tests. Mortar compressive strength testing and CH content of cement pastes can be used as supplements to reactivity testing if further confirmation of performance is desired.

6.2. Use of Non-Traditional Fly Ashes

Most of the non-traditional fly ashes performed comparably to traditional Class F fly ash in most tests, with a few notable exceptions. The following recommendations apply to the use of non-traditional fly ashes in concrete.

- **Sulfate balance:** If using Class F-Class C fly ash blends in concrete, additional gypsum may be needed to modify the sulfate balance. Cement pastes containing these fly ashes exhibited an amplification in the second hydration peak as measured using isothermal calorimetry. This is likely due to the increased number of aluminates in the system coming from crystalline phases in the Class C fly ash in the blend. Since this slight sulfate imbalance is unlikely to cause problems, it is recommended that <u>no action be taken with these materials</u>.

- **Sulfate balance:** On the other hand, it should be cautioned that some non-traditional fly ashes can cause the concrete mixture to be oversulfated. RM-S3 fly ash, which was treated for high sulfate content, led to a delayed setting time, which can cause construction problems in the field. A possible solution when using fly ashes with high sulfate content like RM-S3 could be to add limestone powder to reduce the setting time [83]. This was not done as part of this study but could be the subject of future work to validate this concept. <u>It is recommended that fly ashes treated for high sulfate content be avoided until a solution for the setting time delay is found.</u>

- **Workability:** Most fly ashes had the same impact on workability as traditional Class F fly ash, except for BA-S, a blended Class F-Class C fly ash. This is due to the presence of angular particles in the fly ash, which could have been caused by the blending process. A water reducer can be added to concrete mixtures when using BA-S if a similar workability as a traditional Class F fly ash is desired. Since most blended Class F-Class C fly ashes did not cause workability differences, it is recommended that <u>no action is necessary with regard to workability, except on a case-by-case basis identified through trial mixtures before implementation. In these cases, a water reducing admixture can be utilized.</u>

- **Sulfate resistance:** Fly ashes that contain reactive crystalline phases (C_3A, gehlenite, and anhydrite) were not able to meet the requirements for an ACI 201 [89] sulfate exposure class. The Class F fly ash-milled bottom ash blend, BA-B, also did not meet an ACI 201 sulfate exposure class. This is likely due to the lower reactivity of BA-B compared to other fly ash blends, as expected due to its low amorphous content and observed by its slow

strength gain in mortar and concrete mixtures. <u>Fly ash blends containing reactive crystalline phases or having low reactivity should not be used in concrete that requires sulfate resistance.</u>

Class F fly ash produced through firing of blended coal sources, blending different CCPs, remediation of non-compliant fly ash, or from other countries all show promise as potential sources to extend the supply of fly ash as the availability of traditional Class F fly ash declines. <u>It is recommended that the sulfate content from oxide analysis not exceed the limits in the ASTM C618 [1] specification, and it is suggested that qualitative X-ray diffraction (XRD) testing be conducted on fly ashes that are intended for use in sulfate environments.</u>

References

[1] ASTM C618, Standard Specification for Coal Fly Ash and Raw or Calcined Natural Pozzolan for Use, ASTM International, West Conshohocken, PA, 2019. https://doi.org/10.1520/C0618-19.2.

[2] ACI Committee 232, Use of Fly Ash in Concrete (ACI 232.2R-18), Farmington Hills, MI, 2018. https://doi.org/10.1021/cen-v041n021.p102.

[3] M. Thomas, R. Jewell, R. Jones, Coal fly ash as a pozzolan, in: T. Robl, A. Oberlink, R. Jones (Eds.), Coal Combust. Prod. Charact. Util. Benef., Elsevier Ltd., 2017: pp. 121–154. https://doi.org/10.1016/B978-0-08-100945-1.00005-8.

[4] ACAA, 2019 Coal Combustion Product (CCP) Production & Use Survey Report, Farmington Hills, MI, 2020. https://www.acaa-usa.org/Portals/9/Files/PDFs/2019-Survey-Results.pdf.

[5] ACAA, 2018 Coal Combustion Product (CCP) Production & Use Survey Report, Farmington Hills, MI, 2019. https://www.acaa-usa.org/Portals/9/Files/PDFs/2018-Survey-Results.pdf.

[6] U.S. Energy Information Administration, Annual Energy Outlook 2020: with projections to 2050, Washington, DC, 2020. https://www.eia.gov/outlooks/aeo/pdf/AEO2020 Full Report.pdf.

[7] M.J. McCarthy, T. Robl, L.J. Csetenyi, Recovery, processing, and usage of wet-stored fly ash, Elsevier Ltd., 2017. https://doi.org/10.1016/B978-0-08-100945-1.00014-9.

[8] American Road & Transportation Builders Association, Production and Use of Coal Combustion Products in the U.S. - Market Forecast Through 2033, 2015. https://www.acaa-usa.org/Portals/9/Files/PDFs/ReferenceLibrary/ARTBA-final-forecast.compressed.pdf.

[9] I. Diaz-Loya, M. Juenger, S. Seraj, R. Minkara, Extending supplementary cementitious material resources: Reclaimed and remediated fly ash and natural pozzolans, Cem. Concr. Compos. 101 (2019) 44–51. https://doi.org/10.1016/j.cemconcomp.2017.06.011.

[10] Texas Department of Transportation, Standard Specifications for Construction and Maintenance of Highways, Streets, and Bridges, 2014. ftp://ftp.dot.state.tx.us/pub/txdot-info/des/spec-book-1114.pdf.

[11] ASTM C1567, Standard Test Method for Determining the Potential Alkali-Silica Reactivity of Combinations of Cementitious Materials and Aggregate (Accelerated Mortar-Bar Method), ASTM International, West Conshohocken, PA, 2013. https://doi.org/10.1520/C1567-13.2.

[12] ASTM C1260, Standard Test Method for Potential Alkali Reactivity of Aggregates (Mortar-Bar Method), ASTM International, West

Conshohocken, PA, 2014. https://doi.org/10.1520/C1260-14.2.

[13] A. Naranjo, E. Lukefahr, Fly Ash Supply - Full Version, Texas Dep. Transp. Tech. Advis. (2010) 1–4. https://ftp.dot.state.tx.us/pub/txdot-info/cst/tips/fly_ash.pdf.

[14] G.J. McCarthy, J.K. Solem, O.E. Manz, D.J. Hassett, Use of a Database of Chemical, Mineralogical and Physical Properties of North American Fly Ash to Study the Nature of Fly Ash and its Utiliziation as a Mineral Admixture in Concrete, in: Mater. Res. Soc. Proc., 1990: pp. 3–33.

[15] ASTM C1697, Standard Specification for Blended Supplementary Cementitious Materials, ASTM International, West Conshohocken, PA, 2018. https://doi.org/10.1520/C1697-18.2.

[16] T.R. Naik, S. Singh, B. Ramme, Mechanical Properties and Durability of Concrete Made with Blended Fly Ash, Cem. Concr. Res. 95 (1998) 454–460.

[17] S. Antiohos, V.. Papadakis, K. Maganari, S. Tsimas, the Development of Blended Supplementary Cementing Materials Consisting of High and Low Calcium Fly Ashes, 11th Int. Congr. Chem. Cem. (2003) 747–757.

[18] S. Antiohos, K. Maganari, S. Tsimas, Evaluation of blends of high and low calcium fly ashes for use as supplementary cementing materials, Cem. Concr. Compos. 27 (2005) 349–356. https://doi.org/10.1016/j.cemconcomp.2004.05.001.

[19] EN 197-1, Cement - Part 1: Composition, specifications and conformity criteria for common cements, European Committee for Standardization, Brussels, Belgium, 2011.

[20] S.K. Antiohos, V.G. Papadakis, E. Chaniotakis, S. Tsimas, Improving the performance of ternary blended cements by mixing different types of fly ashes, Cem. Concr. Res. 37 (2007) 877–885. https://doi.org/10.1016/j.cemconres.2007.02.017.

[21] P. Tanikella, Incorporating Physical and Chemical Characteristics of Fly Ash in Statistical Modeling of Binder Properties, Purdue University, 2009.

[22] B. Franklin, D. Rhodes, Influences of Class F and C Fly Ash Blending, 2015 World Coal Ash Conf. Nasvhille. (2015). http://www.flyash.info/2015/087-franklin-2015.pdf.

[23] ASTM C1012/C1012M, Standard Test Method for Length Change of Hydraulic-Cement Mortars Exposed to a Sulfate Solution, ASTM International, West Conshohocken, PA, 2018. https://doi.org/10.1520/C1012.

[24] P.K. Mehta, Effect of Fly Ash Composition on Sulfate Resistance of Cement, ACI J. 83 (1986) 994–1000. https://doi.org/10.14359/1892.

[25] R. Dhole, M.D.A. Thomas, K.J. Folliard, T. Drimalas, Sulfate Resistance of Mortar Mixtures of High-Calcium Fly Ashes and Other Pozzolans, ACI

Mater. J. 108 (2011) 645–654. https://doi.org/10.14359/51683468.

[26] M.H. Shehata, M.D.A. Thomas, Effect of fly ash composition on the expansion of concrete due to alkali-silica reaction, Cem. Concr. Res. 30 (2000) 1063–1072. https://doi.org/10.1016/S0008-8846(00)00283-0.

[27] M.H. Shehata, M.D.A. Thomas, Alkali release characteristics of blended cements, Cem. Concr. Res. 36 (2006) 1166–1175. https://doi.org/10.1016/j.cemconres.2006.02.015.

[28] K.L. Aughenbaugh, R.T. Chancey, P. Stutzman, M.C. Juenger, D.W. Fowler, An examination of the reactivity of fly ash in cementitious pore solutions, Mater. Struct. 46 (2013) 869–880. https://doi.org/10.1617/s11527-012-9939-6.

[29] K.L. Aughenbaugh, P. Stutzman, M.C.G. Juenger, Identifying Glass Compositions in Fly Ash, Front. Mater. 3 (2016). https://doi.org/10.3389/fmats.2016.00001.

[30] R.T. Chancey, P. Stutzman, M.C.G. Juenger, D.W. Fowler, Comprehensive phase characterization of crystalline and amorphous phases of a Class F fly ash, Cem. Concr. Res. 40 (2010) 146–156. https://doi.org/10.1016/j.cemconres.2009.08.029.

[31] S. Diamond, On the Glass Present in Low-Calcium and in High-Calcium Flyashes, Cem. Concr. Res. 13 (1983) 459–464.

[32] P.T. Durdziński, C.F. Dunant, M. Ben Haha, K.L. Scrivener, A new quantification method based on SEM-EDS to assess fly ash composition and study the reaction of its individual components in hydrating cement paste, Cem. Concr. Res. 73 (2015) 111–122. https://doi.org/10.1016/j.cemconres.2015.02.008.

[33] G.J. McCarthy, K.D. Swanson, L.P. Keller, W.C. Blatter, Mineralogy of Western Fly Ash, Cem. Concr. Res. 14 (1984) 471–478. https://doi.org/10.1016/0008-8846(84)90121-2.

[34] P.J. Sandberg, L.R. Roberts, Cement-Admixture Interactions Related to Aluminate Control, J. ASTM Int. 2 (2005) 219–232. https://doi.org/10.1520/jai12296.

[35] R.D. Kalina, S. Al-Shmaisani, R.D. Ferron, M.C.G. Juenger, False Positives in ASTM C618 Specifications for Natural Pozzolans, ACI Mater. J. 116 (2019) 1–8. https://doi.org/10.14359/51712243.

[36] S. Seraj, R. Cano, S. Liu, D. Whitney, D. Fowler, R. Ferron, J. Zhu, M. Juenger, Evaluating the Performance of Alternative Supplementary Cementing Material in Concrete, Austin, TX, 2014.

[37] ASTM C1709, Standard Guide for Evaluation of Alternative Supplementary Cementitious Materials (ASCM) for Use in Concrete, ASTM International, West Conshohocken, PA, 2018. https://doi.org/10.1520/C1709-18.2.

[38] A.R. Pourkhorshidi, M. Najimi, T. Parhizkar, F. Jafarpour, B. Hillemeier, Applicability of the standard specifications of ASTM C618 for evaluation of natural pozzolans, Cem. Concr. Compos. 32 (2010) 794–800. https://doi.org/10.1016/j.cemconcomp.2010.08.007.

[39] K.L. Aughenbaugh, T. Williamson, M.C.G. Juenger, Critical evaluation of strength prediction methods for alkali-activated fly ash, Mater. Struct. 48 (2015) 607–620. https://doi.org/10.1617/s11527-014-0496-z.

[40] NF P 18-513 Annexe A, Détermination de la quantité d'hydroxyde de calcium fixé (essai Chapelle modifié), 2010.

[41] EN 196-5, Method of testing cement - Part 5: Pozzolanicity test for pozzolanic cement, European Committee for Standardization, Brussels, Belgium, 2011.

[42] IS 1727-1967, Methods of Test for Pozzolanic Materials, Bureau of Indian Standards, New Delhi, India, 2004.

[43] CSA A3004-E1, Standard Practice for the Evaluation of Alternative Supplementary Cementing Materials (ASCMs) for use in Concrete, Canadian Standards Association, Mississauga, ON, Canada, 2013.

[44] R. Snellings, K.L. Scrivener, Rapid screening tests for supplementary cementitious materials: past and future, Mater. Struct. 49 (2016) 3265–3279. https://doi.org/10.1617/s11527-015-0718-z.

[45] S. Seraj, M.C.G. Juenger, Evaluation of an accelerated characterization method for pozzolanic reactivity, in: Am. Concr. Institute, ACI Spec. Publ., 2016.

[46] B. Lothenbach, P. Durdziński, K. De Weerdt, Thermogravimetric analysis, in: K. Scrivener, R. Snellings, B. Lothenbach (Eds.), A Pract. Guid. to Microstruct. Anal. Cem. Mater., Taylor & Francis Group, 2016: pp. 177–211. https://doi.org/10.1201/b19074.

[47] S. Al-Shmaisani, R. Kalina, M. Rung, R. Ferron, M. Juenger, Implementation of a Testing Protocol for Approving Alternative Supplementary Cementitious Materials (SCMs): Natural Minerals and Reclaimed and Remediated Fly Ashes, Austin, TX, 2018. http://library.ctr.utexas.edu/ctr-publications/5-6717-01-1.pdf.

[48] T. Kim, J. Olek, Effects of Sample Preparation and Interpretation of Thermogravimetric Curves on Calcium Hydroxide in Hydrated Pastes and Mortars, Transp. Res. Rec. (2012) 10–18. https://doi.org/10.3141/2290-02.

[49] P.T. Durdziński, M. Ben Haha, S.A. Bernal, N. De Belie, E. Gruyaert, B. Lothenbach, E. Menéndez Méndez, J.L. Provis, A. Schöler, C. Stabler, Z. Tan, Y. Villagrán Zaccardi, A. Vollpracht, F. Winnefeld, M. Zając, K.L. Scrivener, Outcomes of the RILEM round robin on degree of reaction of slag and fly ash in blended cements, Mater. Struct. 50 (2017). https://doi.org/10.1617/s11527-017-1002-1.

[50] M. Kasaniya, M.D.A. Thomas, E.G. Moffatt, Development of Rapid and Reliable Pozzolanic Reactivity Test Method, ACI Mater. J. 116 (2019) 145–154. https://doi.org/10.14359/51716718.

[51] ASTM C1897, Standard Test Methods for Measuring the Reactivity of Supplementary Cementitious Materials by Isothermal Calorimetry and Bound Water Measurements, ASTM International, West Conshohocken, PA, 2020. https://doi.org/10.1520/C1897-20.2.

[52] X. Li, R. Snellings, M. Antoni, N.M. Alderete, M. Ben Haha, S. Bishnoi, Ö. Cizer, M. Cyr, K. De Weerdt, Y. Dhandapani, J. Duchesne, J. Haufe, D. Hooton, M. Juenger, S. Kamali-Bernard, S. Kramar, M. Marroccoli, A.M. Joseph, A. Parashar, C. Patapy, J.L. Provis, S. Sabio, M. Santhanam, L. Steger, T. Sui, A. Telesca, A. Vollpracht, F. Vargas, B. Walkley, F. Winnefeld, G. Ye, M. Zajac, S. Zhang, K.L. Scrivener, Reactivity tests for supplementary cementitious materials: RILEM TC 267-TRM phase 1, Mater. Struct. Constr. 51 (2018). https://doi.org/10.1617/s11527-018-1269-x.

[53] P. Suraneni, A. Hajibabaee, S. Ramanathan, Y. Wang, J. Weiss, New insights from reactivity testing of supplementary cementitious materials, Cem. Concr. Compos. 103 (2019) 331–338. https://doi.org/10.1016/j.cemconcomp.2019.05.017.

[54] P. Suraneni, J. Weiss, Examining the pozzolanicity of supplementary cementitious materials using isothermal calorimetry and thermogravimetric analysis, Cem. Concr. Compos. 83 (2017) 273–278. https://doi.org/10.1016/j.cemconcomp.2017.07.009.

[55] D.P. Bentz, A. Durán-Herrera, D. Galvez-Moreno, Comparison of ASTM C311 strength activity index testing versus testing based on constant volumetric proportions, J. ASTM Int. 9 (2011). https://doi.org/10.1520/JAI104138.

[56] V.G. Papadakis, S. Tsimas, Supplementary cementing materials in concrete Part I: efficiency and design, Cem. Concr. Res. 32 (2002) 1525–1532.

[57] M.C.G. Juenger, R. Siddique, Recent advances in understanding the role of supplementary cementitious materials in concrete, Cem. Concr. Res. 78 (2015) 71–80. https://doi.org/10.1016/j.cemconres.2015.03.018.

[58] K.L. Scrivener, B. Lothenbach, N. De Belie, E. Gruyaert, J. Skibsted, R. Snellings, A. Vollpracht, TC 238-SCM: hydration and microstructure of concrete with SCMs: State of the art on methods to determine degree of reaction of SCMs, Mater. Struct. 48 (2015) 835–862. https://doi.org/10.1617/s11527-015-0527-4.

[59] ASTM C1240, Standard Specification for Silica Fume Used in Cementitious Mixtures, ASTM International, West Conshohocken, PA, 2020. https://doi.org/10.1520/C1240-20.2.

[60] M. Antoni, J. Rossen, F. Martirena, K. Scrivener, Cement substitution by a

combination of metakaolin and limestone, Cem. Concr. Res. 42 (2012) 1579–1589. https://doi.org/10.1016/j.cemconres.2012.09.006.

[61] D.P. Bentz, T. Sato, I. De La Varga, W.J. Weiss, Fine limestone additions to regulate setting in high volume fly ash mixtures, Cem. Concr. Compos. 34 (2012) 11–17. https://doi.org/10.1016/j.cemconcomp.2011.09.004.

[62] ASTM C1293, Standard Test Method for Determination of Length Change of Concrete Due to Alkali-Silica Reaction, ASTM International, West Conshohocken, PA, 2020. https://doi.org/10.1520/C1293-20A.2.

[63] ASTM C311/C311M, Standard Test Methods for Sampling and Testing Fly Ash or Natural Pozzolans for Use in Portland-Cement Concrete, ASTM International, West Conshohocken, PA, 2018. https://doi.org/10.1520/C0311.

[64] ASTM C109/C109M, Standard Test Method for Compressive Strength of Hydraulic Cement Mortars (Using 2-in. or [50 mm] Cube Specimens), ASTM International, West Conshohocken, PA, 2020. https://doi.org/10.1520/C0109.

[65] E.I. Diaz-Loya, F. Kinney, C.A.O. Rios, Reactivity indicators for activated high-calcium fly ash-based binders, ACI Spec. Publ. 294 (2013) 1–22.

[66] T. Oey, C. Huang, R. Worley, S. Ho, J. Timmons, K.L. Cheung, A. Kumar, M. Bauchy, G. Sant, Linking Fly Ash Composition to Performance in Cementitious Systems, 2015 World Coal Ash Conf. Nasvhille. (2015). http://www.flyash.info/.

[67] P. Duxson, J.L. Provis, Designing Precursors for Geopolymer Cements, J. Am. Ceram. Soc. 91 (2008) 3864–3869.

[68] S. Al-Shmaisani, R.D. Kalina, R.D. Ferron, M.C.G. Juenger, Evaluation of Beneficiated and Reclaimed Fly Ashes in Concrete, ACI Mater. J. 116 (2019) 79–87. https://doi.org/10.14359/51716713.

[69] B. Lothenbach, K. Scrivener, R.D. Hooton, Supplementary cementitious materials, Cem. Concr. Res. 41 (2011) 1244–1256. https://doi.org/10.1016/j.cemconres.2010.12.001.

[70] R. Snellings, X. Li, F. Avet, K. Scrivener, Rapid, Robust, and Relevant (R3) Reactivity Test for Supplementary Cementitious Materials, ACI Mater. J. 116 (2019) 155–162. https://doi.org/10.14359/51716719.

[71] B. Lothenbach, D.A. Kulik, T. Matschei, M. Balonis, L. Baquerizo, B. Dilnesa, G.D. Miron, R.J. Myers, Cemdata18: A chemical thermodynamic database for hydrated Portland cements and alkali-activated materials, Cem. Concr. Res. 115 (2019) 472–506. https://doi.org/10.1016/j.cemconres.2018.04.018.

[72] B.K. Marsh, R.L. Day, Pozzolanic and cementitious reactions of fly ash in blended cement pastes, Cem. Concr. Res. 18 (1988) 301–310.

[73] S. Ramanathan, P. Suraneni, Cheap Reactivity Testing, (2020).

[74] J.A. Larbi, J.M.J.M. Bijen, Orientation of calcium hydroxide at the portland cement paste-aggregate interface in mortars in the presence of silica fume: A contribution, Cem. Concr. Res. 20 (1990) 461–470. https://doi.org/10.1016/0008-8846(90)90037-X.

[75] B. Lothenbach, M. Zajac, Application of thermodynamic modelling to hydrated cements, Cem. Concr. Res. 123 (2019). https://doi.org/10.1016/j.cemconres.2019.105779.

[76] J. Skibsted, R. Snellings, Reactivity of supplementary cementitious materials (SCMs) in cement blends, Cem. Concr. Res. 124 (2019). https://doi.org/10.1016/j.cemconres.2019.105799.

[77] J.K. Jang, A New Approach to Measuring Pozzolanicity of Supplementary Cementitious Materials Using Existing ASTM Standards, The University of Texas at Austin, 2020.

[78] M. Kasaniya, UNBPRT Thresholds, (2020).

[79] ASTM C226, Standard Specification for Air-Entraining Additions for Use in the Manufacture of Air- Entraining Hydraulic Cement, ASTM International, West Conshohocken, PA, 2019. https://doi.org/10.1520/C0226-19.2.

[80] ASTM C1738/C1738M, Standard Practice for High-Shear Mixing of Hydraulic Cement Pastes, ASTM International, West Conshohocken, PA, 2019. https://doi.org/10.1520/C1738.

[81] M.A. Schultz, L.J. Struble, Use of oscillatory shear to study flow behavior of fresh cement paste, Cem. Concr. Res. 23 (1993) 273–282. https://doi.org/10.1016/0008-8846(93)90092-N.

[82] V.F. Rahhal, Z. Pavlík, A. Tironi, C.C. Castellano, M.A. Trezza, R. Černý, E.F. Irassar, Effect of cement composition on the early hydration of blended cements with natural zeolite, J. Therm. Anal. Calorim. 128 (2017) 721–733. https://doi.org/10.1007/s10973-016-6007-4.

[83] F. Zunino, D.P. Bentz, J. Castro, Reducing setting time of blended cement paste containing high-SO3 fly ash (HSFA) using chemical/physical accelerators and by fly ash pre-washing, Cem. Concr. Compos. 90 (2018) 14–26. https://doi.org/10.1016/j.cemconcomp.2018.03.018.

[84] J.O. Wheeless, Improving the Sulfate Resistance of Class C Fly Ash : A Scientific Approach to Making Bad Ash Concrete, The University of Texas at Austin, 2018.

[85] L. Wadsö, F. Winnefeld, K. Riding, P. Sandberg, Calorimetry, in: K. Scrivener, R. Snellings, B. Lothenbach (Eds.), A Pract. Guid. to Microstruct. Anal. Cem. Mater., Taylor & Francis Group, 2016: pp. 37–74. https://doi.org/10.1201/b19074.

[86] V. Mechtcherine, A. Gram, K. Krenzer, J.H. Schwabe, S. Shyshko, N. Roussel, Simulation of fresh concrete flow using Discrete Element Method

(DEM): Theory and applications, Mater. Struct. 47 (2014) 615–630. https://doi.org/10.1617/s11527-013-0084-7.

[87] ASTM C157/C157M, Standard Test Method for Length Change of Hardened Hydraulic-Cement Mortar and Concrete, ASTM International, West Conshohocken, PA, 2017. https://doi.org/10.1520/C0157.

[88] M. Zajac, A. Rossberg, G. Le Saout, B. Lothenbach, Influence of limestone and anhydrite on the hydration of Portland cements, Cem. Concr. Compos. 46 (2014) 99–108. https://doi.org/10.1016/j.cemconcomp.2013.11.007.

[89] ACI Committee 201, Guide to Durable Concrete (ACI 201.2R-16), Farmington Hills, MI, 2016.

[90] ASTM C143/C143, Standard Test Method for Slump of Hydraulic-Cement Concrete, ASTM International, West Conshohocken, PA, 2020. https://doi.org/10.1520/C0143.

[91] ASTM C231/C231M, Standard Test Method for Air Content of Freshly Mixed Concrete by the Pressure Method, in: ASTM International, West Conshohocken, PA, 2017: pp. 1–10.

[92] ASTM C403, Standard Test Method for Time of Setting of Concrete Mixtures by Penetration Resistance, ASTM International, West Conshohocken, PA, 2016. https://doi.org/10.1520/C0403.

[93] W. Lerch, Plastic Shrinkage, J. Am. Concr. Inst. 28 (1957) 797–802. https://doi.org/10.14359/11555.

[94] ASTM C39/C39M, Standard Test Method for Compressive Strength of Cylindrical Concrete Specimens, ASTM International, West Conshohocken, PA, 2020. https://doi.org/10.1520/C0039.

[95] ASTM C1202, Standard Test Method for Electrical Indication of Concrete's Ability to Resist Chloride Ion Penetration, ASTM International, West Conshohocken, PA, 2019. https://doi.org/10.1520/C1202-19.2.

[96] M. Thomas, Supplementary cementing materials in concrete, Taylor & Francis Group, 2013. https://doi.org/10.1201/b14493.

[97] ASTM C1876, Standard Test Method for Bulk Electrical Resistivity or Bulk Conductivity of Concrete, ASTM International, West Conshohocken, PA, 2019. https://doi.org/10.1520/C1876-19.

[98] A. Gholizadeh Vayghan, J.R. Wright, F. Rajabipour, An extended chemical index model to predict the fly ash dosage necessary for mitigating alkali-silica reaction in concrete, Cem. Concr. Res. 82 (2016) 1–10. https://doi.org/10.1016/j.cemconres.2015.12.014.

[99] J.H. Ideker, A.F. Bentivegna, K.J. Folliard, M.C.G. Juenger, Do Current Laboratory Test Methods Accurately Predict Alkali-Silica Reactivity?, ACI Mater. J. 109 (2012) 395–402. https://doi.org/10.14359/51683914.

[100] J. Tanesi, T. Drimalas, K.S.T. Chopperla, M. Beyene, J.H. Ideker, H. Kim,

L. Montanari, A. Ardani, Divergence between Performance in the Field and Laboratory Test Results for Alkali-Silica Reaction, Transp. Res. Rec. 2674 (2020) 120–134. https://doi.org/10.1177/0361198120913288.

[101] AASHTO T 380, Standard Method of Test for Potential Alkali Reactivity of Aggregates and Effectiveness of ASR Mitigation Measures (Miniature Concrete Prism Test, MCPT), American Association of State Highway and Transportation Officials, Washington, DC, 2019.

Appendix A. X-Ray Diffractograms
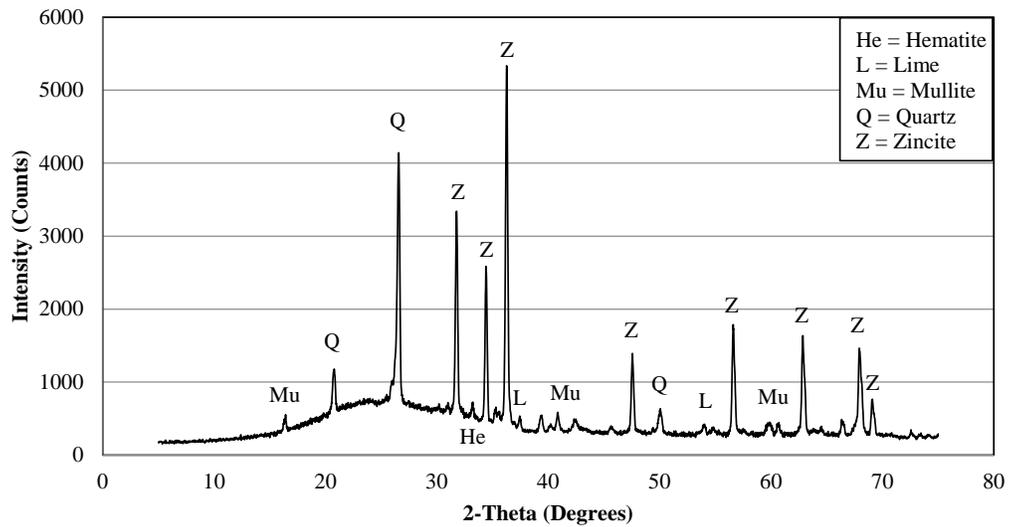
Figure A.1 X-ray diffraction pattern of F-G
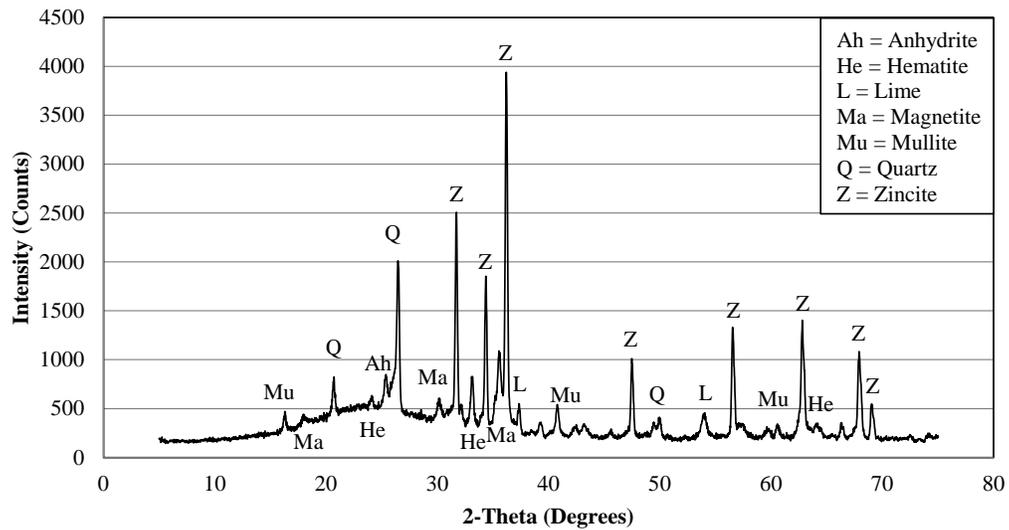
Figure A.2 X-ray diffraction pattern of F-Z
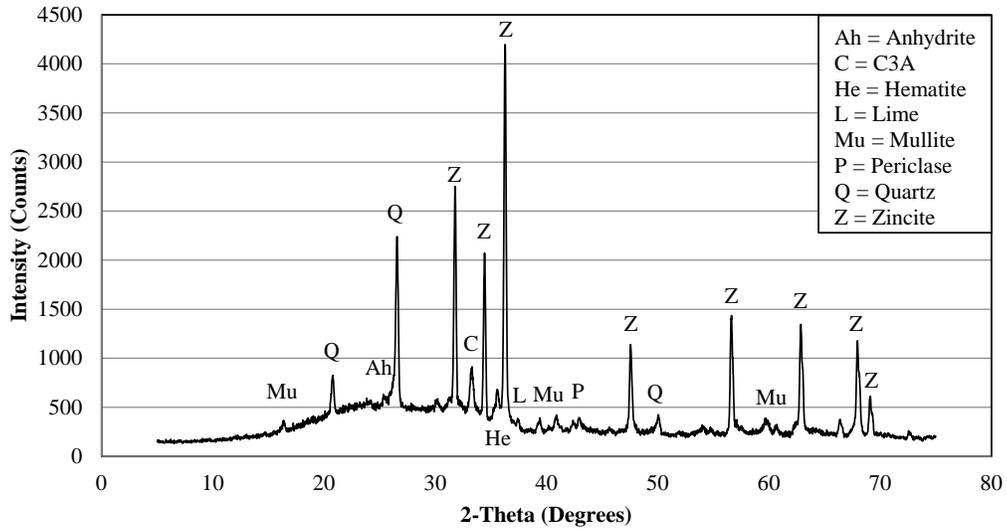
Figure A.3 X-ray diffraction pattern of BA-P
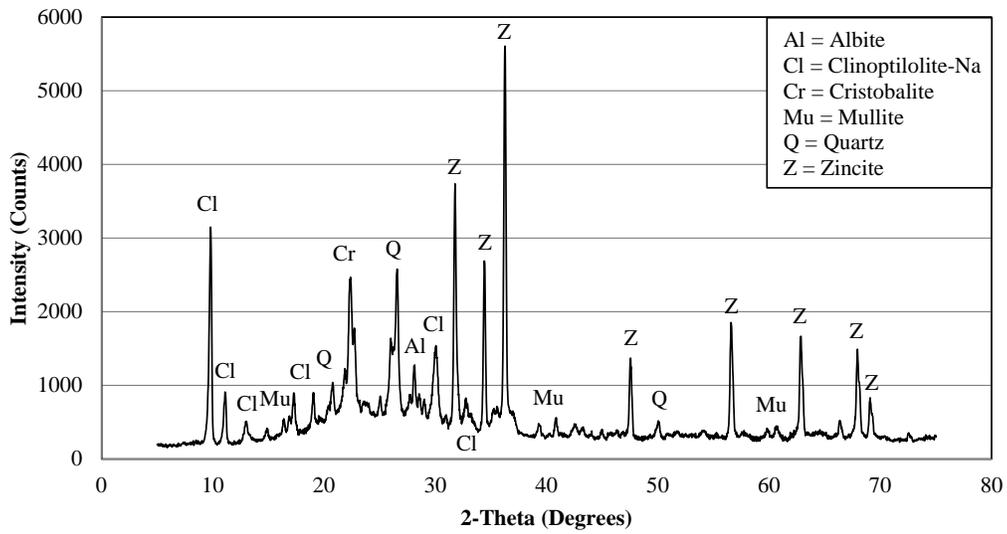
Figure A.4 X-ray diffraction pattern of BA-S
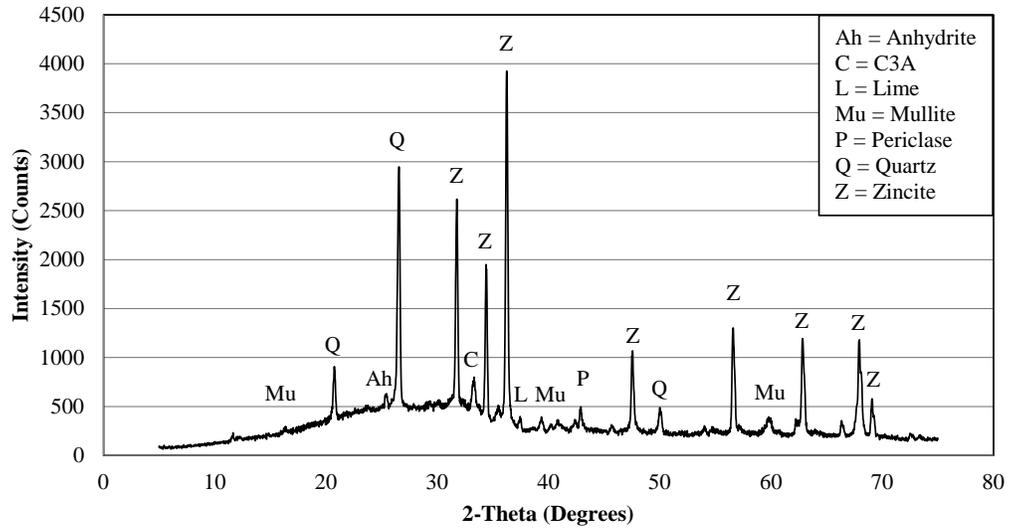
Figure A.5 X-ray diffraction pattern of BA-V
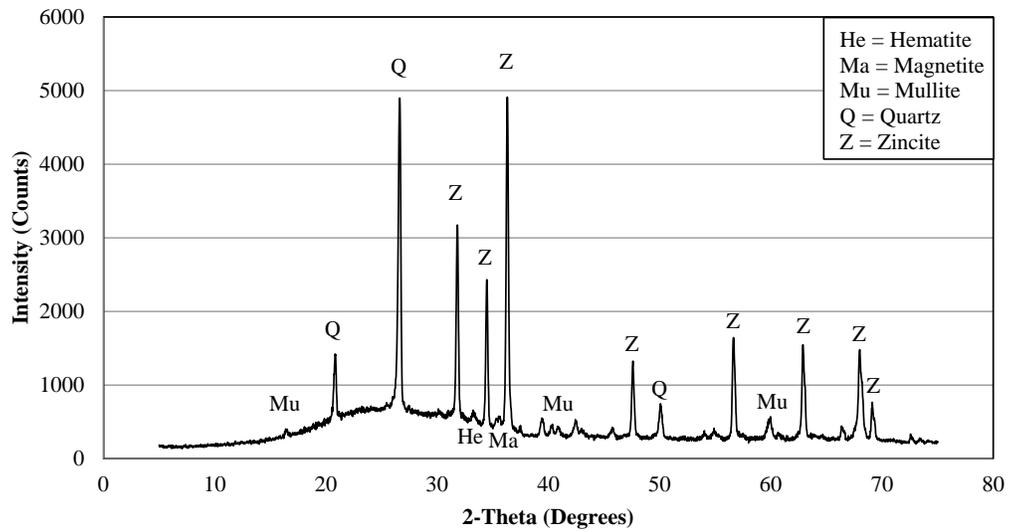
Figure A.6 X-ray diffraction pattern of BC-B

86
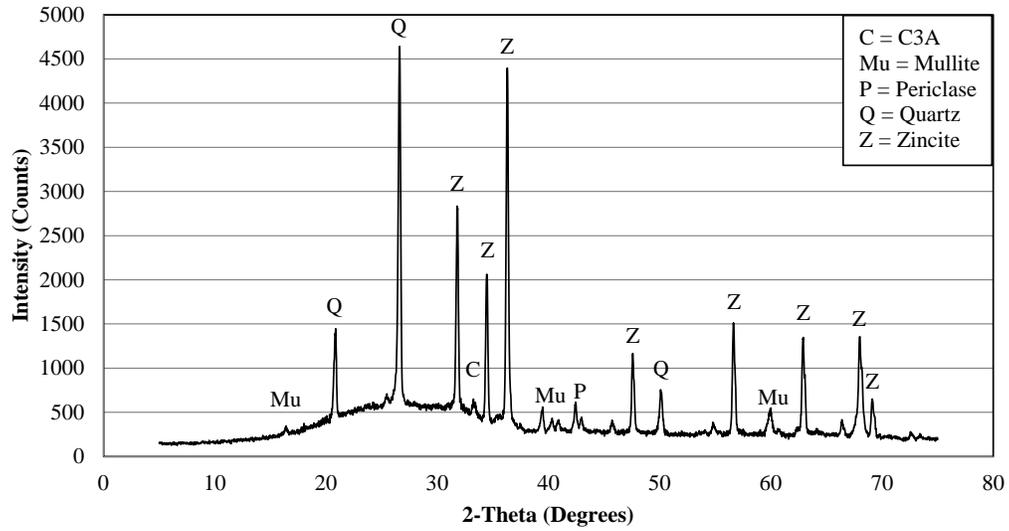
Figure A.7 X-ray diffraction pattern of BC-M
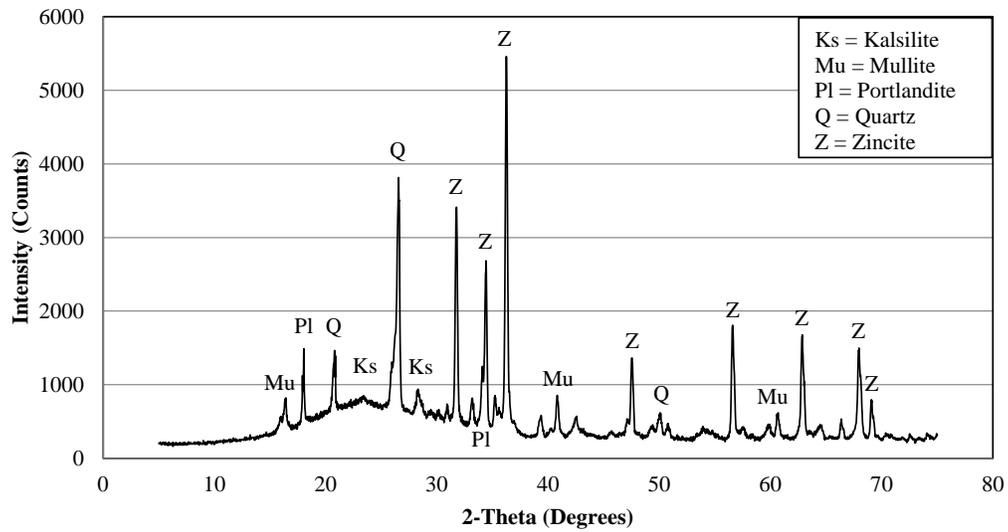
Figure A.8 X-ray diffraction pattern of RM-S3
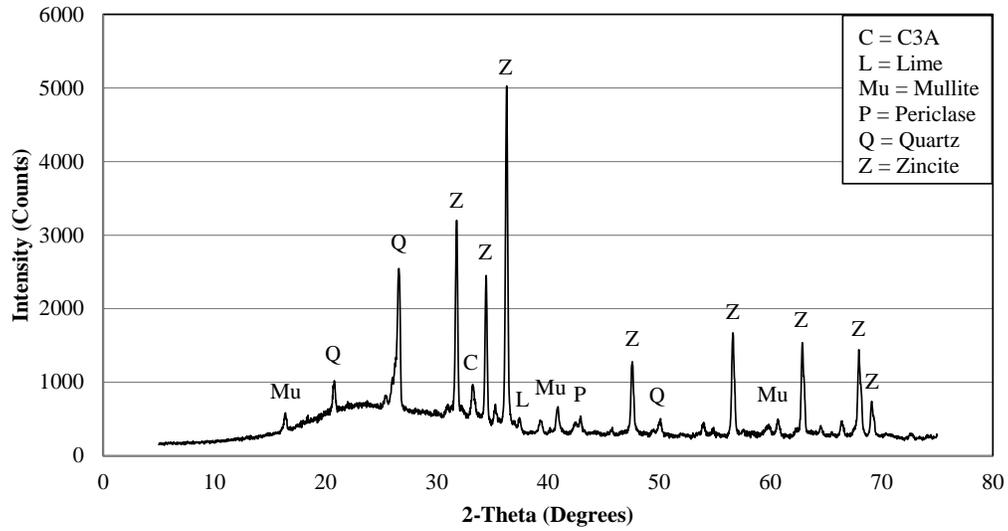
Figure A.9 X-ray diffraction pattern of RM-S9
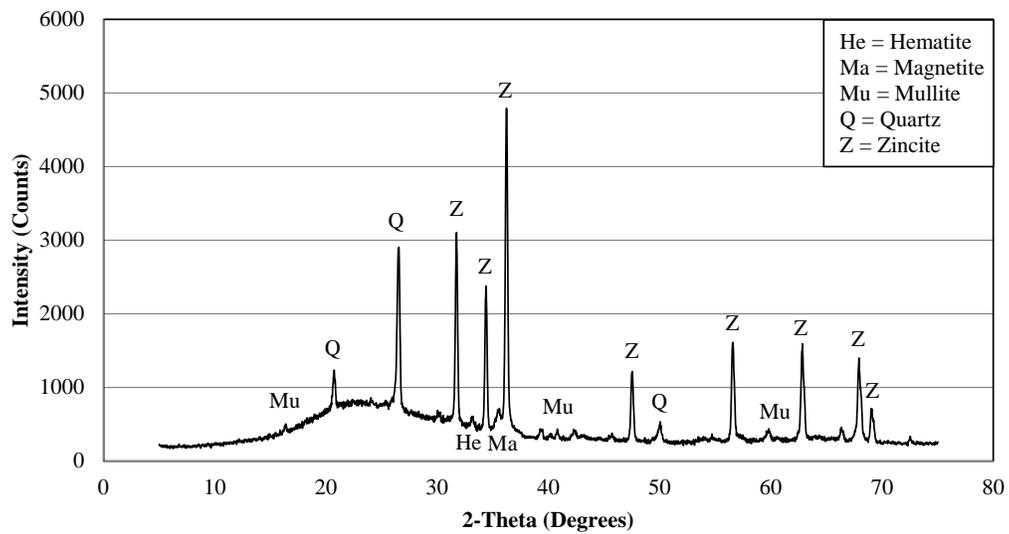
Figure A.10 X-ray diffraction pattern of I-S
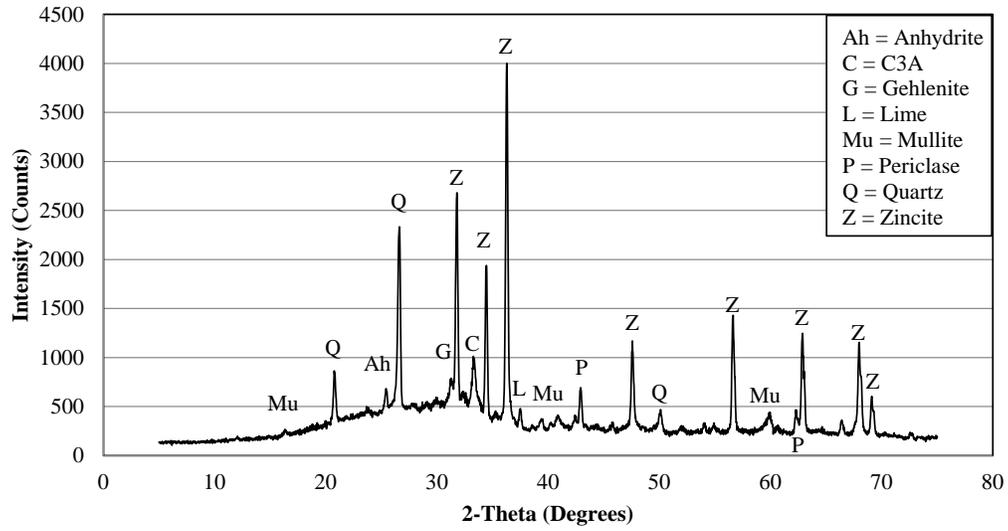
Figure A.11 X-ray diffraction pattern of C-H
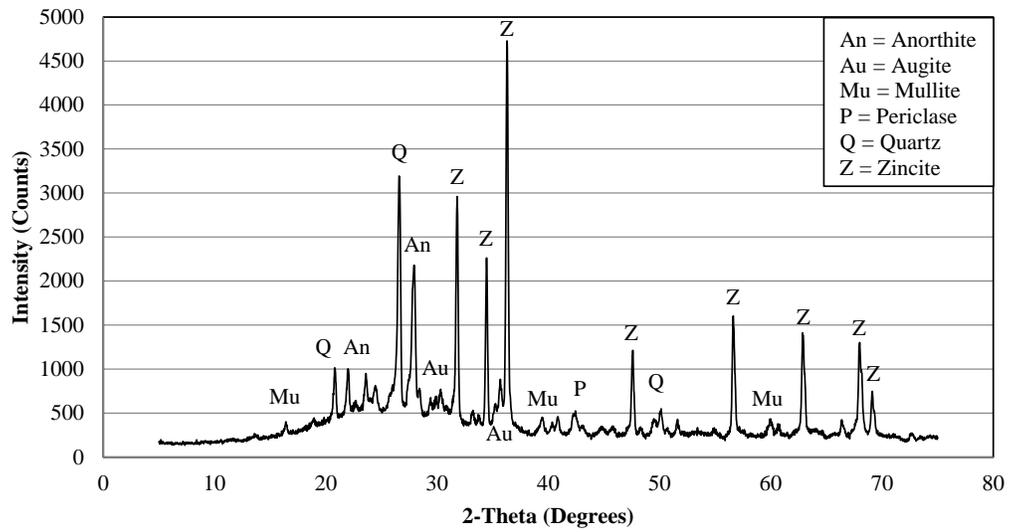
Figure A.12 X-ray diffraction pattern of MBA
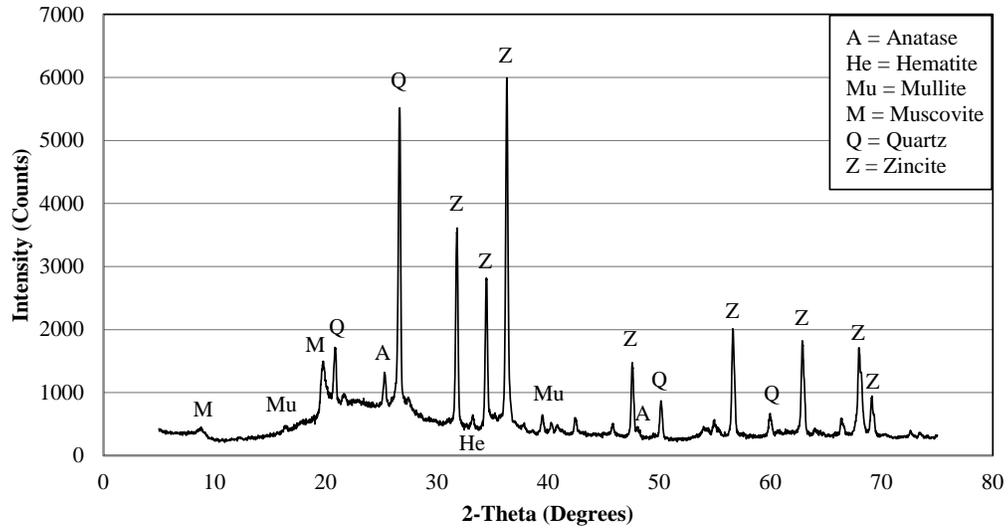
Figure A.13 X-ray diffraction pattern of M-D
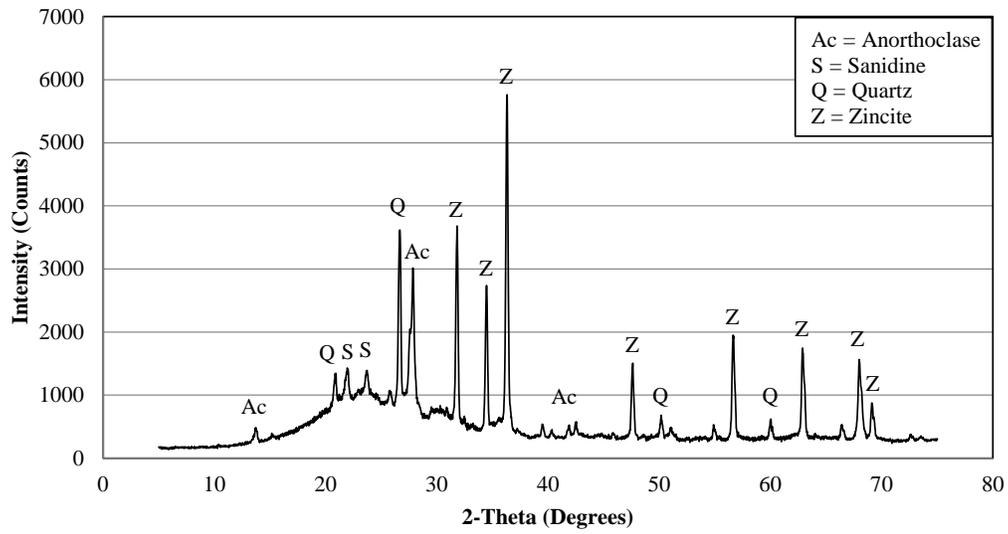
Figure A.14 X-ray diffraction pattern of P-O
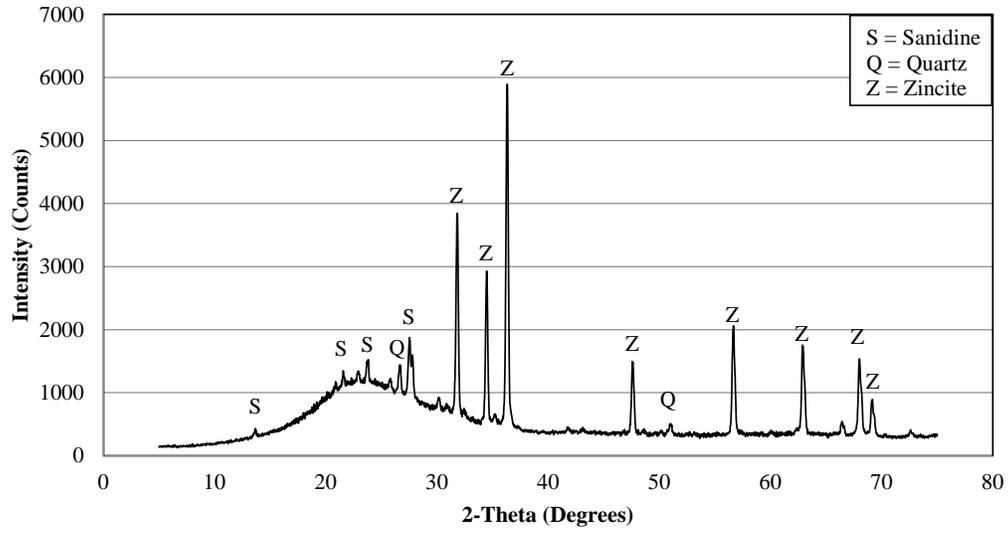
Figure A.15 X-ray diffraction pattern of P-P
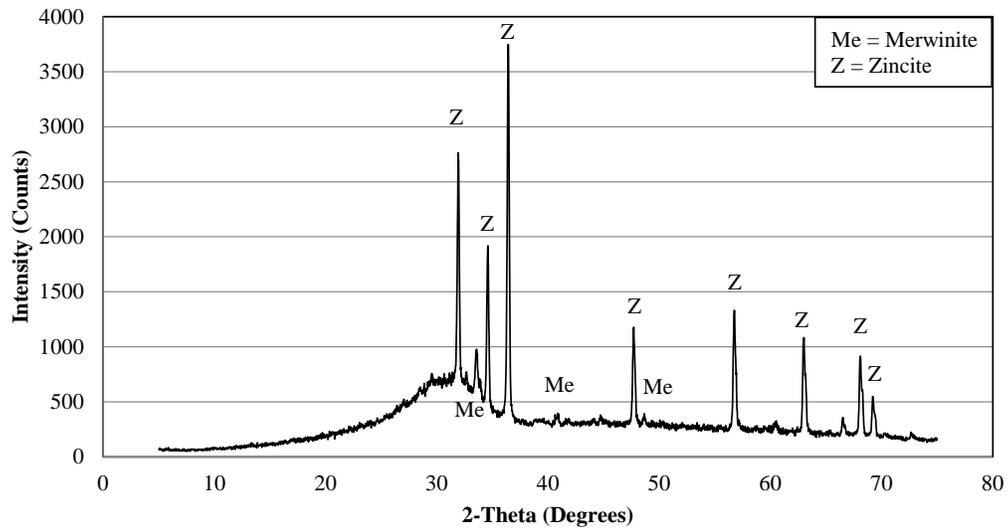
Figure A.16 X-ray diffraction pattern of S
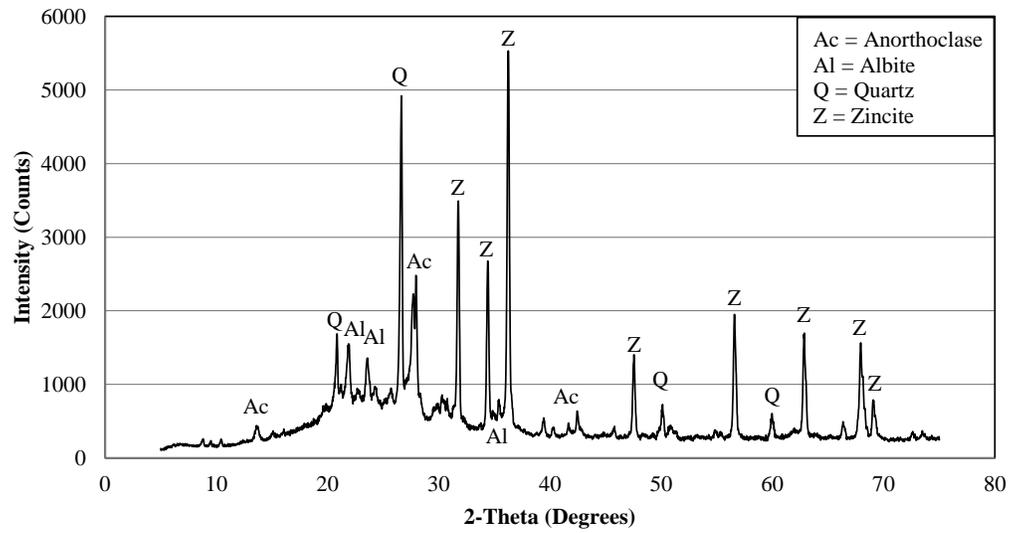
Figure A.17 X-ray diffraction pattern of T-P

Appendix B. Scanning Electron Microscopy Images
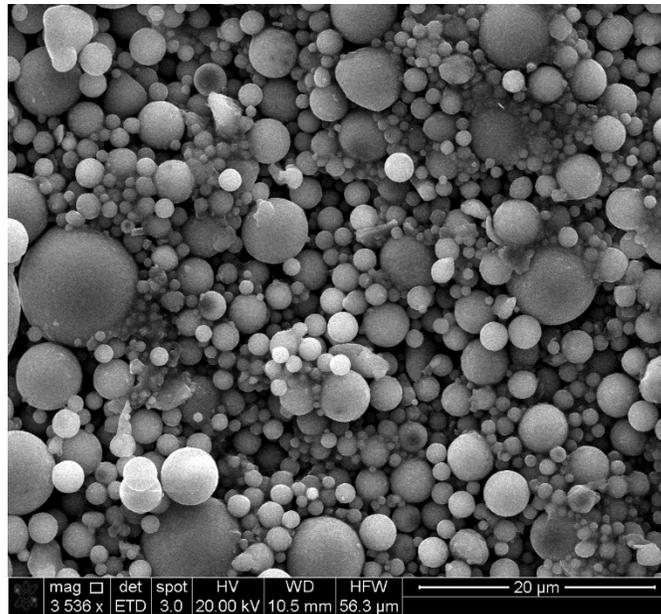
Figure B.1 SEM image of F-G
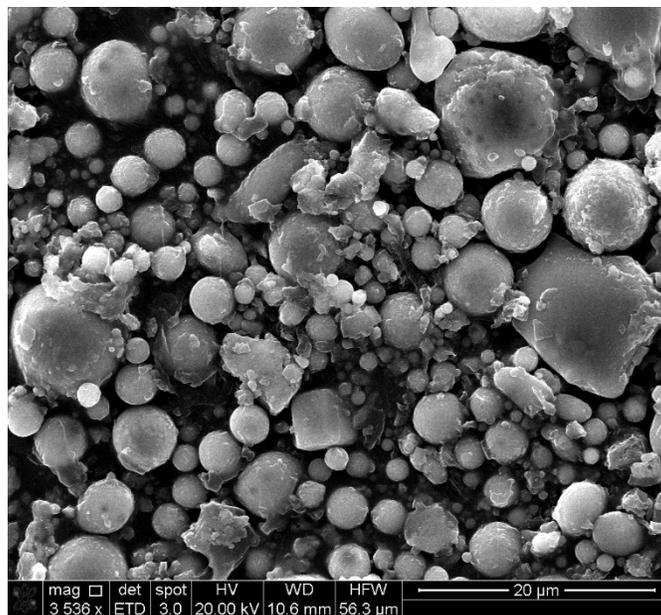
Figure B.2 SEM image of F-Z
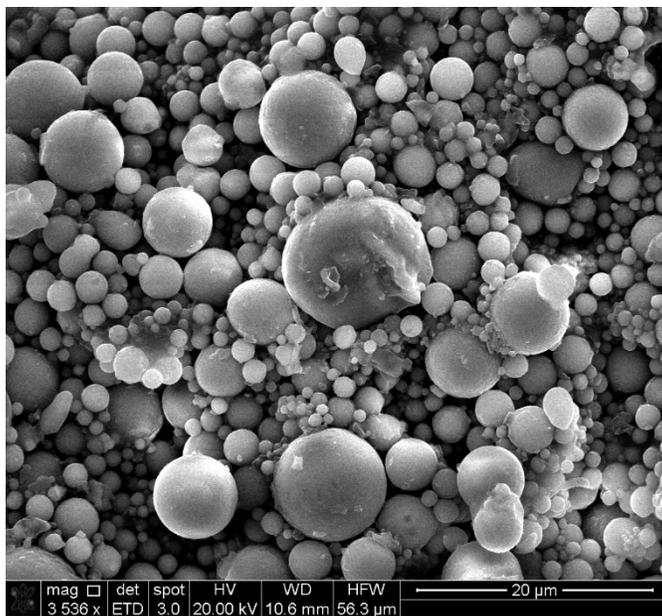
Figure B.3 SEM image of BA-P
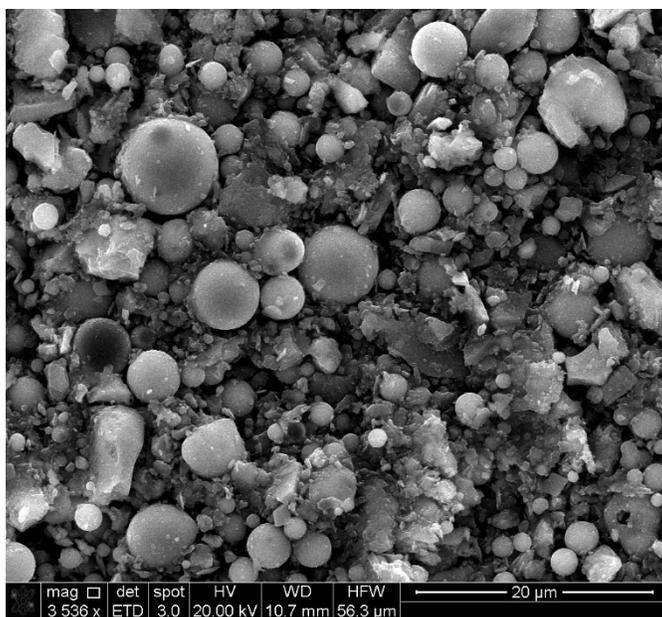
Figure B.4 SEM image of BA-S
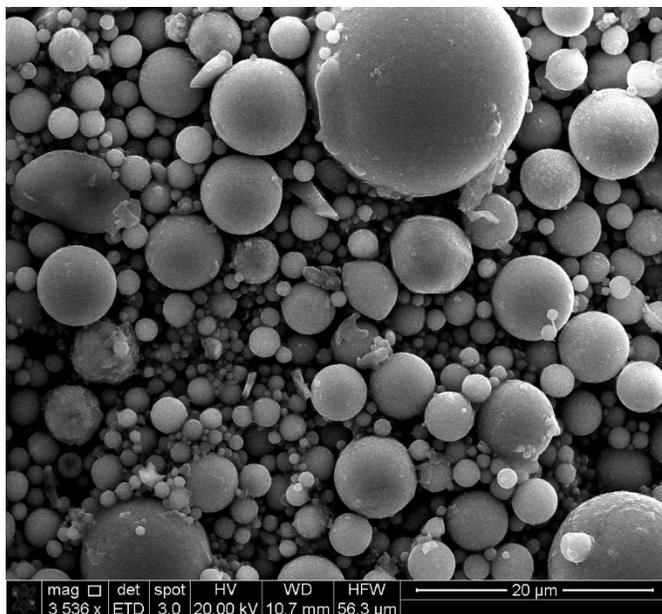
Figure B.5 SEM image of BA-V
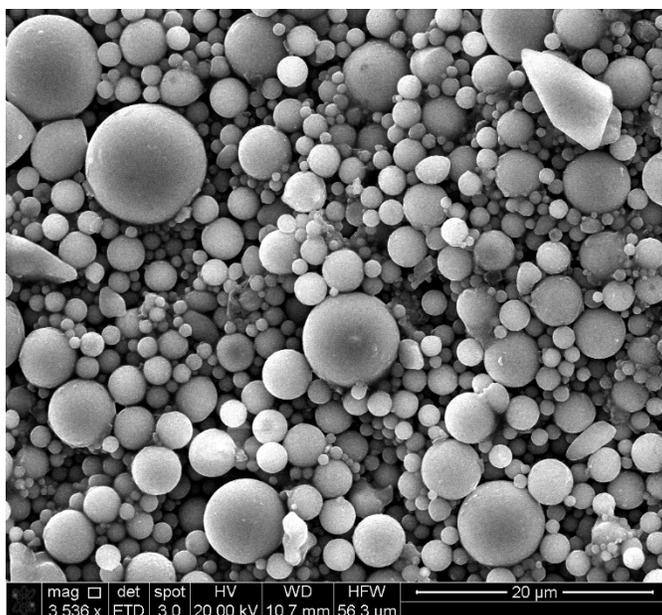
Figure B.6 SEM image of BC-B
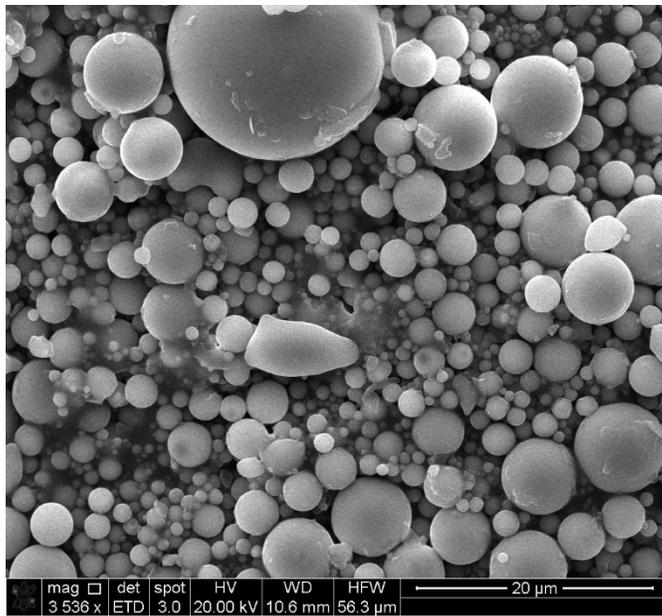
Figure B.7 SEM image of BC-M
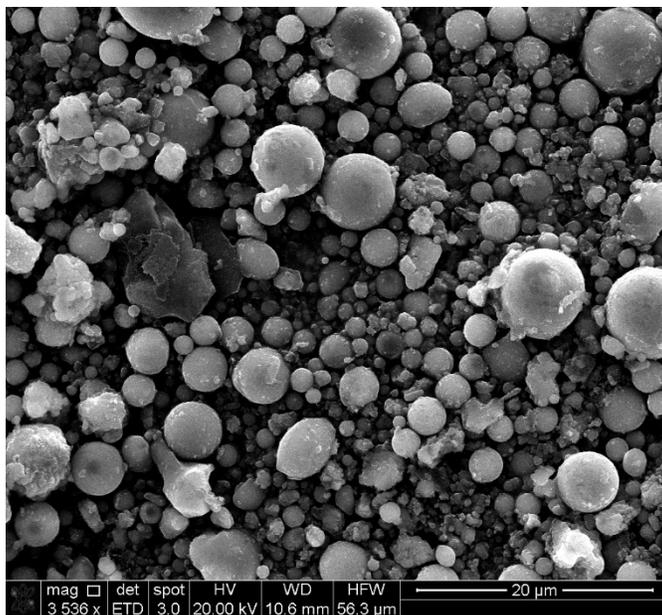
Figure B.8 SEM image of RM-S3
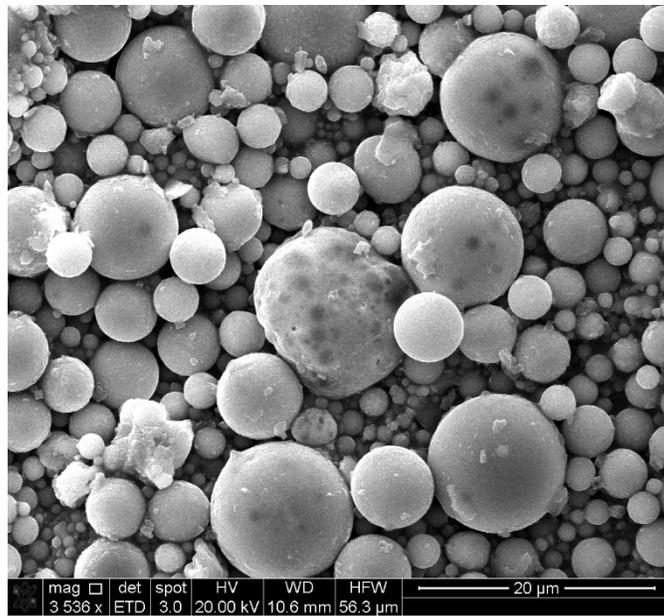
Figure B.9 SEM image of RM-S9
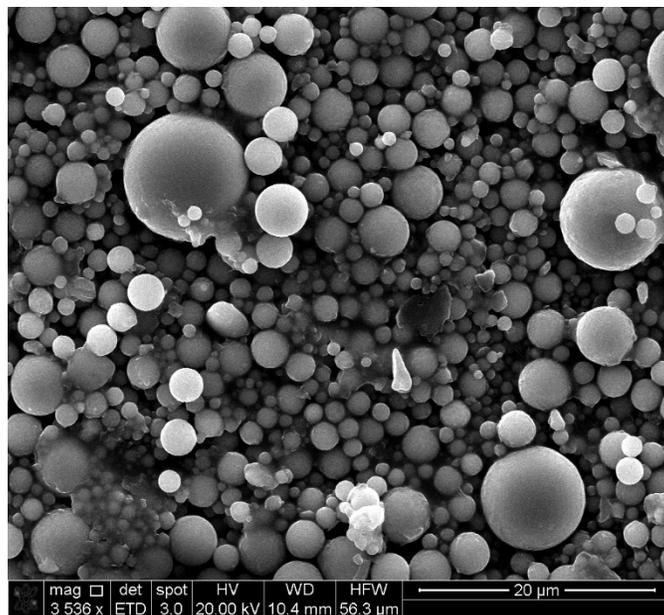
Figure B.10 SEM image of I-S
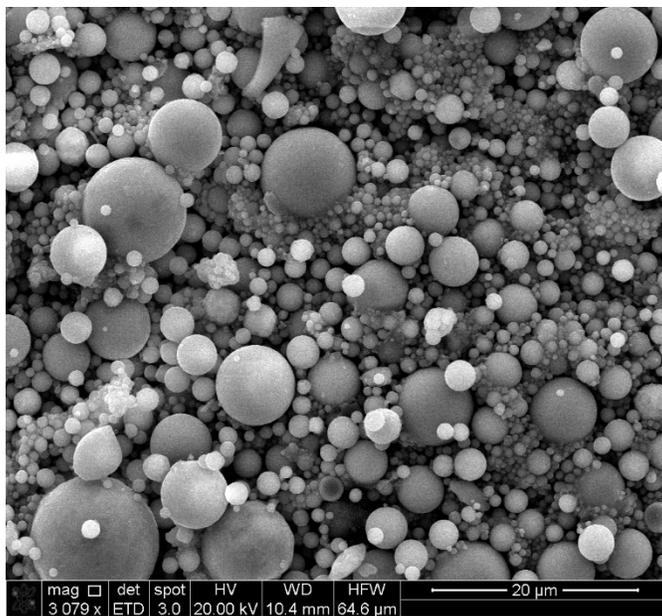
Figure B.11 SEM image of C-H

Figure B.12 SEM image of MBA